Reversibly Neutralized Perfringolysin O for Intracellular Delivery of Macromolecules

by

Nicole J. Yang

B.S. Chemical Engineering
Stanford University, 2009

MASSACHUSETTS INSTITUTE OF TECHNOLOGY
FEB 11 2016
LIBRARIES
ARCHIVES

SUBMITTED TO THE DEPARTMENT OF CHEMICAL ENGINEERING IN
PARTIAL FULFILLMENT OF THE REQUIREMENTS FOR THE DEGREE OF

DOCTOR OF PHILOSOPHY
AT THE
MASSACHUSETTS INSTITUTE OF TECHNOLOGY

FEBRUARY 2016

© Massachusetts Institute of Technology. All rights reserved.

Signature of Author: Signature redacted
Department of Chemical Engineering
October 5th, 2015

Certified by: Signature redacted
K. Dane Wittrup
C.P. Dubbs Professor of Chemical Engineering and Biological Engineering
Thesis Supervisor

Certified by: Signature redacted
Robert S. Langer
David H. Koch Institute Professor
Thesis Supervisor

Accepted by: Signature redacted
Richard D. Braatz
Edwin R. Gilliland Professor of Chemical Engineering
Chairman, Committee for Graduate Students

Thesis Committee

Daniel G. Anderson
Samuel A. Goldblith Professor of Applied Biology
Departments of Chemical Engineering and Health Sciences & Technology
Institute for Medical Engineering and Science
Massachusetts Institute of Technology

Bradley L. Pentelute
Pfizer-Laubach Career Development Assistant Professor
Department of Chemistry
Massachusetts Institute of Technology

David J. Fitzgerald
Senior Investigator, Laboratory of Molecular Biology
Head, Biotherapy Section
Center for Cancer Research
National Cancer Institute

Reversibly Neutralized Perfringolysin O for Intracellular Delivery of Macromolecules

by

Nicole J. Yang

Submitted to the Department of Chemical Engineering on October 5th, 2015
in Partial Fulfillment of the Requirements for the Degree of
Doctor of Philosophy in Chemical Engineering

ABSTRACT

With an increasing understanding of the molecular bases of disease, macromolecules such as proteins and siRNA can potentially be used as therapeutics, modulating biological function with high specificity to reverse pathological progression. However, while certain contexts require manipulating the biology inside the cell, the large size and charge of macromolecules prevent them from spontaneously crossing the cell membrane. For proteins, this problem limits the scope of diseases that are potentially addressable. For siRNA, this prevents access to the cellular machinery responsible for executing gene silencing in the first place. Thus, a safe and effective method to deliver proteins and siRNA into the cytoplasm is desired to fully enable their therapeutic potential.

In this thesis, we describe the development of an intracellular delivery system based on a bacterial pore-forming protein, and demonstrate its efficacy *in vitro* using protein and siRNA payloads. Perfringolysin O (PFO) is a member of the cholesterol-dependent cytolysin (CDC) family of bacterial toxins whose pores, reaching up to 30nm in diameter, allow the passage of large molecules without a specialized transport mechanism. However, the creation of such pores on the cell membrane is accompanied by cytotoxicity, which limits the practical use of these proteins as a delivery tool. Thus, we developed a strategy to selectively activate PFO in endosomal compartments to minimize cytotoxicity. Specifically, we engineered a neutralizing binder against PFO on the fibronection scaffold. The binder was designed to have a higher affinity for PFO at neutral pH, inhibiting pore-formation on the cell membrane, and a lower affinity at acidic pH, promoting pore-formation on endosomal membranes. Fusing this binder to an antibody against EGFR allowed specific targeting and internalization. Using a protein payload—the ribosome-inactivating protein gelonin—administered *in trans*, we demonstrated that this strategy enables efficient delivery with high specificity and low toxicity, increasing the therapeutic window of PFO by orders of magnitude *in vitro*.

One advantage of this delivery system is its modularity, as the payload administered *in trans* is readily swappable with other molecules of interest. Thus, we next demonstrated that the neutralized PFO-based system can also be used for intracellular delivery of siRNA. For this application, we engineered a targeted siRNA carrier based on the dsRNA-binding protein p19 of the Carnation Italian Ringspot Virus (CIRV). In particular, we matured the affinity of p19 to create clones with some of the highest affinities for siRNA reported to date. Higher affinity correlated with higher potency, with the tightest-binding p19 mutant enabling silencing of a reporter gene with pM concentrations of siRNA *in vitro*. This increase in potency was partially due to increased uptake of siRNA. However, we also observed that the high-affinity clones enable stronger silencing even when each clone internalizes similar numbers of siRNA. This observation suggests that prolonging the association of siRNA and its carrier inside the cell may be a strategy for further improving the efficiency of silencing.

Overall, the work described in this thesis demonstrates how neutralizing binders can be used to control the activity of potent membrane-disrupting agents, to deliver exogenous macromolecules into the cytoplasm with low toxicity. Further optimization of the neutralized PFO-based system for *in vivo* use will enhance its utility as a viable therapeutic strategy.

Thesis Supervisor: K. Dane Wittrup
Title: C.P. Dubbs Professor, Chemical Engineering and Biological Engineering

Thesis Supervisor: Robert S. Langer
Title: David H. Koch Institute Professor

Acknowledgements

I am deeply grateful to the many people who made this work possible. My advisor Dane Wittrup, first and foremost, imparted in me an approach to science that I will strive to carry on in my future endeavors. He was a constant source of ideas, regarding big picture directions to small experimental details, and consequently was a driving force behind this project. His trust in my abilities motivated me to do my best, and his support and patience allowed me to pursue my interests. My co-advisor Bob Langer kept me on track throughout my graduate career, while being extremely available for even the smallest advice. Members of my committee, Dan Anderson, Brad Pentelute and David Fitzgerald provided scientific advice that was indispensable for moving my project forward. I am also grateful for their generous mentorship.

I am most fortunate to have met and learned from an outstanding group of people who made the Wittrup lab the incredible place that it is. My labmates provided the advice and support that sustained me throughout graduate school, to which I am indebted. In particular, David Liu and Chris Pirie laid the foundations for the intracellular delivery work that eventually became my project. Jamie Spangler mentored me through my first learning curve in the lab and taught me everything from pHing buffers to culturing cells. Tiffany Chen and Xiaosai Yao have been my closest friends, who not only taught me science but also made Boston feel like home. Cary Opel set a standard of scientific rigor and organization I will forever strive to meet. Seymour de Picciotto taught me the value of persistence (and having fun while you're at it). Alice Tzeng repeatedly came to my rescue with all manners of lab: with reagents I ran out, protocols I needed, and lab duties I forgot. Jim Van Deventer supported and advised me as I decided to further pursue an academic career. Alessandro Angelini and Michael Traxlmayr inspired me with their genuine love of learning and meticulous approach to science, and their mentorship and friendship greatly enriched my graduate experience. Annie Gai, Jordi Mata-Fink, John Rhoden, Byron Kwan, Eric Zhu, Katie Maass, Monique Kauke, Ryan Kelly, Adrienne Rothschilds, Naveen Mehta and Alison Tisdale were amazing labmates, always willing to help, who made my years here thoroughly enjoyable. In the Langer lab, Abigail Lytton-Jean taught me bioconjugation; Gaurav Sahay helped me with numerous imaging experiments; and Chris Alabi provided scientific guidance. I was also fortunate to work with undergraduates with contagious enthusiasm—Fangdi Sun, Demetra Sklaviadis, Keerti Shukla, Jacob Laux, Lucy Yang and Eta Atolia—who contributed significantly to the project while also teaching me how to be a better mentor. Finally, the Koch Institute was an incredible environment to do research. Richard Cook and members of the Biopolymers Facility sequenced countless tubes of DNA for me. Glenn Paradis, Michael Jennings, Michele Griffin and Merve Saturno-Condon from the Flow Cytometry Core advised and assisted with sorting, which was essential for my project. Jaime Cheah and Christian Soule from the High Throughput Screening Facility introduced me to the future of science. Ermelinda provided friendship and moral support through the late nights.

Outside of lab, my classmates in Chemical Engineering and friends throughout MIT supported me during our shared journey through graduate school. My in-laws, Jay and Yun, cared and looked out for me ever since we first met. My grandparents were my biggest and most dedicated cheerleaders. My parents were an unwavering source of unconditional love and support. Without their dedication and sacrifice I would not be where I am today to write this thesis. Finally, my husband Dan, with his infinite patience and understanding, supported me through it all. Dan cooked me yummy food then did all the dishes; he helped me with experiments and edited all my papers. He kept me sane through moments of difficulty, and celebrated my achievements, however small, with unfailingly greater enthusiasm than myself. Thank you for being there for me in every single way.

Dedicated to my parents

Table of Contents

Chapter 1. Introduction

1. The Intracellular Delivery Problem

Macromolecules such as proteins and siRNA can potentially be used to modulate biological function with high specificity for the treatment of disease[1,2]. However, while certain therapeutic strategies require manipulating biology inside the cell, the large size and charge of macromolecules prevent them from spontaneously crossing the cell membrane. This problem limits the scope of diseases that are potentially addressable with proteins, and prevents siRNA from accessing the cellular machinery responsible for executing gene silencing in the first place. Thus, an effective method to deliver proteins and siRNA into the cytoplasm is desired to fully enable their therapeutic potential.

Proteins as Drugs. The high affinity of binding and specificity of interaction intrinsic to protein-protein interactions have made proteins, as a class of molecules, successful therapeutics[3]. For example, protein drugs are in clinical use to inhibit (e.g. antibodies), augment (e.g. immunostimulatory cytokines) or reconstitute (e.g. hormones) biological function[1] by interacting with extracellular receptors. In contrast, there is a lack of engagement with intracellular targets, in part reflecting the difficulty of reliably delivering intact and functional protein into the cytoplasm[4].

Currently, the relatively most robust method to introduce exogenous proteins into the cytoplasm is to introduce the genetic material (typically DNA, but also mRNA) encoding the protein of interest. Various gene delivery techniques are routinely used in the laboratory, including electroporation, chemical transfection and viral transduction. However, the advantages and disadvantages of delivering genetic material versus the protein product itself should be considered within the context of the disease. For example, for proteins requiring long-term persistence, it may be most appropriate to deliver its DNA that can be stably maintained. Alternatively, mRNA, although less stable and more immunogenic than DNA, does not risk genomic integration. Its transient nature, in fact, may further increase its safety profile from a clinical perspective. However, the recipient cell must be capable of expressing the protein of interest at therapeutic levels in a consistent manner. In contrast, delivering protein allows the highest degree of control over the dose and duration of the active product. Protein are also non-integrative and transient, and thus particularly appropriate for applications requiring only a single, one-time manipulation (such as

This chapter was reproduced in part with permission from Yang et al. *Methods Mol Biol.* **2015**; 1266:29-53.
Copyright © 2015 Springer Science+Business Media New York.

genome editing[5,6]).

Proof-of-concept studies have demonstrated that intracellular delivery of proteins can be achieved in vitro and to some degree, in vivo, as discussed below (see "Intracellular Delivery Systems for Protein and siRNA Payloads"). However, targeted delivery of proteins is "in its infancy"[4] and preclinical studies demonstrating therapeutic efficacy from intracellularly delivered proteins are yet to be reported.

siRNA as Drugs. RNA interference (RNAi) is an endogenous, post-transcriptional gene silencing mechanism[7] that can be triggered by exogenously introduced siRNA[8]. Synthetic siRNAs are loaded directly onto Argonaute and unwound to form the RNA-induced silencing complex (RISC). mRNA with perfect complementarity to the guide strand in RISC is cleaved between the 10^{th} and 11^{th} nucleotide (counting from the 5' of the guide strand)[8]. To note, cleavage occurs only with Argonaute 2 (AGO2), as the other three human AGO proteins lack catalytic activity[9]. An active RISC has been estimated to cleave approximately 10 molecules of mRNA[10], and depending on the doubling rate of cells, gene silencing below 50% can be maintained for approximately 2-8 days[11].

siRNAs are attractive therapeutics from a drug-development perspective, because a single delivery platform can be readily expanded towards multiple gene targets. In theory, siRNAs can be designed against any gene, including those that code for "undruggable" proteins that lack an enzymatic pocket for a small-molecule to bind. In addition, although extensive optimization is required to identify an effective sequence[12], this process may be achieved in a relatively short period of 4-8 weeks[13].

Multiple preclinical studies have demonstrated proof-of-concept using siRNA-mediated gene silencing for the treatment of cancer, either with siRNA alone or in combination with another drug (typically a chemotherapeutic). For example, a liposomal siRNA formulation targeting Protein Kinase N3 (PKN3) delayed growth of primary tumors and reduced metastases in orthotopic tumor models in mice[14,15]. This system completed Phase I clinical trials and evaluation in combination with gemcitabine is planned (NCT01808638). Other lipid-based siRNA formulations are also under clinical evaluation for the treatment of cancer[16].

2. Naturally Occurring Intracellular Delivery Systems

Certain bacterial toxins and viruses have evolved mechanisms to shuttle protein or genetic material across the mammalian cell membrane. While the mechanisms of many such processes are not yet fully elucidated, bacterial and viral systems have inspired numerous engineering efforts and are thus briefly surveyed below.

Bacterial toxins. A number of bacterial toxins are potent inhibitors of central cellular functions such as protein synthesis. Typically, a separate domain (typically denoted the B domain, translocation domain, or translocation complex when oligomerization occurs) is responsible for binding to cellular receptors and translocating the catalytic domain (denoted the A domain) into the cytoplasm[17].

Some toxins form their own pores, such as the diphtheria and anthrax toxins. The translocation domains of anthrax toxin, known as the protective antigen (PA), oligomerizes into a pre-pore complex following proteolytic activation. Subsequent internalization and endosomal acidification is thought to trigger its conversion into a full pore, through which catalytic domains translocate into the cytosol[18].

A number of other toxins, such as the plant toxin ricin, *Pseudomonas* exotoxin A and cholera toxin, take advantage of the ERAD machinery to enter the cell[19–21]. Following binding to gangliosides via its B domains, cholera toxin is internalized and trafficked to the ER where the A domain is reduced, unfolded and subsequently refolded in the cytoplasm[22,23].

Viruses. Viruses can be classified into enveloped viruses, which are encased in a lipid membrane containing glycoproteins, or non-enveloped viruses, which lack a membrane. In general, enveloped viruses are thought to orchestrate the fusion of host and viral membranes using viral fusion proteins, which expose hydrophobic peptides upon environmental triggers such as receptor binding, low pH or proteolytic cleavage. For example, influenza A exposes a hydrophobic segment of hemagglutinin (HA) upon endosomal acidification[24]. With this mechanism, there is no need to translocate across the cell membrane.

Non-enveloped viruses, in contrast, have to cross the membrane in order to access the cell interior. In general, non-enveloped viruses are thought to mediate the disruption of cellular membranes by exposing or releasing lytic peptides that are amphipathic or hydrophobic[25–27] Alternatively, members of the polyomavirus family such as the simian virus (SV40) use a strategy similar to the aforementioned cholera toxin, and hijack the ERAD machinery[28,29].

3. Engineered Intracellular Delivery Systems

3.1. Methods of Evaluating Delivery Systems.

Whereas the permeability of small molecules can be quantitatively measured by standardized assays using model membranes[30], such universally adopted assays are lacking for objectively comparing

the performances of different macromolecule delivery systems. Accurately quantifying the number of functional peptides or proteins that successfully enter the cytoplasm is technically challenging, although selective isolation of the cytosol (and not endosomal compartments) using cellular fractionation[31,32] or digitonin-mediated permeabilization of the plasma membrane[33] have been reported. Immunoprecipitation demonstrating the intended disruption of the target intracellular protein-protein interaction has also been presented as evidence of permeation[34,35].

Fluorescence-microscopy based methods or biological assays measuring the activity of the payload in the cytoplasm have also been employed. In microscopy, diffuse cytosolic staining (indicating endosomal release) is frequently contrasted with punctate signal (indicating endosomal entrapment) to provide a qualitative assessment of permeation, although payloads in the intracellular space that have aggregated or are associated with subcellular organelles may also produce punctate patterns. In some cases, automated image analyses have been reported to identify endosomal release events[36]. However, the presence of labeled payload in the cytoplasm does not guarantee that it has retained its function, and the label itself or fixation steps may cause artifacts in cellular distribution[37,38]. Flow cytometry may potentially be used as an alternative when the fluorescence spectra are distinct in the endosomal compartment and the cytoplasm[39].

Alternatively, cytosolic uptake can be confirmed by measuring a biological effect that is generated only when the payload is in the cytoplasm. For example, a protein payload fused with the avi tag, when delivered to cells stably expressing biotin ligase (BirA), is expected to become biotinylated only in the cytoplasm[40]. When intracellular kinases are targeted, such as with an affibody against Raf-1, downstream signaling pathways are expected to be perturbed only when the protein inhibitor has reached the cytoplasm[41]. In addition, peptide payloads have been conjugated to dexamethasone (Dex) derivatives, which bind to transiently expressed gluococorticoid receptor (GR)-fusion proteins in the cytosol, to induce a reporter[42] or alter its localization[43]. It should be noted that reporter gene expression inherently amplifies the signal through multiple rounds of transcription and translation, whereas microscopically observing the altered localization of a fluorescent reporter is subject to the detection threshold of the instrument.

In cases where the biological activity of the payload is reported, one must be mindful that certain payloads can require fewer numbers in the cytoplasm to generate the measured, macroscopic effect. This is particularly true for catalytic proteins. For example, approximately 50 molecules of β-lactamase in a single cell have been reported to generate a detectable signal from catalyzing a fluorogenic substrate, albeit over a long period of time (16hrs)[44]. Similarly, in theory, four molecules of Cre recombinase can repeatedly catalyze multiple recombination events to promote recombined gene expression[45]. Single

molecules of toxins such as diphtheria and ricin have been estimated to kill a cell [46,47], relevant in instances where cell death is used as the readout for delivery.

3.2. Intracellular Delivery Systems for Protein and siRNA Payloads.

Although some proteins have been reported to spontaneously cross the cell membrane, such examples are rare and have not adopted widespread use. Alternatively, naked siRNA can be delivered by hydrodynamic injections in mice[48–50], but such methods are unsuitable for use in humans. Thus, both proteins and siRNA typically require a delivery vehicle (or technique) that allows them to cross the cell membrane.

Physical disruption of the membrane. Varying physical methods of disrupting the cell membrane, such as microinjection and electroporation[51], have been used to deliver compounds ranging from small molecules to proteins. Sharei et al. developed a microfluidic device that induces transient disruption of the plasma membrane through physical constriction[52]. Silicon "nanowires" have also been reported which pierce through the cell membrane[53,54]. From a clinical perspective, such mechanical methods are likely limited to in vitro or ex vivo applications, such as modulating immune cells for vaccination[55] or adoptive T cell transfer.

Chemical disruption of the membrane. A chemical cocktail consisting of NaCl, a transduction compound (NDSB-201 or GABA), glycine and glycerol has been reported to transduce proteins and small RNAs in both immortalized cell lines and primary cells[6]. This method, termed "iTOP," was reported to be approximately four-times more efficient than the cell-penetrating peptide oligoarginine (R11) at transducing primary fibroblasts with a model protein.

Small-molecule conjugates. For siRNA payloads, conjugation to small molecules such as cholesterol[56] or N-acetylgalactosamine (GalNAc)[57] has been shown to mediate gene silencing in the liver. Analogous strategies for protein payloads have not been demonstrated.

Nucleic acid-based strategies. For siRNA payloads, aptamer-siRNA chimeras have been reported to mediate gene silencing in mouse models of cancer expressing the target receptor[58,59]. A tetrahedral DNA particle, conjugated to siRNA and folate (for targeting) was reported to have favorable biodistribution properties and mediate gene silencing in vivo[60]. In addition, RNA "microsponges" have been reported, which are composed entirely of RNA hairpins that are converted to siRNAs by Dicer intracellularly[61].

Lipid-based strategies. For protein payloads, lipid formulations that successfully transfect DNA or RNA have been attempted for use with proteins. For example, a formulation based on a mixture of cationic and neutral lipids was reported to translocate negatively charged proteins[62]. Alternatively, molecular "handles" such as DNA oligos[63] or negatively-charged GFP[5] have been attached to the protein of interest to promote its complexation with lipids.

Lipid-based formulations are one of the most advanced delivery platforms for siRNA, with multiple formulations undergoing clinical evaluation[16], including stable nucleic acid lipid particles (SNALPs)[64], lipidoid nanoparticles[65,66] and lipoplexes[15]. In addition, combinatorial synthesis and screening approaches have identified lipid-like materials with increasing potency[67,68].

Polymer-based strategies. For protein payloads, polymer-based formulations that have been used successfully for nucleic acid transfections, such as poly-β-amino esters (PBAEs), have been examined for their ability to deliver proteins. Alternatively, Yan et al. reported a technology to encapsulate single proteins in a polymeric shell ("nanocapsule") after attaching the monomeric building blocks of the polymer directly to the protein [69,70].

For siRNA payloads, cyclodextrin-based formulations first demonstrated RNAi-mediated gene silencing in humans from a targeted nanoparticle delivery system[71–73]. Alternative polymeric vehicles include Dynamic polyconjugates (DPCs) based on a poly(butyl amino vinyl ether) (PBAVE) backbone, to which GalNAc and PEG are conjugated via an acid-labile linker, and siRNA via a disulfide bridge[74]. The design of DPCs has evolved to formulations where cholesterol-conjugated siRNA is co-injected with the PBAVE-based masked polymer[75] or a membrane-lytic peptide[76]. In addition, cationic polymers that complex siRNA have been chemically conjugated to antibodies for receptor-specific delivery[77].

Peptide-based strategies. Cell-penetrating peptides have been reported to enhance the permeability of various macromolecules. For protein payloads, early studies showed that the TAT peptide can mediate the translocation of covalently coupled proteins[78–80]. Later on, an amphiphilic CPP Pep-1 was reported to non-covalently complex and translocate peptide and protein cargo[81]. Substance P (SP), an 11-residue neuropeptide, has also been proposed to mediate the cytosolic delivery of synthetic antibody fragments[82] and nucleic acids[83] following covalent conjugation.

For siRNA payloads, cell-penetrating peptides such as TAT[84], MPG[85], poly arginine[86] and CADY[87] have been conjugated to or complexed with siRNA to aid in their delivery. The CPP transportan conjugated to stearyl[88] or myristol groups[89] have also been reported.

Protein-based strategies. Various pore- or channel-forming proteins of bacterial origin have been utilized to translocate exogenous protein cargo. Doerner et al. reported the functional expression of an engineered bacterial channel (MscL) in mammalian cells, which could be controlled by covalent modifications to introduce various cargo into the cytoplasm[90]. Alternatively, protein payloads conjugated to the anthrax toxin lethal factor (LF) have been transported across pores formed by protective antigen (PA)[40,41]. The cholesterol-dependent cytolysin (CDC) family of pore-forming toxins have also been proposed as "reversible permeabilization" reagents to translocate exogenous proteins[91,92], as further discussed below (see "Cholesterol-Dependent Cytolysins as a Delivery Tool"). Certain translocation domains of bacterial toxins which do not form pores have also been proposed as a modular tool that can be fused to, and enhance the intracellular delivery of, various cargo including proteins[93].

Alternatively, "supercharged" GFP, a variant engineered to have high net positive charge (+36)[94], and certain human proteins with naturally high positive charge[95,96] have been reported to translocate across the cell membrane. Curiously, 3E10, an autoantibody proposed to bind to dsDNA [97], has also been reported to penetrate into the nucleus and impair DNA repair[98] or translocate an exogenous phosphatase across the cell membrane[99].

Protein vehicles for siRNA payloads are typically composed of a RNA-binding moiety that is fused to either a cell-penetrating moiety or a receptor-targeting moiety[100]. In certain cases, the positively charged RNA-binding moiety is thought to mediate translocation in addition. For example, protamine (or truncated protamine) has been fused to scFvs[101–103] or DARPins[104] and polyarginine (R9) has been fused to scFvs[86] for targeted delivery of siRNA. Non-cationic dsRNA-binding moieties have also been reported, such as the double-stranded RNA binding domain (dsRBD) of PKR, which was fused to cell-penetrating peptides[84,105], or the viral dsRNA binding protein p19, which was fused to a targeting peptide (YSA)[106]. Alternatively, without using a protein-based RNA carrier, siRNA has been directly conjugated to targeting antibodies using chemical linkers[107].

Exosome-based strategies. Exosomes, endogenously generated vesicles containing proteins, lipids and nucleic acids[108], have been reported to deliver exogenous siRNA that have been loaded into the vesicle by electroporation[109].

Virus-based strategies. For protein payloads, encapsulation in virus-like particles[110] or attachment to an engineered bacteriophage T4 head[111] have been reported to enhance cytosolic delivery. For siRNA payloads, short hairpin RNA (shRNA) expression cassettes[112–114] can be delivered virally.

Bacteria-based strategies. The type III secretion system (T3SS) is a bacterial organelle that delivers bacterial proteins directly into eukaryotic cells. Bacterial "minicells" containing the T3SS have been reported to deliver antigens to the cytosol of antigen-presenting cells[115]. Alternatively, *E. Coli* expressing shRNA, invasin and listeriolysin O (LLO) were reported to induce "trans-kingdom RNAi" upon oral or intravenous administration[116].

Inorganic material-based strategies. A variety of inorganic materials have been proposed to deliver protein and siRNA cargo intracellularly, including silica, carbon nanotubes, quantum dots and gold nanoparticles[117–120].

4. Cholesterol-Dependent Cytolysins as a Delivery Tool

Background. Cholesterol-dependent cytolysins (CDCs) are a family of pore-forming toxins secreted (mainly) by Gram-positive bacteria[121], including Perfringolysin O (PFO), Listeriolysin O (LLO), Streptolysin O (SLO) and Pneumolysin (PLY). CDCs share approximately 40-80% pairwise identity[122] and those whose structure has been solved share an analogous 4-domain structure. CDCs are secreted as water-soluble toxins, and PFO has been reported to form anti-parallel dimers in solution[123]. Most CDCs bind to cholesterol on mammalian cell membranes (with the exception of ILY, which also binds to human CD59[124]), and the affinity of this interaction has been reported to be on the order of hundreds of nM[125,126].

CDCs are thought to recognize cholesterol through a Thr-Leu pair conserved in all CDCs[126]. Following this initial interaction, the loops in domain 4 are thought to anchor into the membrane. Insertion of the highly conserved Trp-rich loop (also known as the undecapeptide, with the sequence ECTGLAWEWWR) has been proposed to trigger allosteric changes that allow the membrane-bound monomers to interact with each other[127]. Structural transitions in domain 3 are thought to expose a previously buried oligomerization interface, which allows hydrogen bonding interactions to form between neighboring β-strands, and π-stacking interactions between Tyr181 and Phe318 which lie on each strand[128]. Following the formation of a pre-pore complex, two bundles of alpha helices in domain 3 each unfold into amphipathic β-hairpins that insert into the membrane[129]. The transmembrane hairpins form a β-barrel pore composed of 35-50 monomers, which reaches 25-30nm in diameter[121]. The pores formed by CDCs are one of the largest bacterial toxin pores that have been reported to date[130].

Motivation for use as a delivery tool. Because the pores formed by CDCs are remarkably large, they are thought to allow macromolecules to directly diffuse across without requiring a specialized transport

mechanism. The ability to shuttle multiple types of payloads across the cell membrane enables CDCs to be used as a generalizable tool independent of the chemical and biological identity of the payload. In addition, interestingly, CDCs share a remarkably analogous structure with human perforin[131]. This structural similarity indicates that these pore-forming proteins may also share a similar mechanism of action. As such, successful engineering strategies developed for CDCs have the potential to be translated to perforin, a non-immunogenic alternative.

CDCs have previously been demonstrated to deliver a wide range of payloads to both established and primary cell types[132]. Early studies showed that CDCs such as SLO, PFO and LLO can be used as transfection regents to introduce various membrane-impermeable payloads into cells, including plasmid DNA[133], antisense oligonucleotides[134], siRNA[135], glycopeptides (bleomycin)[136] and various proteins[137]. In particular, targeted LLO and PFO constructs (fused to binding moieties against tumor associated antigens) successfully delivered macromolecular payloads such as the ribosome-inactivating toxin gelonin[92] and siRNA[138] to antigen-positive cells more efficiently than their untargeted counterparts.

5. P19 as an siRNA Carrier

Background. Viral suppressors of RNA silencing (VSRs) are a family of viral proteins that inhibit the RNA interference pathway in its host, such as by binding to AGO or dsRNA to prevent the assembly of RISC[139]. All plant viruses and certain insect and mammalian viruses express VSRs[140].

P19, the structures of which from the Tomato Bushy Stunt Virus (TBSV)[141] and the Carnation Italian Ringspot Virus (CIRV)[142] are available, is one of the most extensively studied VSRs. P19 forms a tail-to-tail homodimer, which creates a positively charged, concave surface of β-sheets that wrap around one side of the siRNA. Basic and polar residues from p19 interact with the phosphate groups and 2' hydroxyls on the siRNA backbone, directly or through water. In addition, two tryptophan residues from each monomer form stacking interactions with the terminal bases of the siRNA. This end-capping interaction acts as a "molecular caliper" that confers a size-selectivity for siRNAs approximately 21 base pairs in length. Overall, p19's recognition of siRNA is thought to be independent of sequence, as the aforementioned interactions with the siRNA backbone or terminal bases do not rely on the chemical identity of specific bases. Interestingly, although p19 forms hydrogen bonds with both the 3' 2-nt overhangs and 5' phosphates of siRNA, the former has been shown to be dispensable for binding whereas the latter was required to maintain affinity[141,142].

The reported affinities of p19 towards siRNA have varied, ranging from the picomolar (170pM[142], 200pM[143] and 370pM[144]) to the nanomolar range (7nM, 12nM[145], 97nM[146] and 450nM[147]). In

addition, p19 has been reported to have extremely rapid on- and off-rates (1.69×10^8 $M^{-1}s^{-1}$ and 6.2×10^{-2} s^{-1}, respectively), based on a solution-based fluorescence quenching assay[144]. Native p19 contains three free cysteines, two of which are solvent exposed, and mutating them to either alanine or serine did not significantly affect affinity[146]. Tandem dimers of p19, where two monomers were linked with flexible Gly_4Ser linkers, were reported to have 2-3 fold improvement in affinity[147] compared to the unlinked dimer. Additionally, the affinity of p19 has been reported to depend pH but in conflicting directions, either increasing[148] or decreasing[106] with decreasing pH.

The high affinity of p19 for dsRNA has fueled its use in various biological applications[140], including miRNA/siRNA detection and RNAi suppression. Typically, to detect and quantify miRNA from biological samples, a complementary RNA probe is used to create a dsRNA hybrid that can then be captured by p19[149–157]. p19-coated magnetics beads are commercially available as a miRNA detection kit using this approach[158]. Similarly, p19 has been used to immunoprecipitate endogenous siRNAs[159–161]. In addition, the natural function of p19 inhibiting RNAi[162] has been utilized in plants to reduce transgene silencing for enhanced recombinant protein yields[163–165], or in mammalian cells for enhanced recombinant adenovirus titers[166]. Rauschhuber et al. further demonstrated the utility of p19-mediated inhibition of RNAi inhibition in vivo, by virally delivering p19 under tissue-specific promoters[166]. Additionally, p19 has been used to stabilize siRNAs in bacteria for "recombinant" production of siRNA[167] and to deliver siRNA intracellularly for gene silencing[106].

Motivation for use as a siRNA delivery vehicle. As noted by Liu et al.[138], protein-based siRNA delivery vehicles, compared to nanoparticulate formulations, have the advantages that they can be synthesized and purified in a relatively straightforward manner to monodispersity, and that their relatively smaller size favors extravasation to and diffusion within the tumor[168]. As summarized earlier (see "Intracellular Delivery Systems for Protein and siRNA Payloads"), there is precedent demonstrating gene silencing using protein-based delivery vehicles, but few have adopted widespread use or advanced towards more extensive preclinical or clinical evaluations. This may be due to the generally lower efficiencies of silencing, complicated preparation and purification strategies involving chemical conjugation or protein refolding, or poor pharmacokinetics and biodistribution properties stemming from the polycationic nature of previous delivery vehicles[138].

As such, we had previously reported the development of a double-stranded RNA binding domain (dsRBD)-based, three-agent siRNA delivery system targeting EGFR[138]. The dsRBD was that of human Protein Kinase R (PKR). While this system achieved specific silencing in vitro with an EC_{50} of approximately 10 nM siRNA, the low affinity of the dsRBD against its payload prevented efficient delivery to xenografted tumors following intravenous administration. Indeed, we observed the siRNA

dissociating prematurely from the dsRBD-based vehicle and accumulating primarily in the kidney, in a similar manner to naked siRNA (data not shown). However, subsequent efforts to mature the affinity of the dsRBD via yeast surface display methodologies were unsuccessful (data not shown), initiating the need for a dsRNA-binding protein that has higher affinity naturally.

Several factors make p19 an attractive alternative as the siRNA binding moiety. Similar to dsRBDs, p19 binds to siRNA independent of sequence, allowing association with any siRNA in theory, through non-covalent interactions that allow eventual release and simple preparation (mixing, instead of conjugation). In addition, the starting affinity of p19 is higher than that of dsRBDs (see "Background" above), whose monovalent affinity is approximately 200nM[169] and apparent affinity in bivalent form is 3.5nM[138]. In addition, the charge density of p19 is lower and more negative than the dsRBD of PKR, with an expected net charge of -2, in contrast to +5 for PKR dsRBD. Positively-charged proteins are thought to become absorbed non-specifically onto the negatively-charged surfaces of mammalian cell membranes[95,170–172]. Finally, the end-capping mechanism of binding present only in p19 ensures 1:1 binding between a p19 dimer and one molecule of siRNA, and thus true monodispersity. In contrast, one double-stranded RNA binding motif (dsRBM) occupies approximately 12 base pairs of dsRNA[173], allowing two dsRBMs to bind to one molecule of siRNA. Such a setup can potentially cause crosslinking and aggregation (the dsRBD of PKR is composed of two homologous dsRBMs).

Works cited

1 Leader B, Baca QJ, Golan DE. Protein therapeutics: a summary and pharmacological classification. *Nat Rev Drug Discov* 2008; **7**: 21–39.

2 Kanasty R, Dorkin JR, Vegas A, Anderson D. Delivery materials for siRNA therapeutics. *Nat Mater* 2013; **12**: 967–977.

3 Kariolis MS, Kapur S, Cochran JR. Beyond antibodies: using biological principles to guide the development of next-generation protein therapeutics. *Curr Opin Biotechnol* 2013; **24**: 1072–1077.

4 Carter PJ. Introduction to current and future protein therapeutics: A protein engineering perspective. *Exp Cell Res* 2011; **317**: 1261–1269.

5 Zuris JA, Thompson DB, Shu Y, Guilinger JP, Bessen JL, Hu JH *et al.* Cationic lipid-mediated delivery of proteins enables efficient protein-based genome editing in vitro and in vivo. *Nat Biotechnol* 2015; **33**: 73–80.

6 Astolfo DS D', Pagliero RJ, Pras A, Karthaus WR, Clevers H, Prasad V *et al.* Efficient Intracellular Delivery of Native Proteins. *Cell* 2015; **161**: 674–690.

7 Fire A, Xu S, Montgomery MK, Kostas SA, Driver SE, Mello CC. Potent and specific genetic interference by double-stranded RNA in Caenorhabditis elegans. *Nature* 1998; **391**: 806–811.

8 Elbashir SM, Harborth J, Lendeckel W, Yalcin A, Weber K, Tuschl T. Duplexes of 21-nucleotide RNAs mediate RNA interference in cultured mammalian cells. *Nature* 2001; **411**: 494–498.

9 Wilson RC, Doudna JA. Molecular Mechanisms of RNA Interference. *Annu Rev Biophys* 2013; **42**: 217–239.

10 Hutvágner G, Zamore PD. A microRNA in a Multiple-Turnover RNAi Enzyme Complex. *Science* 2002; **297**: 2056–2060.

11 Bartlett DW, Davis ME. Insights into the kinetics of siRNA-mediated gene silencing from live-cell and live-animal bioluminescent imaging. *Nucleic Acids Res* 2006; **34**: 322–333.

12 Reynolds A, Leake D, Boese Q, Scaringe S, Marshall WS, Khvorova A. Rational siRNA design for RNA interference. *Nat Biotechnol* 2004; **22**: 326–330.

13 Vaishnaw AK, Gollob J, Gamba-Vitalo C, Hutabarat R, Sah D, Meyers R *et al.* A status report on RNAi therapeutics. *Silence* 2010; **1**: 14.

14 Aleku M, Schulz P, Keil O, Santel A, Schaeper U, Dieckhoff B *et al.* Atu027, a Liposomal Small Interfering RNA Formulation Targeting Protein Kinase N3, Inhibits Cancer Progression. *Cancer Res* 2008; **68**: 9788–9798.

15 Santel A, Aleku M, Röder N, Möpert K, Durieux B, Janke O *et al.* Atu027 Prevents Pulmonary Metastasis in Experimental and Spontaneous Mouse Metastasis Models. *Clin Cancer Res* 2010; **16**: 5469–5480.

16 Yin H, Kanasty RL, Eltoukhy AA, Vegas AJ, Dorkin JR, Anderson DG. Non-viral vectors for gene-based therapy. *Nat Rev Genet* 2014; **15**: 541–555.

17 Falnes PØ, Sandvig K. Penetration of protein toxins into cells. *Curr Opin Cell Biol* 2000; **12**: 407–413.

18 Collier RJ. Membrane translocation by anthrax toxin. *Mol Aspects Med* 2009; **30**: 413–422.

19 de Virgilio M, Lombardi A, Caliandro R, Fabbrini MS. Ribosome-Inactivating Proteins: From Plant Defense to Tumor Attack. *Toxins* 2010; **2**: 2699–2737.

20 Spooner RA, Lord JM. How Ricin and Shiga Toxin Reach the Cytosol of Target Cells: Retrotranslocation from the Endoplasmic Reticulum. In: Mantis N (ed). *Ricin and Shiga Toxins.* Springer Berlin Heidelberg, 2012, pp 19–40.

21 Sandvig K, Skotland T, van Deurs B, Klokk TI. Retrograde transport of protein toxins through the Golgi apparatus. *Histochem Cell Biol* 2013; **140**: 317–326.

22 Wernick NLB, Chinnapen DJ-F, Cho JA, Lencer WI. Cholera Toxin: An Intracellular Journey into the Cytosol by Way of the Endoplasmic Reticulum. *Toxins* 2010; **2**: 310–325.

23 Cho JA, Chinnapen DJ-F, Aamar E, Welscher YM te, Lencer WI, Massol R. Insights on the trafficking and retro-translocation of glycosphingolipid-binding bacterial toxins. *Front Cell Infect Microbiol* 2012; **2**. doi:10.3389/fcimb.2012.00051.

24 Sriwilaijaroen N, Suzuki Y. Molecular basis of the structure and function of H1 hemagglutinin of influenza virus. *Proc Jpn Acad Ser B Phys Biol Sci* 2012; **88**: 226–249.

25 Tsai B. Penetration of nonenveloped viruses into the cytoplasm. *Annu Rev Cell Dev Biol* 2007; **23**: 23–43.

26 Johnson J, Banerjee M. Activation, Exposure and Penetration of Virally Encoded, Membrane-Active Polypeptides During Non-Enveloped Virus Entry. *Curr Protein Pept Sci* 2008; **9**: 16–27.

27 Moyer CL, Nemerow GR. Viral Weapons of Membrane Destruction: Variable Modes of Membrane Penetration by Non-Enveloped Viruses. *Curr Opin Virol* 2011; **1**: 44–99.

28 Inoue T, Tsai B. How Viruses Use the Endoplasmic Reticulum for Entry, Replication, and Assembly. *Cold Spring Harb Perspect Biol* 2013; **5**: a013250.

29 Suomalainen M, Greber UF. Uncoating of non-enveloped viruses. *Curr Opin Virol* 2013; **3**: 27–33.

30 Sugano K, Kansy M, Artursson P, Avdeef A, Bendels S, Di L *et al.* Coexistence of passive and carrier-mediated processes in drug transport. *Nat Rev Drug Discov* 2010; **9**: 597–614.

31 Shamu CE, Story CM, Rapoport TA, Ploegh HL. The Pathway of Us11-Dependent Degradation of Mhc Class I Heavy Chains Involves a Ubiquitin-Conjugated Intermediate. *J Cell Biol* 1999; **147**: 45–58.

32 Bartz R, Fan H, Zhang J, Innocent N, Cherrin C, Beck SC *et al.* Effective siRNA delivery and target mRNA degradation using an amphipathic peptide to facilitate pH-dependent endosomal escape. *Biochem J* 2011; **435**: 475–487.

33 Bittner MA, Holz RW. Effects of Tetanus Toxin on Catecholamine Release from Intact and Digitonin-Permeabilized Chromaffin Cells. *J Neurochem* 1988; **51**: 451–456.

34 Moellering RE, Cornejo M, Davis TN, Bianco CD, Aster JC, Blacklow SC *et al.* Direct inhibition of the NOTCH transcription factor complex. *Nature* 2009; **462**: 182–188.

35 Chang YS, Graves B, Guerlavais V, Tovar C, Packman K, To K-H *et al.* Stapled α–helical peptide drug development: A potent dual inhibitor of MDM2 and MDMX for p53-dependent cancer therapy. *Proc Natl Acad Sci* 2013; **110**: E3445–E3454.

36 Bonner DK, Leung C, Chen-Liang J, Chingozha L, Langer R, Hammond PT. Intracellular Trafficking of Polyamidoamine–Poly(ethylene glycol) Block Copolymers in DNA Delivery. *Bioconjug Chem* 2011; **22**: 1519–1525.

37 Richard JP, Melikov K, Vives E, Ramos C, Verbeure B, Gait MJ *et al.* Cell-penetrating Peptides: a re-evaluation of the mechanism of cellular uptake. *J Biol Chem* 2003; **278**: 585–590.

38 Bechara C, Sagan S. Cell-penetrating peptides: 20 years later, where do we stand? *FEBS Lett* 2013; **587**: 1693–1702.

39 Cebrian I, Visentin G, Blanchard N, Jouve M, Bobard A, Moita C *et al.* Sec22b Regulates Phagosomal Maturation and Antigen Crosspresentation by Dendritic Cells. *Cell* 2011; **147**: 1355–1368.

40 Verdurmen WPR, Luginbühl M, Honegger A, Plückthun A. Efficient cell-specific uptake of binding proteins into the cytoplasm through engineered modular transport systems. *J Controlled Release* 2015; **200**: 13–22.

41 Liao X, Rabideau AE, Pentelute BL. Delivery of Antibody Mimics into Mammalian Cells via Anthrax Toxin Protective Antigen. *ChemBioChem* 2014; **15**: 2458–2466.

42 Yu P, Liu B, Kodadek T. A high-throughput assay for assessing the cell permeability of combinatorial libraries. *Nat Biotechnol* 2005; **23**: 746–751.

43 Holub JM, LaRochelle JR, Appelbaum JS, Schepartz A. Improved Assays for Determining the Cytosolic Access of Peptides, Proteins, and Their Mimetics. *Biochemistry (Mosc)* 2013; **52**: 9036–9046.

44 Zlokarnik G, Negulescu PA, Knapp TE, Mere L, Burres N, Feng L *et al.* Quantitation of Transcription and Clonal Selection of Single Living Cells with β-Lactamase as Reporter. *Science* 1998; **279**: 84–88.

45 Bordonaro M. Modular Cre/lox System and Genetic Therapeutics for Colorectal Cancer. *J Biomed Biotechnol* 2009; **2009**. doi:10.1155/2009/358230.

46 Yamaizumi M, Mekada E, Uchida T, Okada Y. One molecule of diphtheria toxin fragment a introduced into a cell can kill the cell. *Cell* 1978; **15**: 245–250.

47 Eiklid K, Olsnes S, Pihl A. Entry of lethal doses of abrin, ricin and modeccin into the cytosol of HeLa cells. *Exp Cell Res* 1980; **126**: 321–326.

48 Lewis DL, Hagstrom JE, Loomis AG, Wolff JA, Herweijer H. Efficient delivery of siRNA for inhibition of gene expression in postnatal mice. *Nat Genet* 2002; **32**: 107–108.

49 McCaffrey AP, Meuse L, Pham T-TT, Conklin DS, Hannon GJ, Kay MA. Gene expression: RNA interference in adult mice. *Nature* 2002; **418**: 38–39.

50 Song E, Lee S-K, Wang J, Ince N, Ouyang N, Min J *et al.* RNA interference targeting Fas protects mice from fulminant hepatitis. *Nat Med* 2003; **9**: 347–351.

51 Zhang Y, Yu L-C. Microinjection as a tool of mechanical delivery. *Curr Opin Biotechnol* 2008; **19**: 506–510.

52 Sharei A, Zoldan J, Adamo A, Sim WY, Cho N, Jackson E *et al.* A vector-free microfluidic platform for intracellular delivery. *Proc Natl Acad Sci* 2013; **110**: 2082–2087.

53 Shalek AK, Robinson JT, Karp ES, Lee JS, Ahn D-R, Yoon M-H *et al.* Vertical silicon nanowires as a universal platform for delivering biomolecules into living cells. *Proc Natl Acad Sci* 2010; **107**: 1870–1875.

54 Yosef N, Shalek AK, Gaublomme JT, Jin H, Lee Y, Awasthi A *et al.* Dynamic regulatory network controlling TH17 cell differentiation. *Nature* 2013; **496**: 461–468.

55 Lee Szeto G, Van Egeren D, Worku H, Sharei A, Alejandro B, Park C *et al.* Microfluidic squeezing for intracellular antigen loading in polyclonal B-cells as cellular vaccines. *Sci Rep* 2015; **5**. doi:10.1038/srep10276.

56 Soutschek J, Akinc A, Bramlage B, Charisse K, Constien R, Donoghue M *et al.* Therapeutic silencing of an endogenous gene by systemic administration of modified siRNAs. *Nature* 2004; **432**: 173–178.

57 Nair JK, Willoughby JLS, Chan A, Charisse K, Alam MR, Wang Q *et al.* Multivalent N-Acetylgalactosamine-Conjugated siRNA Localizes in Hepatocytes and Elicits Robust RNAi-Mediated Gene Silencing. *J Am Chem Soc* 2014; **136**: 16958–16961.

58 McNamara JO, Andrechek ER, Wang Y, Viles KD, Rempel RE, Gilboa E *et al.* Cell type–specific delivery of siRNAs with aptamer-siRNA chimeras. *Nat Biotechnol* 2006; **24**: 1005–1015.

59 Dassie JP, Liu X, Thomas GS, Whitaker RM, Thiel KW, Stockdale KR *et al.* Systemic administration of optimized aptamer-siRNA chimeras promotes regression of PSMA-expressing tumors. *Nat Biotechnol* 2009; **27**: 839–846.

60 Lee H, Lytton-Jean AKR, Chen Y, Love KT, Park AI, Karagiannis ED *et al.* Molecularly self-assembled nucleic acid nanoparticles for targeted in vivo siRNA delivery. *Nat Nanotechnol* 2012; **7**: 389–393.

61 Lee JB, Hong J, Bonner DK, Poon Z, Hammond PT. Self-assembled RNA interference microsponges for efficient siRNA delivery. *Nat Mater* 2012; **11**: 316–322.

62 Zelphati O, Wang Y, Kitada S, Reed JC, Felgner PL, Corbeil J. Intracellular Delivery of Proteins with a New Lipid-mediated Delivery System. *J Biol Chem* 2001; **276**: 35103–35110.

63 Eltoukhy AA, Chen D, Veiseh O, Pelet JM, Yin H, Dong Y *et al.* Nucleic acid-mediated intracellular protein delivery by lipid-like nanoparticles. *Biomaterials* 2014; **35**: 6454–6461.

64 Zimmermann TS, Lee ACH, Akinc A, Bramlage B, Bumcrot D, Fedoruk MN *et al.* RNAi-mediated gene silencing in non-human primates. *Nature* 2006; **441**: 111–114.

65 Frank-Kamenetsky M, Grefhorst A, Anderson NN, Racie TS, Bramlage B, Akinc A *et al.* Therapeutic RNAi targeting PCSK9 acutely lowers plasma cholesterol in rodents and LDL cholesterol in nonhuman primates. *Proc Natl Acad Sci* 2008; **105**: 11915–11920.

66 Tabernero J, Shapiro GI, LoRusso PM, Cervantes A, Schwartz GK, Weiss GJ *et al.* First-in-Humans Trial of an RNA Interference Therapeutic Targeting VEGF and KSP in Cancer Patients with Liver Involvement. *Cancer Discov* 2013; **3**: 406–417.

67 Love KT, Mahon KP, Levins CG, Whitehead KA, Querbes W, Dorkin JR *et al.* Lipid-like materials for low-dose, in vivo gene silencing. *Proc Natl Acad Sci* 2010; **107**: 1864–1869.

68 Dong Y, Love KT, Dorkin JR, Sirirungruang S, Zhang Y, Chen D *et al.* Lipopeptide nanoparticles for potent and selective siRNA delivery in rodents and nonhuman primates. *Proc Natl Acad Sci* 2014; **111**: 3955–3960.

69 Gu Z, Yan M, Hu B, Joo K-I, Biswas A, Huang Y *et al.* Protein Nanocapsule Weaved with Enzymatically Degradable Polymeric Network. *Nano Lett* 2009; **9**: 4533–4538.

70 Yan M, Du J, Gu Z, Liang M, Hu Y, Zhang W *et al.* A novel intracellular protein delivery platform based on single-protein nanocapsules. *Nat Nanotechnol* 2010; **5**: 48–53.

71 Hu-Lieskovan S, Heidel JD, Bartlett DW, Davis ME, Triche TJ. Sequence-Specific Knockdown of EWS-FLI1 by Targeted, Nonviral Delivery of Small Interfering RNA Inhibits Tumor Growth in a Murine Model of Metastatic Ewing's Sarcoma. *Cancer Res* 2005; **65**: 8984–8992.

72 Heidel JD, Yu Z, Liu JY-C, Rele SM, Liang Y, Zeidan RK *et al.* Administration in non-human primates of escalating intravenous doses of targeted nanoparticles containing ribonucleotide reductase subunit M2 siRNA. *Proc Natl Acad Sci* 2007; **104**: 5715–5721.

73 Davis ME, Zuckerman JE, Choi CHJ, Seligson D, Tolcher A, Alabi CA *et al.* Evidence of RNAi in humans from systemically administered siRNA via targeted nanoparticles. *Nature* 2010; **464**: 1067–1070.

74 Rozema DB, Lewis DL, Wakefield DH, Wong SC, Klein JJ, Roesch PL *et al.* Dynamic PolyConjugates for targeted in vivo delivery of siRNA to hepatocytes. *Proc Natl Acad Sci* 2007; **104**: 12982–12987.

75 Wong SC, Klein JJ, Hamilton HL, Chu Q, Frey CL, Trubetskoy VS *et al.* Co-Injection of a Targeted, Reversibly Masked Endosomolytic Polymer Dramatically Improves the Efficacy of Cholesterol-Conjugated Small Interfering RNAs In Vivo. *Nucleic Acid Ther* 2012; **22**: 380–390.

76 Wooddell CI, Rozema DB, Hossbach M, John M, Hamilton HL, Chu Q *et al.* Hepatocyte-targeted RNAi Therapeutics for the Treatment of Chronic Hepatitis B Virus Infection. *Mol Ther* 2013; **21**: 973–985.

77 Lu H, Wang D, Kazane S, Javahishvili T, Tian F, Song F *et al.* Site-Specific Antibody–Polymer Conjugates for siRNA Delivery. *J Am Chem Soc* 2013; **135**: 13885–13891.

78 Lo S, Wang S. Peptide-Based Nanocarriers for Intracellular Delivery of Biologically Active Proteins. In: *Organelle-Specific Pharmaceutical Nanotechnology*. John Wiley & Sons, 2010.

79 Koren E, Torchilin VP. Cell-penetrating peptides: breaking through to the other side. *Trends Mol Med* 2012; **18**: 385–393.

80 Nakase I, Tanaka G, Futaki S. Cell-penetrating peptides (CPPs) as a vector for the delivery of siRNAs into cells. *Mol Biosyst* 2013; **9**: 855–861.

81 Morris MC, Depollier J, Mery J, Heitz F, Divita G. A peptide carrier for the delivery of biologically active proteins into mammalian cells. *Nat Biotechnol* 2001; **19**: 1173–1176.

82 Rizk SS, Luchniak A, Uysal S, Brawley CM, Rock RS, Kossiakoff AA. An engineered substance P variant for receptor-mediated delivery of synthetic antibodies into tumor cells. *Proc Natl Acad Sci* 2009; **106**: 11011–11015.

83 Rizk SS, Misiura A, Paduch M, Kossiakoff AA. Substance P Derivatives as Versatile Tools for Specific Delivery of Various Types of Biomolecular Cargo. *Bioconjug Chem* 2011; **23**: 42–46.

84 Eguchi A, Meade BR, Chang Y-C, Fredrickson CT, Willert K, Puri N *et al.* Efficient siRNA delivery into primary cells by a peptide transduction domain–dsRNA binding domain fusion protein. *Nat Biotechnol* 2009; **27**: 567–571.

85 Simeoni F, Morris MC, Heitz F, Divita G. Insight into the mechanism of the peptide-based gene delivery system MPG: implications for delivery of siRNA into mammalian cells. *Nucleic Acids Res* 2003; **31**: 2717–2724.

86 Kumar P, Ban H-S, Kim S-S, Wu H, Pearson T, Greiner DL *et al.* T Cell-Specific siRNA Delivery Suppresses HIV-1 Infection in Humanized Mice. *Cell* 2008; **134**: 577–586.

87 Crombez L, Aldrian-Herrada G, Konate K, Nguyen QN, McMaster GK, Brasseur R *et al.* A New Potent Secondary Amphipathic Cell–penetrating Peptide for siRNA Delivery Into Mammalian Cells. *Mol Ther* 2008; **17**: 95–103.

88 Ezzat K, Andaloussi SE, Zaghloul EM, Lehto T, Lindberg S, Moreno PMD *et al.* PepFect 14, a novel cell-penetrating peptide for oligonucleotide delivery in solution and as solid formulation. *Nucleic Acids Res* 2011; **39**: 5284–5298.

89 Ren Y, Hauert S, Lo JH, Bhatia SN. Identification and Characterization of Receptor-Specific Peptides for siRNA Delivery. *ACS Nano* 2012; **6**: 8620–8631.

90 Doerner JF, Febvay S, Clapham DE. Controlled delivery of bioactive molecules into live cells using the bacterial mechanosensitive channel MscL. *Nat Commun* 2012; **3**: 990.

91 Provoda CJ, Stier EM, Lee K-D. Tumor Cell Killing Enabled by Listeriolysin O-liposome-mediated Delivery of the Protein Toxin Gelonin. *J Biol Chem* 2003; **278**: 35102–35108.

92 Pirie CM, Liu DV, Wittrup KD. Targeted Cytolysins Synergistically Potentiate Cytoplasmic Delivery of Gelonin Immunotoxin. *Mol Cancer Ther* 2013; **12**: 1774–1782.

93 Prior TI, FitzGerald DJ, Pastan I. Translocation mediated by domain II of Pseudomonas exotoxin A: transport of barnase into the cytosol. *Biochemistry (Mosc)* 1992; **31**: 3555–3559.

94 Lawrence MS, Phillips KJ, Liu DR. Supercharging Proteins Can Impart Unusual Resilience. *J Am Chem Soc* 2007; **129**: 10110–10112.

95 Cronican JJ, Thompson DB, Beier KT, McNaughton BR, Cepko CL, Liu DR. Potent Delivery of Functional Proteins into Mammalian Cells in Vitro and in Vivo Using a Supercharged Protein. *ACS Chem Biol* 2010; **5**: 747–752.

96 Cronican JJ, Beier KT, Davis TN, Tseng J-C, Li W, Thompson DB *et al.* A Class of Human Proteins that Deliver Functional Proteins into Mammalian Cells In Vitro and In Vivo. *Chem Biol* 2011; **18**: 833–838.

97 Weisbart RH, Noritake DT, Wong AL, Chan G, Kacena A, Colburn KK. A conserved anti-DNA antibody idiotype associated with nephritis in murine and human systemic lupus erythematosus. *J Immunol* 1990; **144**: 2653–2658.

98 Hansen JE, Chan G, Liu Y, Hegan DC, Dalal S, Dray E *et al.* Targeting Cancer with a Lupus Autoantibody. *Sci Transl Med* 2012; **4**: 157ra142–157ra142.

99 Lawlor MW, Armstrong D, Viola MG, Widrick JJ, Meng H, Grange RW *et al.* Enzyme replacement therapy rescues weakness and improves muscle pathology in mice with X-linked myotubular myopathy. *Hum Mol Genet* 2013; **22**: 1525–1538.

100 Watanabe K, Ohtsuki T. Intracellular Delivery of RNA via RNA-Binding Proteins or Peptides. In: Prokop A, Iwasaki Y, Harada A (eds). *Intracellular Delivery II.* Springer Netherlands, 2014, pp 403–416.

101 Song E, Zhu P, Lee S-K, Chowdhury D, Kussman S, Dykxhoorn DM *et al.* Antibody mediated in vivo delivery of small interfering RNAs via cell-surface receptors. *Nat Biotechnol* 2005; **23**: 709–717.

102 Peer D, Zhu P, Carman CV, Lieberman J, Shimaoka M. Selective gene silencing in activated leukocytes by targeting siRNAs to the integrin lymphocyte function-associated antigen-1. *Proc Natl Acad Sci* 2007; **104**: 4095–4100.

103 Yao Y, Sun T, Huang S, Dou S, Lin L, Chen J *et al.* Targeted Delivery of PLK1-siRNA by ScFv Suppresses Her2+ Breast Cancer Growth and Metastasis. *Sci Transl Med* 2012; **4**: 130ra48–130ra48.

104 Winkler J, Martin-Killias P, Plückthun A, Zangemeister-Wittke U. EpCAM-targeted delivery of nanocomplexed siRNA to tumor cells with designed ankyrin repeat proteins. *Mol Cancer Ther* 2009; **8**: 2674–2683.

105 Geoghegan JC, Gilmore BL, Davidson BL. Gene Silencing Mediated by siRNA-binding Fusion Proteins Is Attenuated by Double-stranded RNA-binding Domain Structure. *Mol Ther — Nucleic Acids* 2012; **1**: e53.

106 Choi K, Park GL, Hwang KY, Lee J-W, Ahn HJ. Efficient siRNA Delivery into Tumor Cells by p19-YSA Fusion Protein. *Mol Pharm* 2013; **10**: 763–773.

107 Cuellar TL, Barnes D, Nelson C, Tanguay J, Yu S-F, Wen X *et al.* Systematic evaluation of antibody-mediated siRNA delivery using an industrial platform of THIOMAB–siRNA conjugates. *Nucleic Acids Res* 2015; **43**: 1189–1203.

108 Colombo M, Raposo G, Théry C. Biogenesis, Secretion, and Intercellular Interactions of Exosomes and Other Extracellular Vesicles. *Annu Rev Cell Dev Biol* 2014; **30**: 255–289.

109 Alvarez-Erviti L, Seow Y, Yin H, Betts C, Lakhal S, Wood MJA. Delivery of siRNA to the mouse brain by systemic injection of targeted exosomes. *Nat Biotechnol* 2011; **29**: 341–345.

110 Kaczmarczyk SJ, Sitaraman K, Young HA, Hughes SH, Chatterjee DK. Protein delivery using engineered virus-like particles. *Proc Natl Acad Sci* 2011; **108**: 16998–17003.

111 Tao P, Mahalingam M, Marasa BS, Zhang Z, Chopra AK, Rao VB. In vitro and in vivo delivery of genes and proteins using the bacteriophage T4 DNA packaging machine. *Proc Natl Acad Sci* 2013; **110**: 5846–5851.

112 Brummelkamp TR, Bernards R, Agami R. A System for Stable Expression of Short Interfering RNAs in Mammalian Cells. *Science* 2002; **296**: 550–553.

113 Paddison PJ, Caudy AA, Hannon GJ. Stable suppression of gene expression by RNAi in mammalian cells. *Proc Natl Acad Sci* 2002; **99**: 1443–1448.

114 Paul CP, Good PD, Winer I, Engelke DR. Effective expression of small interfering RNA in human cells. *Nat Biotechnol* 2002; **20**: 505–508.

115 Carleton HA, Lara-Tejero M, Liu X, Galán JE. Engineering the type III secretion system in non-replicating bacterial minicells for antigen delivery. *Nat Commun* 2013; **4**: 1590.

116 Xiang S, Fruehauf J, Li CJ. Short hairpin RNA–expressing bacteria elicit RNA interference in mammals. *Nat Biotechnol* 2006; **24**: 697–702.

117 Du J, Jin J, Yan M, Lu Y. Synthetic Nanocarriers for Intracellular Protein Delivery. *Curr Drug Metab* 2012; **13**: 82–92.

118 Malmsten M. Inorganic nanomaterials as delivery systems for proteins, peptides, DNA, and siRNA. *Curr Opin Colloid Interface Sci* 2013; **18**: 468–480.

119 Hong CA, Nam YS. Functional Nanostructures for Effective Delivery of Small Interfering RNA Therapeutics. *Theranostics* 2014; **4**: 1211–1232.

120 Lytton-Jean AKR, Langer R, Anderson DG. Five Years of siRNA Delivery: Spotlight on Gold Nanoparticles. *Small* 2011; **7**: 1932–1937.

121 Johnson BB, Heuck AP. Perfringolysin O Structure and Mechanism of Pore Formation as a Paradigm for Cholesterol-Dependent Cytolysins. In: Anderluh G, Gilbert R (eds). *MACPF/CDC Proteins - Agents of Defence, Attack and Invasion*. Springer Netherlands, 2014, pp 63–81.

122 Rossjohn J, Polekhina G, Feil SC, Morton CJ, Tweten RK, Parker MW. Structures of Perfringolysin O Suggest a Pathway for Activation of Cholesterol-dependent Cytolysins. *J Mol Biol* 2007; **367**: 1227–1236.

123 Solovyova AS, Nollmann M, Mitchell TJ, Byron O. The Solution Structure and Oligomerization Behavior of Two Bacterial Toxins: Pneumolysin and Perfringolysin O. *Biophys J* 2004; **87**: 540–552.

124 Giddings KS, Zhao J, Sims PJ, Tweten RK. Human CD59 is a receptor for the cholesterol-dependent cytolysin intermedilysin. *Nat Struct Mol Biol* 2004; **11**: 1173–1178.

125 Shimada Y, Maruya M, Iwashita S, Ohno-Iwashita Y. The C-terminal domain of perfringolysin O is an essential cholesterol-binding unit targeting to cholesterol-rich microdomains. *Eur J Biochem* 2002; **269**: 6195–6203.

126 Farrand AJ, LaChapelle S, Hotze EM, Johnson AE, Tweten RK. Only two amino acids are essential for cytolytic toxin recognition of cholesterol at the membrane surface. *Proc Natl Acad Sci* 2010; **107**: 4341–4346.

127 Dowd KJ, Tweten RK. The Cholesterol-Dependent Cytolysin Signature Motif: A Critical Element in the Allosteric Pathway that Couples Membrane Binding to Pore Assembly. *PLoS Pathog* 2012; **8**. doi:10.1371/journal.ppat.1002787.

128 Ramachandran R, Tweten RK, Johnson AE. Membrane-dependent conformational changes initiate cholesterol-dependent cytolysin oligomerization and intersubunit β-strand alignment. *Nat Struct Mol Biol* 2004; **11**: 697–705.

129 Shatursky O, Heuck AP, Shepard LA, Rossjohn J, Parker MW, Johnson AE *et al.* The Mechanism of Membrane Insertion for a Cholesterol-Dependent Cytolysin: A Novel Paradigm for Pore-Forming Toxins. *Cell* 1999; **99**: 293–299.

130 Gonzalez MR, Bischofberger M, Pernot L, van der Goot FG, Frêche B. Bacterial pore-forming toxins: The (w)hole story? *Cell Mol Life Sci* 2008; **65**: 493–507.

131 Law RHP, Lukoyanova N, Voskoboinik I, Caradoc-Davies TT, Baran K, Dunstone MA *et al.* The structural basis for membrane binding and pore formation by lymphocyte perforin. *Nature* 2010; **468**: 447–451.

132 Provoda CJ, Lee K-D. Bacterial pore-forming hemolysins and their use in the cytosolic delivery of macromolecules. *Adv Drug Deliv Rev* 2000; **41**: 209–221.

133 Gottschalk S, Tweten RK, Smith LC, Woo SL. Efficient gene delivery and expression in mammalian cells using DNA coupled with perfringolysin O. *Gene Ther* 1995; **2**: 498–503.

134 El B, Fa G, Pa F. Introduction of antisense oligonucleotides into cells by permeabilization with streptolysin O. *BioTechniques* 1993; **15**: 1016–8, 1020.

135 Brito JLR, Davies FE, Gonzalez D, Morgan GJ. Streptolysin-O reversible permeabilisation is an effective method to transfect siRNAs into myeloma cells. *J Immunol Methods* 2008; **333**: 147–155.

136 Kerr DE, Wu GY, Wu CH, Senter PD. Listeriolysin O Potentiates Immunotoxin and Bleomycin Cytotoxicity. *Bioconjug Chem* 1997; **8**: 781–784.

137 Walev I, Bhakdi SC, Hofmann F, Djonder N, Valeva A, Aktories K *et al.* Delivery of proteins into living cells by reversible membrane permeabilization with streptolysin-O. *Proc Natl Acad Sci* 2001; **98**: 3185–3190.

138 Liu DV, Yang NJ, Wittrup KD. A Nonpolycationic Fully Proteinaceous Multiagent System for Potent Targeted Delivery of siRNA. *Mol Ther — Nucleic Acids* 2014; **3**: e162.

139 Csorba T, Kontra L, Burgyán J. viral silencing suppressors: Tools forged to fine-tune host-pathogen coexistence. *Virology* 2015; **479–480**: 85–103.

140 Danielson DC, Pezacki JP. Studying the RNA silencing pathway with the p19 protein. *FEBS Lett* 2013; **587**: 1198–1205.

141 Ye K, Malinina L, Patel DJ. Recognition of small interfering RNA by a viral suppressor of RNA silencing. *Nature* 2003; **426**: 874–878.

142 Vargason JM, Szittya G, Burgyán J, Hall TMT. Size Selective Recognition of siRNA by an RNA Silencing Suppressor. *Cell* 2003; **115**: 799–811.

143 Cheng J, Danielson DC, Nasheri N, Singaravelu R, Pezacki JP. Enhanced Specificity of the Viral Suppressor of RNA Silencing Protein p19 toward Sequestering of Human MicroRNA-122. *Biochemistry (Mosc)* 2011; **50**: 7745–7755.

144 Rawlings RA, Krishnan V, Walter NG. Viral RNAi Suppressor Reversibly Binds siRNA to Outcompete Dicer and RISC via Multiple Turnover. *J Mol Biol* 2011; **408**: 262–276.

145 Cheng J, Sagan SM, Jakubek ZJ, Pezacki JP. Studies of the Interaction of the Viral Suppressor of RNA Silencing Protein p19 with Small RNAs Using Fluorescence Polarization†. *Biochemistry (Mosc)* 2008; **47**: 8130–8138.

146 Cheng J, Koukiekolo R, Kieliszkiewicz K, Sagan SM, Pezacki JP. Cysteine residues of Carnation Italian Ringspot virus p19 suppressor of RNA silencing maintain global structural integrity and stability for siRNA binding. *Biochim Biophys Acta BBA - Proteins Proteomics* 2009; **1794**: 1197–1203.

147 Cheng J, Sagan SM, Assem N, Koukiekolo R, Goto NK, Pezacki JP. Stabilized recombinant suppressors of RNA silencing: Functional effects of linking monomers of Carnation Italian Ringspot virus p19. *Biochim Biophys Acta BBA - Proteins Proteomics* 2007; **1774**: 1528–1535.

148 Koukiekolo R, Sagan SM, Pezacki JP. Effects of pH and salt concentration on the siRNA binding activity of the RNA silencing suppressor protein p19. *FEBS Lett* 2007; **581**: 3051–3056.

149 Khan N, Cheng J, Pezacki JP, Berezovski MV. Quantitative Analysis of MicroRNA in Blood Serum with Protein-Facilitated Affinity Capillary Electrophoresis. *Anal Chem* 2011; **83**: 6196–6201.

150 Labib M, Khan N, Ghobadloo SM, Cheng J, Pezacki JP, Berezovski MV. Three-Mode Electrochemical Sensing of Ultralow MicroRNA Levels. *J Am Chem Soc* 2013; **135**: 3027–3038.

151 Hong C-Y, Chen X, Li J, Chen J-H, Chen G, Yang H-H. Direct detection of circulating microRNAs in serum of cancer patients by coupling protein-facilitated specific enrichment and rolling circle amplification. *Chem Commun* 2014; **50**: 3292–3295.

152 Kilic T, Nur Topkaya S, Ozsoz M. A new insight into electrochemical microRNA detection: A molecular caliper, p19 protein. *Biosens Bioelectron* 2013; **48**: 165–171.

153 Nasheri N, Cheng J, Singaravelu R, Wu P, McDermott MT, Pezacki JP. An enzyme-linked assay for the rapid quantification of microRNAs based on the viral suppressor of RNA silencing protein p19. *Anal Biochem* 2011; **412**: 165–172.

154 Torrente-Rodríguez RM, Campuzano S, López-Hernández E, Montiel VR-V, Barderas R, Granados R *et al.* Simultaneous detection of two breast cancer-related miRNAs in tumor tissues using p19-based disposable amperometric magnetobiosensing platforms. *Biosens Bioelectron* 2015; **66**: 385–391.

155 Ramnani P, Gao Y, Ozsoz M, Mulchandani A. Electronic Detection of MicroRNA at Attomolar Level with High Specificity. *Anal Chem* 2013; **85**: 8061–8064.

156 Wanunu M, Dadosh T, Ray V, Jin J, McReynolds L, Drndić M. Rapid electronic detection of probe-specific microRNAs using thin nanopore sensors. *Nat Nanotechnol* 2010; **5**: 807–814.

157 He Y-C, Yin B-C, Jiang L, Ye B-C. The rapid detection of microRNA based on p19-enhanced fluorescence polarization. *Chem Commun* 2014; **50**: 6236–6239.

158 Jin J, Cid M, Poole C, McReynolds L. Protein mediated miRNA detection and siRNA enrichment using p19. *BioTechniques* 2010; **48**: xvii–xxiii.

159 Calabrese JM, Sharp PA. Characterization of the short RNAs bound by the P19 suppressor of RNA silencing in mouse embryonic stem cells. *RNA* 2006; **12**: 2092–2102.

160 van den Beek M, Antoniewski C, Carré C. Isolation of small interfering RNAs using viral suppressors of RNA interference. *Methods Mol Biol Clifton NJ* 2014; **1173**: 147–155.

161 Jin J, McReynolds LA, Gullerova M. p19-mediated enrichment and detection of siRNAs. *Methods Mol Biol Clifton NJ* 2014; **1173**: 99–111.

162 Lakatos L, Szittya G, Silhavy D, Burgyán J. Molecular mechanism of RNA silencing suppression mediated by p19 protein of tombusviruses. *EMBO J* 2004; **23**: 876–884.

163 Voinnet O, Rivas S, Mestre P, Baulcombe D. An enhanced transient expression system in plants based on suppression of gene silencing by the p19 protein of tomato bushy stunt virus. *Plant J* 2003; **33**: 949–956.

164 Garabagi F, Gilbert E, Loos A, McLean MD, Hall JC. Utility of the P19 suppressor of gene-silencing protein for production of therapeutic antibodies in Nicotiana expression hosts. *Plant Biotechnol J* 2012; **10**: 1118–1128.

165 Gao S-J, Damaj MB, Park J-W, Beyene G, Buenrostro-Nava MT, Molina J *et al.* Enhanced Transgene Expression in Sugarcane by Co-Expression of Virus-Encoded RNA Silencing Suppressors. *PLoS ONE* 2013; **8**: e66046.

166 Rauschhuber C, Mueck-Haeusl M, Zhang W, Nettelbeck DM, Ehrhardt A. RNAi suppressor P19 can be broadly exploited for enhanced adenovirus replication and microRNA knockdown experiments. *Sci Rep* 2013; **3**. doi:10.1038/srep01363.

167 Huang L, Lieberman J. Production of highly potent recombinant siRNAs in Escherichia coli. *Nat Protoc* 2013; **8**: 2325–2336.

168 Thurber GM, Schmidt MM, Wittrup KD. Antibody tumor penetration: Transport opposed by systemic and antigen-mediated clearance. *Adv Drug Deliv Rev* 2008; **60**: 1421–1434.

169 Bevilacqua PC, Cech TR. Minor-Groove Recognition of Double-Stranded RNA by the Double-Stranded RNA-Binding Domain from the RNA-Activated Protein Kinase PKR. *Biochemistry (Mosc)* 1996; **35**: 9983–9994.

170 Boswell CA, Tesar DB, Mukhyala K, Theil F-P, Fielder PJ, Khawli LA. Effects of Charge on Antibody Tissue Distribution and Pharmacokinetics. *Bioconjug Chem* 2010; **21**: 2153–2163.

171 Niesner U, Halin C, Lozzi L, Günthert M, Neri P, Wunderli-Allenspach H *et al.* Quantitation of the Tumor-Targeting Properties of Antibody Fragments Conjugated to Cell-Permeating HIV-1 TAT Peptides. *Bioconjug Chem* 2002; **13**: 729–736.

172 Lee HJ, Pardridge WM. Pharmacokinetics and Delivery of Tat and Tat-Protein Conjugates to Tissues in Vivo. *Bioconjug Chem* 2001; **12**: 995–999.

173 Ucci JW, Kobayashi Y, Choi G, Alexandrescu AT, Cole JL. Mechanism of Interaction of the Double-Stranded RNA (dsRNA) Binding Domain of Protein Kinase R with Short dsRNA Sequences†. *Biochemistry (Mosc)* 2007; **46**: 55–65.

Chapter 2. Antibody-Mediated Neutralization of Perfringolysin O for Intracellular Protein Delivery

Introduction

The ability to safely and efficiently deliver exogenous proteins to the cytoplasm of target cells is highly desired to enable potential therapeutic interventions. While much progress has been made in the development of delivery systems, as discussed in Chapter 1, their practical implementation remains a significant challenge[1].

Members of the cholesterol-dependent cytolysin (CDC) family of bacterial pore-forming toxins have previously been demonstrated to deliver a wide range of payloads to both established and primary cell types[2], but their widespread use as a delivery system has been limited by their cytotoxicity. Early studies showed that CDCs such as Streptolysin O (SLO), Perfringolysin O (PFO) and Listeriolysin O (LLO) can be used as versatile transfection regents to introduce various membrane-impermeable payloads into cells, including plasmid DNA[3], antisense oligonucleotides[4], siRNA[5], glycopeptides (bleomycin)[6], and various proteins[7]. However, the cytotoxicity of the CDCs often required them to be removed after a brief incubation to avoid cell killing[8,9]. Because such manipulations are not possible in an in vivo setting, alternative delivery methods are needed.

Among those proposed are encapsulating or conjugating LLO into or onto liposomes, which are modified with targeting antibodies in some cases, to shield or inactivate the protein until they are internalized into target cells[10,11]. Although the specificity of delivery were greatly increased when using these approaches in in vitro models, such nanoparticulate formulations often suffer from poor pharmacokinetics and biodistribution, accumulating in the reticuloendothelial system[12] to cause dose-limiting toxicity. Indeed, in vivo demonstrations of LLO-encapsulating liposomes have been limited to vaccination applications targeting phagocytic cells[13,14]. Alternatively, to allow specific targeting of CDCs with favorable biodistribution properties, we previously generated targeted LLO and PFO constructs fused to binding moieties against cancer antigens. While the targeted constructs delivered macromolecular payloads such as the ribosome-inactivating toxin gelonin[15] and siRNA[16] to antigen-positive cells more efficiently than their untargeted counterparts, they remained equally toxic.

In this study, we report a novel, non-particulate engineering strategy that widens the therapeutic

This chapter was reproduced in part with permission from Yang et al. *Mol. Pharmaceutics*, **2015**, *12* (6), pp 1992–2000. Copyright © 2015 American Chemical Society.

window of PFO by greater than five orders of magnitude, substantially improving its potential translatability. The guiding principle of this engineering strategy, first attempted by Lee et al. with liposomal delivery[2], is to direct pore formation to preferentially occur in endosomal compartments rather than on the plasma membrane, to eliminate the deleterious toxicities associated with breaching the latter while efficiently releasing co-endocytosed payloads to the cytoplasm. To such ends, we created a bi-specific neutralizing antibody capable of binding to PFO, inhibiting its pore-forming activity in the extracellular space, and the cancer-associated antigen EGFR, promoting receptor-mediated internalization in target cells. In vitro, complexed with an attenuated PFO mutant, this antibody-PFO system delivered the payload gelonin with comparable efficacy to the previously reported targeted PFO construct, while achieving unprecedented low levels of cytotoxicity. Antibody-mediated internalization of PFO was necessary for efficient delivery, supporting the model of endosomal release.

Our findings support the exploration of CDCs as a versatile, safe and effective delivery vehicle that can enhance the intracellular access of exogenous proteins. Furthermore, we demonstrate the concept of antibody-mediated neutralization as a novel strategy to control the activity of potent membrane-disrupting agents. This approach can potentially be extended to other pore-forming proteins including human perforin, further advancing the practical implementation of a highly efficient, pore-forming protein-based intracellular delivery system.

Results

Engineering of PFO binder for reversible neutralization. PFO is capable of forming pores very efficiently, but its activity is not readily tunable in a rational manner due to its mechanism of action requiring multiple intermolecular interactions and conformational change[17]. Yeast surface display, a well-established technique for directed evolution, was not applicable to engineer PFO directly because the protein was too toxic to express in yeast (data not shown). In contrast, yeast surface display techniques can be applied in a straightforward manner to obtain proteins that bind to PFO and alter its function (**Figure 2.1A**) in a similar manner to certain neutralizing antibodies[18,19].

To isolate neutralizing binders against PFO, we first sorted through yeast libraries previously developed from the fibronectin scaffold[20] to obtain a collection of distinct binders. The 10th type III domain of fibronectin (Fn3) is a stable, cysteine-free scaffold that has been shown to effectively mediate molecular recognition[21], and to be readily expressed as a genetic fusion with other proteins of interest. The Fn3 libraries were subject to multiple rounds of mutagenesis via error-prone PCR and enriched for binders via magnetic bead selection and fluorescence activated cell sorting (FACS). Selections were

performed using PFO of which the cysteine at position 459 was mutated to an alanine[22] to prevent crosslinking. This PFO^{C459A} mutant is herein referred to as "PFO." 18 individual clones from the resulting library could be grouped into six distinct families based on sequence similarity, suggesting that binders were isolated against multiple epitopes on PFO.

To investigate whether any of these PFO binders interacted with functionally important epitopes, representative members from each group were expressed as soluble proteins and analyzed for their ability to inhibit the hemolytic activity of PFO. The Fn3 clones were pre-incubated with PFO at saturating concentrations, and maintained at such after red blood cells were added. Among the binders tested, clone 1.1 (**Figure 2.1C**) had an equilibrium dissociation constant (K_D) of 13.5 ± 2.9 nM as measured by yeast-surface titrations (**Figure 2.1B**), and displayed the greatest degree of functional inhibition by reducing the EC_{50} of hemolysis by approximately 3-fold (from 0.24 ± 0.02nM in the absence of 1.1, to 0.74 ± 0.23nM in the presence of 1.1) (**Figure 2.1D**).

We further matured the affinity of clone 1.1 via additional rounds of mutagenesis and FACS to obtain clone 1.2 (**Figure 2.1C**) with a K_D of 0.53 ± 0.26 nM (**Figure 2.1B**). 1.2 inhibited the hemolytic activity of PFO by approximately 11-fold to an EC_{50} of 2.7 ± 0.21nM (**Figure 2.1D**). Interestingly, increasing the affinity of the PFO binder increased the degree of inhibition even at saturating concentrations. This observation suggests that the binding interaction between the Fn3 and PFO, the duration of which is prolonged by a reduced off-rate in the higher-affinity binder, prevents hemolysis. Furthermore, it suggests that the reversible binding interaction between the Fn3 and PFO can allow pores to form over time as PFO dissociates from the binder and becomes sequestered on the cell membrane before rebinding to 1.2. Both 1.1 and 1.2 were engineered to bind tighter to PFO at pH 7.4 compared to pH 5.5 (**Figure 2.1B**), reducing the degree of inhibition at endosomal pH (**Figure 2.1D**).

To better understand the molecular basis of how clone 1.2 is inhibiting the activity of PFO, we measured how well this Fn3 bound to known PFO mutants. Previously, it has been proposed that residues T490 and L491 of PFO are involved in binding to cholesterol [23], the natural cell-surface receptor of PFO, whereas residues Y181 and F318 provide stacking interactions between neighboring monomers to stabilize the oligomeric complex [24]. Thus 1.2 was displayed on the surface of yeast and incubated with fluorescently labeled PFO clones harboring point mutations in the aforementioned residues.

1.2 bound significantly weaker to PFO^{Y181A} compared to PFO (**Figure 2.1E**), suggesting it may prevent the formation or subsequent stabilization of the oligomeric complex by sterically occluding the PFO stacking surface. PFO^{Y181A} was previously shown to retain the ability to bind and oligomerize on liposomal membranes [25], indicating that it was unlikely the observed loss of binding was due to gross misfolding of the mutant. Mutants of F318 were not tested because this residue is not surface-exposed in the soluble monomer. There was no difference in 1.2 binding to PFO and $PFO^{T490G,L491G}$, suggesting that

the epitope of 1.2 is physically distinct and separated in distance from the membrane-binding region of PFO.

Engineering of a bi-specific neutralizing antibody for specific targeting of PFO. Next, to target the reversibly attenuated PFOs to endosomal compartments, we genetically fused 1.2 to Cetuximab (C225), a monoclonal antibody against EGFR (**Figure 2.2A**). C225 was chosen as the antibody backbone because EGFR has been reported to be constitutively internalized with a half-time of approximately 30 minutes, followed by multiple rounds of recycling and internalization[26], and thus compatible with our engineering strategy to promote pore formation in endocytic vesicles. Furthermore, EGFR is therapeutically relevant due to its overexpression in various cancer types. The N terminus of C225's heavy chain was chosen as the site of fusion because the resulting bi-specific antibody had superior yields compared to other fusion topologies (data not shown). 1.2 was linked to C225 by a flexible $(Gly_4Ser)_2$ linker to allow modular binding to PFO without interfering with C225's interaction with EGFR.

To reduce the presence of uncomplexed proteins that can obscure downstream analysis, we developed a hydrophobic interaction chromatography (HIC)-based purification strategy to obtain C225.2/PFO complexes with high monodispersity. In the purified complex, the molar ratio of PFO and C225.2 was consistently close to 2 (PFO : C225.2 = 2.2 ± 0.2 : 1, from 20 separate preparations), as analyzed by fluorescence densitometry following SDS-PAGE (**Figure 2.2B**). In addition, 89% of the complex fit to a single peak as analyzed by sedimentation velocity (SV) analytical ultracentrifugation (AUC) (**Figure 2.2C**), illustrating that the complex was highly monodisperse.

Next, we confirmed that the 1.2 portion of C225.2 maintained its ability to bind to and inhibit the hemolytic activity of PFO. Indeed, PFO was 31-fold less active when complexed to C225.2, with an EC_{50} of hemolysis of 7.57 ± 0.37nM (**Figure 2.2D**). To confirm that C225.2 maintained its ability to engage EGFR and improve the targeting specificity of PFO, fluorescently labeled PFO was complexed with C225.2 or a control bi-specific antibody (sm3e.2) where 1.2 was fused to an antibody against the carcinoembryonic antigen (CEA) (sm3e) in the same topology as in C225.2. A431 cells express undetectable levels of surface CEA, making sm3e.2 a suitable negative control. Binding was measured on the A431 cell line, which expresses high levels of EGFR and is thus widely used as a model system to study EGFR-based therapeutics[27]. The CHO-K1 cell line, which does not express human EGFR (C225 is not cross-reactive with murine EGFR) served as an antigen-negative control. All binding measurements were performed at 4°C to prevent cell lysis, as the activity of PFO is significantly attenuated at the lower temperature (data not shown)

Free PFO bound with moderate affinity to both cell lines as expected, due to its interaction with membrane cholesterol, which is ubiquitous (**Figure 2.3B**). Interestingly, binding was detectable only at

concentrations much higher than those required for cell lysis (**Figure 2.1D**), highlighting that only a few pores can potently influence membrane barrier properties. sm3e.2 prevented PFO from binding to both cell lines, likely due to steric hindrance provided by the bulky antibody framework. In contrast, C225.2/PFO bound only to A431s in a specific manner, as the signal was abrogated with excess C225.

Next, based on our previous observations which suggested that (a) PFO, after dissociating from C225.2, may associate with either C225.2 or the cell membrane with competing kinetics, and that (b) free PFO is capable of binding to membrane cholesterol and lysing cells with high efficiency, we reasoned that decreasing the affinity of PFO towards the membrane will favor its rebinding to C225.2 and endocytosis. Based on previous reports which demonstrated that this affinity can be fine-tuned via mutagenesis of residues T490 and L491[23], we employed the mutant $PFO^{T490A,L491V}$, which showed no detectable binding to either cell lines by itself in the concentration range tested (**Figure 2.3C**). $PFO^{T490A,L491V}$ was less hemolytically active than PFO as expected (**Figure 2.3A**), based on its attenuated ability to anchor onto the cell membrane. However, we anticipated that this attenuation would not significantly affect the performance of C225.2/PFO as a delivery system as even a few pores may potently permeablize the membrane barrier, and the complex may reach high local concentrations in endocytic compartments following clathrin-mediated concentration and endocytosis of the receptors. As 1.2 does not interact with the residues T490 and L491 (**Figure 2.1E**), $PFO^{T490A,L491V}$ could be complexed with C225.2 and purified to monodispersity in a manner identical to PFO. As expected, the resulting C225.2/$PFO^{T490A,L491V}$ complex bound specifically to A431s, but not CHO-K1s (**Figure 2.3C**).

Specific and efficient intracellular delivery enabled by the C225.2/PFO system. To determine whether the neutralized and endosomally targeted C225.2/PFO system retained PFO's ability to deliver exogenous payloads, we analyzed its dose-dependent cytotoxicity and efficacy in vitro. The efficacy of delivery was assessed with the payload E6rGel, an EGFR-targeted gelonin construct developed previously[28]. As a type I ribosome-inactivating protein (RIP) that lacks its own membrane translocation domain, gelonin is modestly cytotoxic as a single agent but can potently kill cells when artificially introduced into the cytoplasm, as demonstrated by prior studies[29,30]. In addition, the targeting moiety, E6, a binder against EGFR engineered on the Fn3 scaffold, does not to compete with C225 for binding[31], allowing C225.2/PFO and E6rGel to engage the same receptor molecule. This setup enabled maximal overlap of C225.2/PFO and E6rGel in endosomal compartments, the intended site of release, following EGFR-mediated internalization.

The concentration of E6rGel was fixed at a value (10nM) above the K_D of E6 (0.26nM[31]) to saturate the available receptors. E6rGel by itself caused no cell death under these conditions (**Figure 2.4A**). Consequently, any synergistic cell killing between PFO and E6rGel could be attributed to PFO

enhancing gelonin's access to the cytoplasm (in the absence of cell killing caused by PFO itself). Minimal synergy was observed when PFO was combined with E6rGel in either cell line, highlighting how the intrinsic cytotoxicity of PFO can cause cell death before sufficient quantities of E6rGel can be delivered (**Figure 2.4C**). Similarly, the targeted PFO construct reported previously[16], where PFO is fused to an Fn3 that binds to EGFR, increased E6rGel-mediated cell killing in A431 cells but remained severely cytotoxic to both cell lines (**Figure 2.4B**). In contrast, C225.2/PFO and C225.2/PFO^{T490A,L491V} markedly synergized with E6rGel only in A431s, but not CHO-K1s, consistent with our model where PFO mediates the release of gelonin from endocytic compartments following EGFR-mediated internalization (**Figure 2.4C**). Notably, in A431s, C225.2/PFO^{T490A,L491V} efficiently delivered E6rGel at low (pM) concentrations while being completely inert by itself in the concentration range tested (up to 3μM), creating a therapeutic window spanning greater than five orders of magnitude. Furthermore, equivalent delivery was observed in CHO-K1 cells only at very high (μM) concentrations. Overall, the C225.2/PFO^{T490A,L491V} system was a significant improvement over the starting PFO clone, in terms of the safety, efficacy and specificity of delivery.

To confirm that the observed cell killing was indeed caused by E6rGel in the cytoplasm, we measured protein synthesis levels in A431s following treatment with C225.2/PFO^{T490A,L491V} and E6rGel (**Figure 2.5A**). A significant reduction was observed only when wild-type gelonin (E6rGel^{wt}), but not its enzymatically inactive counterpart (E6rGel$^{mut\ 32}$) was used, demonstrating that gelonin in the cytoplasm cleaved the corresponding ribosomes via its catalytic residues. Cell viability judged by gross cell morphology was not significantly affected during the incubation period (data not shown), and thus the observed reduction in protein synthesis was not a result of fewer cells being analyzed. Protein synthesis was unaffected when cells were treated with C225.2/PFO^{T490A,L491V} or E6rGel alone (**Figure 2.5A**).

To gain a deeper understanding of the delivery mechanism, we further probed the role of EGFR-mediated endocytosis in the C225.2/PFO^{T490A,L491V} system. First, we repeated the translation inhibition assay in the presence of excess C225 to block the specific binding interaction between C225.2 and EGFR. C225 completely abolished the reduction in protein synthesis (**Figure 2.5B**), illustrating that this binding interaction is necessary to enable intracellular delivery. Furthermore, decreasing the rate of EGFR-mediated internalization using the clathrin inhibitor Pitstop 2 significantly increased protein synthesis, indicating that clathrin-mediated endocytosis is required for efficient delivery (**Figure 2.5C**). Protein synthesis did not return to basal levels, however, which may be due to incomplete inhibition of endocytosis by Pitstop 2, or residual delivery of gelonin across the cell membrane in addition to its endosomal release. Pitstop 2 did not affect the translational inhibition produced by the analogous but endocytosis-independent system composed of untargeted PFO^{T490A,L491V} and untargeted gelonin (**Figure 2.5C**), confirming that it does not influence the gelonin-mediated inactivation of ribosomes. Eliminating

the EGFR-targeting Fn3 moiety (E6) of E6rGel also caused a significant increase in protein synthesis (**Figure 2.5C**). Collectively, these results support the model in which C225.2/PFO^{T490A,L491V} and E6rGel bind to and internalize with EGFR via clathrin-mediated endocytosis, followed by PFO^{T490A,L491V} mediating gelonin's release from endocytic compartments.

Discussion

In this study, we have described the development of a novel PFO-based intracellular delivery system, which successfully increased the therapeutic window of PFO from being negligible to spanning greater than five orders of magnitude in vitro. Specifically, we engineered a bi-specific, neutralizing antibody composed of an inhibitory binder against PFO and a monoclonal antibody against an internalizing antigen, to deliver reversibly inhibited PFO to endosomal compartments. This system allows pore formation in endocytic vesicles and blocks such on the cell membrane, greatly reducing the cytotoxicity associated with PFO while allowing the efficient release of co-targeted macromolecular payloads into the cytoplasm.

The delivery system described herein is highly modular, and can be expanded to alternative antigens, pore-forming proteins and payloads. First, as the PFO binder can be fused with other antibody frameworks using standard molecular biology techniques, bi-specific antibodies analogous to C225.2 can be created for other antibody-antigen pairs. Of note, while we have investigated a system in which PFO and the payload were targeted to the same internalizing receptor, previous work has demonstrated that the two agents can also be targeted to distinct receptors that colocalize in endosomal compartments [15]. Second, the antibody-based neutralization strategy is compatible with other pore-forming proteins, particularly with those for which neutralizing antibodies have already been obtained [33–35]. The neutralizing antibody, converted to a single-chain variable fragment (scFv), is functionally analogous to the inhibitory PFO binder reported in our study. Perforin, which has been shown to possess remarkable structural similarities to CDCs [36], is of particular interest as it can potentially circumvent immunogenicity concerns that rise when considering bacterial proteins for therapeutic applications. Lastly, we anticipate this delivery system to be seamlessly compatible with non-proteinaceous payloads in addition to proteins, as demonstrated with unmodified CDCs.

The exact mechanism of how PFO was preferentially activated in endosomal compartments in this system remains to be elucidated, although several explanations can be proposed. First, 1.2 bound weaker to PFO at pH 5.5 compared to pH 7.4 (**Supplementary Figure 2**), producing a modest but consistent increase in PFO's hemolytic activity (by 4-fold) at the lower pH (**Supplementary Figure 3**).

Given the potent membrane-permeablizing ability of PFO pores, moderate differences in hemolytic activity may result in amplified differences in biological activity. Second, the superior stability of PFO over C225.2 may have led to preferential unfolding and degradation of C225.2 in maturing endosomes and lysosomes, releasing PFO from inhibition. Third, following the internalization of C225.2/PFO into endocytic compartments, the reversible binding interaction between the two components may have been simply competed off over time by the irreversible process of pore formation. Finally, any combination of the aforementioned possibilities could have collectively activated PFO in endocytic vesicles. Incorporating additional responsive elements for finer control of pore-forming activity before and after endocytosis is a subject of future studies.

The C225.2/PFO system described in this study involves multiple kinetic processes, including the internalization and recycling of EGFR, the association and dissociation between multiple components (C225.2 and EGFR, C225.2 and PFO, and PFO and the lipid membrane), the gradual maturation of endosomes into lysosomes and subsequent degradation of proteins, and the uptake and release of payloads into and out of such intracellular vesicles. Thus, quantitative modeling of the system can be beneficial for better understanding the relative importance of each kinetic process and refining the system for in vivo delivery. For example, in an in vivo setting, prolonged circulation of C225.2/PFO in the blood compartment prior to reaching the target site is expected to greatly reduce the probability of dissociated PFO rebinding to C225.2, particularly in the presence of active clearance mechanisms such as renal filtration and reticuloendothelial uptake.

In addition, as a two-component system where the payload (E6rGel) is physically separate from the agent mediating endosomal release (C225.2/PFO), the present system is expected to have unique advantages and disadvantages as a delivery strategy in vivo. Notably, as the two agents are expected to have differing clearance and tumor accumulation kinetics, their dosing scheme will require empirical optimization to achieve maximal co-localization in target cells. Prior work demonstrating proof-of-concept that non-neutralized PFO, *in trans*, can potentiate the cytotoxicity of gelonin in a xenograft tumor model [15], supports the feasibility of co-localizing two agents in vivo. In addition, the minimal toxicity of C225.2/PFO and E6rGel towards bystander cells is expected to allow high dosages to be administered, driving the accumulation of both agents to working concentrations in the tumor interstitium. Of note, separating the payload from PFO may provide additional benefits: First, such a *trans* administration strategy preserves the modularity of the system, as it allows E6rGel to be substituted with other payloads without further adjusting the C225.2/PFO component. Second, physically separating the two agents may further improve the specificity of targeting by decreasing the likelihood of bystander cells receiving both agents simultaneously. Individually, C225.2/PFO and E6rGel are inert within the concentration ranges we have tested.

Overall, the current study provides strong evidence that the activity of pore-forming proteins can be successfully controlled via neutralizing binders, antibody-mediated targeting and mutagenesis approaches to allow the safe and specific delivery of macromolecular payloads to the cytosolic space. As EGFR is already a validated cancer antigen and C225 a validated therapeutic antibody, considerable therapeutic opportunities exist in combining C225-mediated antibody therapy with C225.2/PFO-mediated delivery of various macromolecular drugs for synergistic treatment.

Materials and Methods

Cell lines. The A431 and CHO-K1 cell lines (ATCC, Manassas, VA) were cultured in DMEM and F-12K medium (ATCC, Manassas, VA), respectively, supplemented with 10% heat-inactivated FBS (Life Technologies, Grand Island, NY). HEK 293F cells were cultured in suspension in FreeStyle 293 expression medium (Life Technologies, Grand Island, NY). All cell lines were maintained at 37°C and 5% CO_2 in a humidified incubator.

Protein expression and purification. Fn3, E6rGel and PFO variants were expressed from the pE-SUMO vector (LifeSensors, Malvern, PA) in Rosetta 2 (DE3) *E. coli* (Novagen, San Diego, CA). Point mutations in PFO and E6rGel (C459A/T490A/L491V and Y74A/Y133A/E166K/R169Q, respectively) were introduced by QuikChange site-directed mutagenesis (Agilent, Santa Clara, CA). Briefly, bacterial cultures were grown to OD_{600} = 2 in terrific broth (TB) and induced with 1mM IPTG at 20°C overnight. The proteins of interest were purified from sonicated pellets using Talon metal affinity chromatography (Clontech, Mountain View, CA) per manufacturer's protocol. Following an overnight digestion with SUMO protease at 4°C overnight, cleaved SUMO and SUMO protease were removed by Talon metal affinity chromatography. C225.2 was expressed and purified from HEK 293F cells as previously described [37]. All proteins were subjected to endotoxin removal as described below and stored in PBS.

Endotoxin removal. The protein of interest was exchanged into a 20mM buffer suitable for anion-exchange chromatography at a pH 1 unit below its isoelectric point, with 150mM NaCl in addition. The isoelectric points were calculated using Geneious software (Biomatters, Auckland, New Zealand). The flow-through was collected after repeated passages through a 5mL HiTrap Q HP anion exchange column (GE Healthcare, Pittsburgh, PA) and endotoxin levels were measured using the QCL-1000 LAL assay following manufacturer's instructions (Lonza, Basel, Switzerland).

Purification of C225.2/PFO complexes. PFO mutants were pre-complexed with C225.2 at a molar ratio of 1:1.25 (PFO:C225.2) with C225.2 (and corresponding PFO binding sites) in excess to ensure complete capture of PFO. The mixture was incubated at 4°C for 30min, diluted 5-fold into running buffer (50mM sodium phosphate, 100mM ammonium sulfate, pH 7.4), and purified using a 1mL HiTrap Butyl HP column (GE Healthcare, Pittsburgh, PA) to separate unbound C225.2 captured on the column from the C225.2/PFO complexes present in the flow-through. Purified complexes were analyzed by SDS-PAGE stained with Sypro Orange (Life Technologies, Grand Island, NY) and imaged on the Typhoon Trio imager (GE Healthcare, Pittsburgh, PA). The concentration of C225.2 and PFO were determined by densitometry using a standard curve generated with known amounts of PFO.

Sedimentation Velocity Analytical Ultracentrifugation. Velocity AUC of the C225.2/PFO^{C215A} complex was performed in a Beckman XL-I Analytical Ultracentrifuge (Beckman Coulter, Fullerton, CA) using an An-60 Ti rotor at 42,000 rpm and 4°C. The proteins were at AU = 0.2 in PBS. Data were collected at radial steps of 0.003cm and analyzed with Sedfit using the c(s) method [38].

Isolation of inhibitory binders against PFO. Binders to PFO based on the fibronectin scaffold (Fn3) were engineered using standard yeast surface display techniques as previously described [39], with modified selection schemes to identify inhibitory clones. A pooled combination of the YS, G2 and G4 Fn3 libraries previously developed [20] were first screened with biotinylated PFO captured on magnetic beads [40], followed by fluorescence activated cell sorting (FACS). Random mutagenesis was performed after every 2-3 selections to maintain high library diversity. For FACS, one round of positive selection at pH 7.4 was followed by one round of negative selection at pH 5.5, to enrich for binders with favorable pH-sensitivity. Individual clones from the resulting library were expressed solubly and screened for their ability to inhibit the hemolytic activity of PFO at pH 7.4 as described under "Hemolysis assays." The most effective clone was subjected to additional rounds of mutagenesis and FACS-based selections.
The binding affinities of all individual clones were analyzed by yeast surface titration using biotinylated PFO as previously described [20]. Sorting was performed on MoFlo (Beckman Coulter, Brea, CA) or Aria (BD Biosciences, San Jose, CA) instruments.

Binding assays. To compare the binding affinity of the Fn3 clone 1.2 towards different PFO mutants, EBY100 yeast were transformed with 1.2 using the EZ Yeast transformation kit (Zymo Research, Irvine, CA) and induced to display the Fn3 as previously described [39]. Soluble PFO clones were labeled with Alexa 647 per manufacturer's instructions (Life Technologies, Grand Island, NY). 0.3 million yeast displaying 1.2 were incubated with 500nM PFO for 30 minutes at 4°C, and analyzed on an Accuri C6

cytometer (BD Accuri Cytometers, Ann Arbor, MI). The measured fluorescence intensities were normalized to that of PFO.

To analyze the binding specificity of the C225.2/PFO complex to model cell lines, fluorescently-labeled PFO clones were pre-incubated with C225.2 or the control sm3e.2 at an equimolar ratio of PFO to its binding site, for 30 minutes at 4°C. The PFO mixtures were then diluted in PBSA to the desired concentrations, incubated with A431 or CHO-K1 cells for 1.5 hours at 4°C in suspension, and analyzed on the Accuri C6 cytometer (BD Accuri Cytometers, Ann Arbor, MI). Fluorescence intensities were normalized to the maximum value obtained for each PFO clone, respectively.

Hemolysis assays. CPDA-1 stabilized human red blood cells (Research Blood Components, Boston, MA) were washed with and resuspended to a 50% suspension in PBSA (to approximately 10^{10} cells/mL). 50μL of red blood cells were incubated with 50μL of PFO or C225.2/PFO at varying concentrations for 30 min at 37°C. Following centrifugation at 2500g for 10 minutes, the absorbance of the supernatant was measured at 541nm using the Infinite 200 Pro plate reader (Tecan, Männedorf, Switzerland). The background absorbance from the negative control (PBSA) was subtracted from all measurements, after which all values were normalized to that of the positive control (1% Triton-X 100).

To identify PFO binders that inhibit the pore-forming activity of PFO, hemolysis assays were performed as described, but varying concentrations of PFO were pre-complexed with 3μM (1.1) or 300nM (1.2) Fn3s in PBSA for 20 minutes at 4°C before incubation with red blood cells. The Fn3s were present at these concentrations also during the incubation to drive binding to PFO.

Viability assays. Cells were plated at a density of 12,000 (A431) or 10,000 (CHO-K1) cells/well in 96 well plates 16-20 hours prior to the experiment. PFO or C225.2/PFO complexes were diluted to the desired concentrations in complete medium with or without 10nM E6rGel, and incubated with cells for 16 hours overnight. To measure viability, cells were incubated with 100μL of WST-1 cell proliferation reagent (Roche, Indianapolis, IN) diluted 1:10 in complete medium, for 30 minutes at 37°C. The absorbance of the supernatant was measured at 450nm using the Infinite 200 Pro plate reader (Tecan, Männedorf, Switzerland). The background absorbance of the reagent in medium was subtracted from all measurements, after which all values were normalized to that of untreated cells.

Translation inhibition assays. A431 cells were plated at a density of 20,000 cells/well in 96 well plates 16-20 hours prior to the experiment. The appropriate protein samples were prepared in complete medium and incubated with cells for 2 hours. Cells were then incubated with DMEM containing 1μCi/mL of 1-^{14}C leucine for 30 minutes at 37°C. The media used was free of unlabeled leucine and supplemented with

10% dialyzed serum. 1-^{14}C was used to track protein synthesis exclusively. Following washes with PBS, cells were lysed with RIPA buffer and transferred to a LumaPlate-96 (PerkinElmer, Waltham, MA) for counting on a TopCount NXT Microplate Scintillation and Luminescence Counter (PerkinElmer, Waltham, MA). The background counts from untreated cells incubated with media lacking 1-^{14}C leucine was subtracted from all measurements, after which all values were normalized to that of untreated cells.

To determine the importance of PFO binding to and internalizing with EGFR, translation inhibition assays were performed as above with the following modifications. First, to block C225.2/PFO from associating with EGFR, the assay was performed in the presence of C225 maintained at a 10-fold molar excess relative to C225.2. To reduce the rate of clathrin-mediated endocytosis, cells were pre-treated with 2.5μM Pitstop 2 (Abcam, Cambridge, MA) or an equivalent concentration of DMSO in serum-free media for 15 minutes, incubated with protein samples at 37°C for 45 minutes and labeled with 1-^{14}C leucine (1μCi/mL) at 37°C for 45 minutes. Pitstop 2 or DMSO was present throughout the incubation and radiolabeling steps. Following background subtraction as previous, all measurements were normalized to that of cells treated with Pitstop 2 or DMSO only.

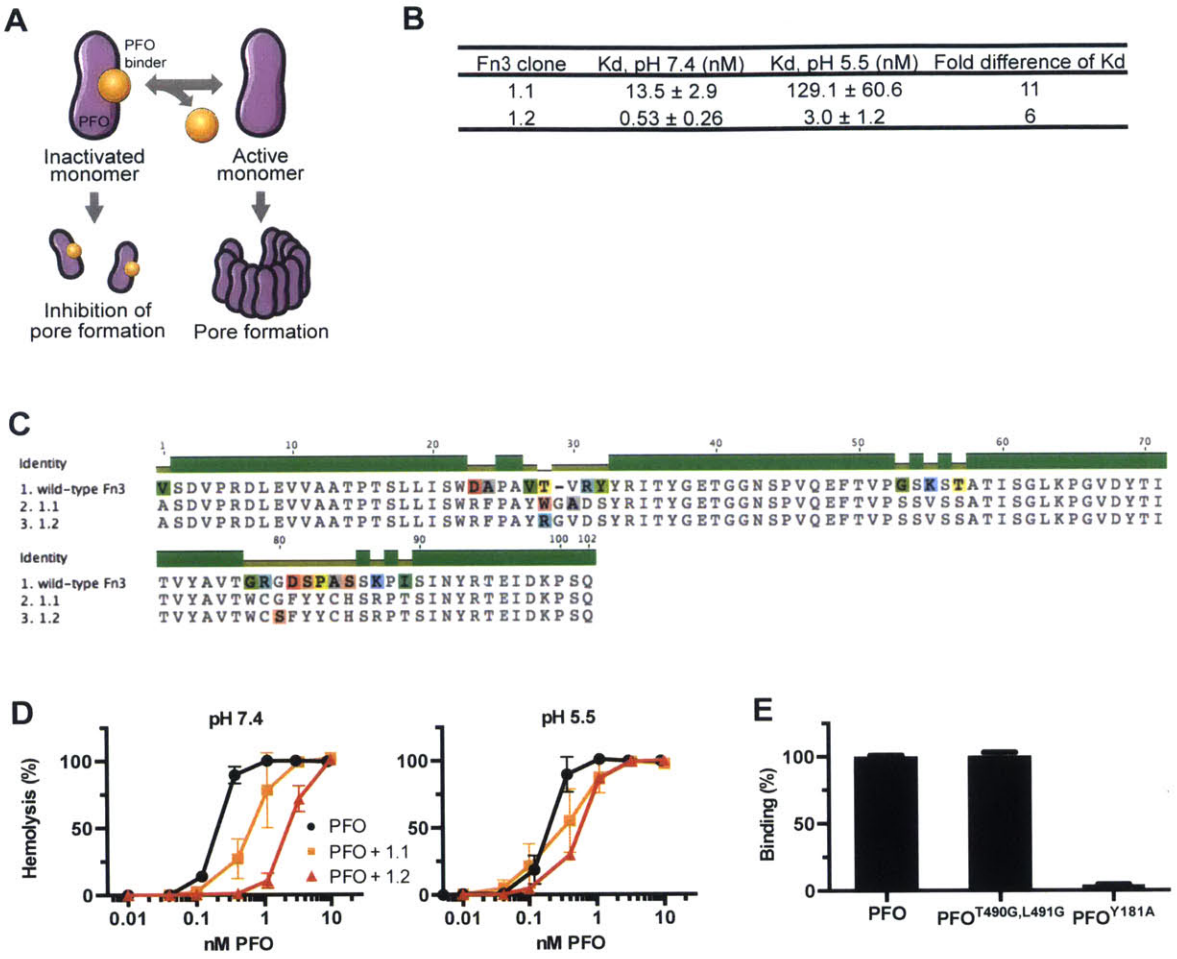

Fn3 clone	Kd, pH 7.4 (nM)	Kd, pH 5.5 (nM)	Fold difference of Kd
1.1	13.5 ± 2.9	129.1 ± 60.6	11
1.2	0.53 ± 0.26	3.0 ± 1.2	6

Figure 2.1. Engineered PFO binder reversibly inhibits the hemolytic activity of PFO. **(a)** Schematic of PFO neutralization. Binders to PFO were engineered on the Fn3 scaffold using yeast surface display techniques, and selected for those that inhibit PFO function. The binder prevents pore formation when associated with PFO but allows normal activity following dissociation, enabling reversible inhibition. **(b)** Equilibrium dissociation constants of the isolated PFO binders measured by yeast-surface titrations at pH 7.4 and 5.5. Errors denote the 95% confidence interval of the global fit to a monovalent binding isotherm. **(c)** Amino acid sequences of the wild-type Fn3 and the engineered PFO binders 1.1 and 1.2. **(d)** Hemolytic activity of PFO in the presence of PFO binders. The Fn3s 1.1 and 1.2 were pre-complexed with PFO at saturating concentrations (3μM and 300nM, respectively), and maintained at such after red blood cells were added. **(e)** Clone 1.2 interacts with residue Y181 involved in oligomerization. 1.2 was displayed on the surface of yeast and tested for its ability to bind fluorescently labeled, soluble PFO mutants at 10nM. The relative fluorescence units were normalized to that measured with PFO.

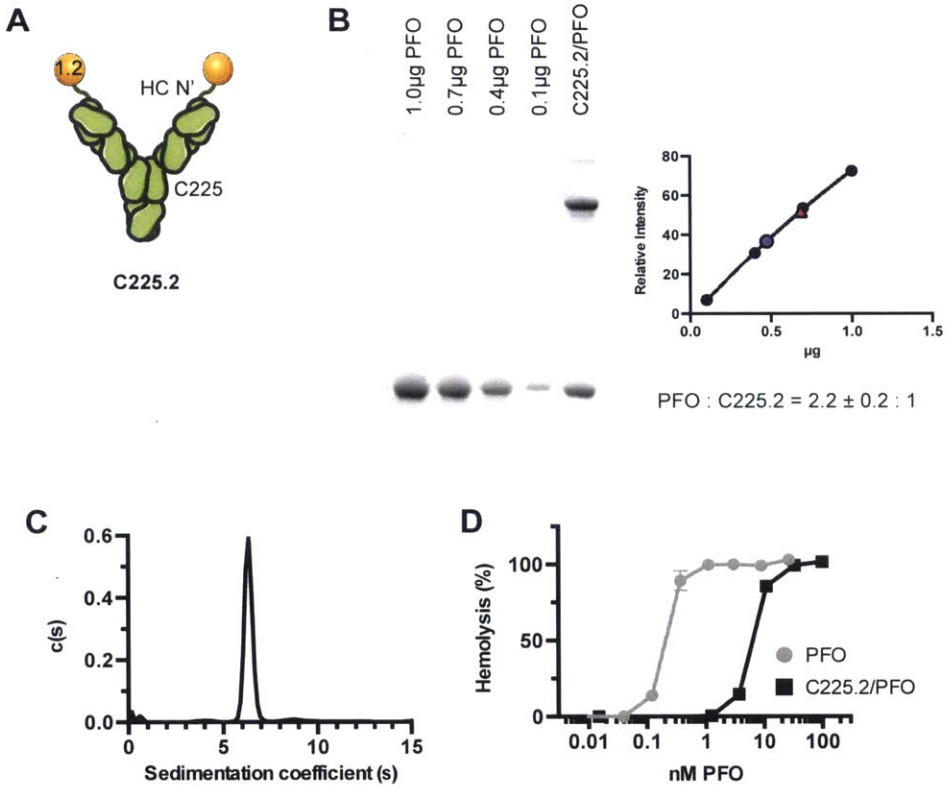

Figure 2.2. C225.2 forms monodisperse complexes with PFO and potently inhibits its activity. (a) Schematic of the bi-specific, neutralizing antibody C225.2 against PFO and EGFR. The PFO binder 1.2 was genetically fused to the heavy chain N terminus of C225 via a flexible $(Gly_4Ser)_2$ linker. **(b) Left:** Non-reducing SDS-PAGE of C225.2/ PFO and PFO stained with SYPRO orange and scanned on the Typhoon Trio imager. The lower bands are PFO, the upper band C225.2. **Right:** Corresponding quantification of the protein gel using Image J. The interpolated values for C225.2 (pink triangle) and PFO (purple circle) are plotted on the standard curve (black) generated from fitting the median intensities of the bands containing known amounts of PFO (black circles). **(c)** The distribution of sedimentation coefficients in the purified C225.2/PFO complex obtained from sedimentation velocity AUC. **(d)** PFO or C225.2/PFO complexes were incubated with human red blood cells at varying concentrations. The molar concentrations denote that of PFO, either in free form or complexed to C225.2. The corresponding concentrations of C225.2 in the mixture can be estimated as half of that of PFO based on the molar ratios shown in (a).

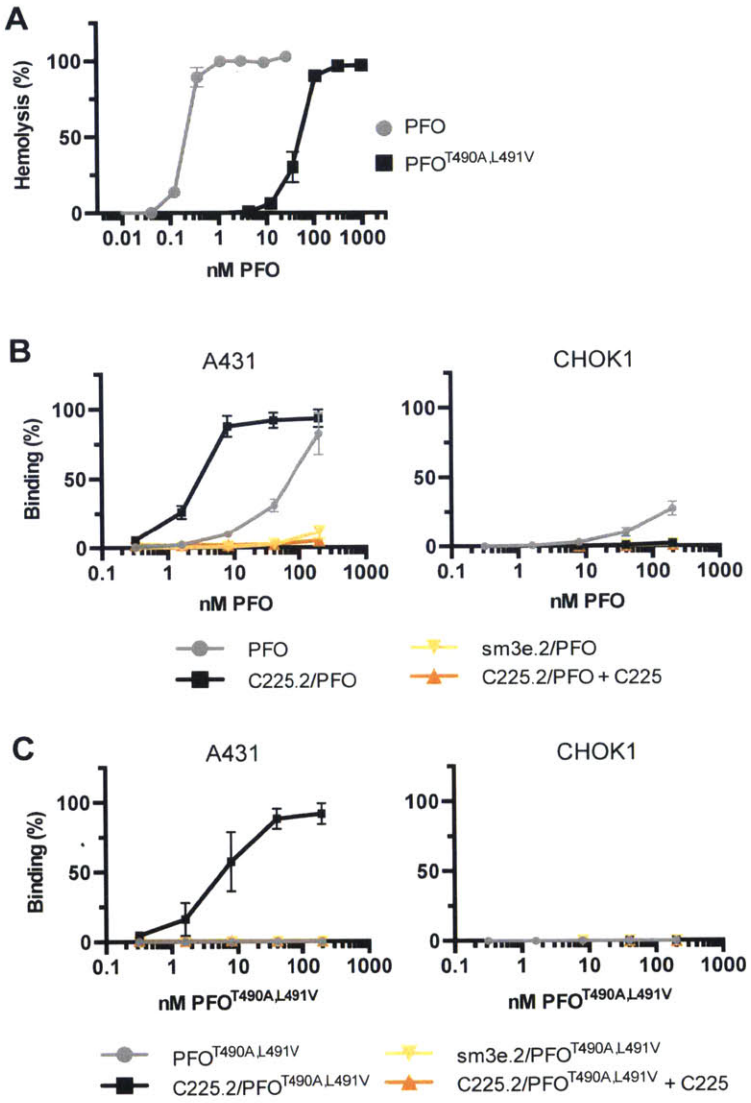

Figure 2.3. C225.2 improves the targeting specificity of PFO. (a) Comparison of the hemolytic activities of PFO and PFO^{T490A,L491V}. Values were normalized to that of the positive control (1% Triton X-100). **(b)** Fluorescently labeled PFO was incubated with the indicated cell lines at 4°C for 1.5 hours, either in free form or as a complex with the neutralizing antibodies C225.2 or sm3e.2. To determine the specificity of the binding interaction, C225 was included at a ten-fold molar excess over C225.2 to compete for EGFR. All fluorescence intensities were normalized to the maximum value obtained on A431 cells. **(c)** Equivalent analysis with fluorescently labeled PFO^{T490A,L491V}.

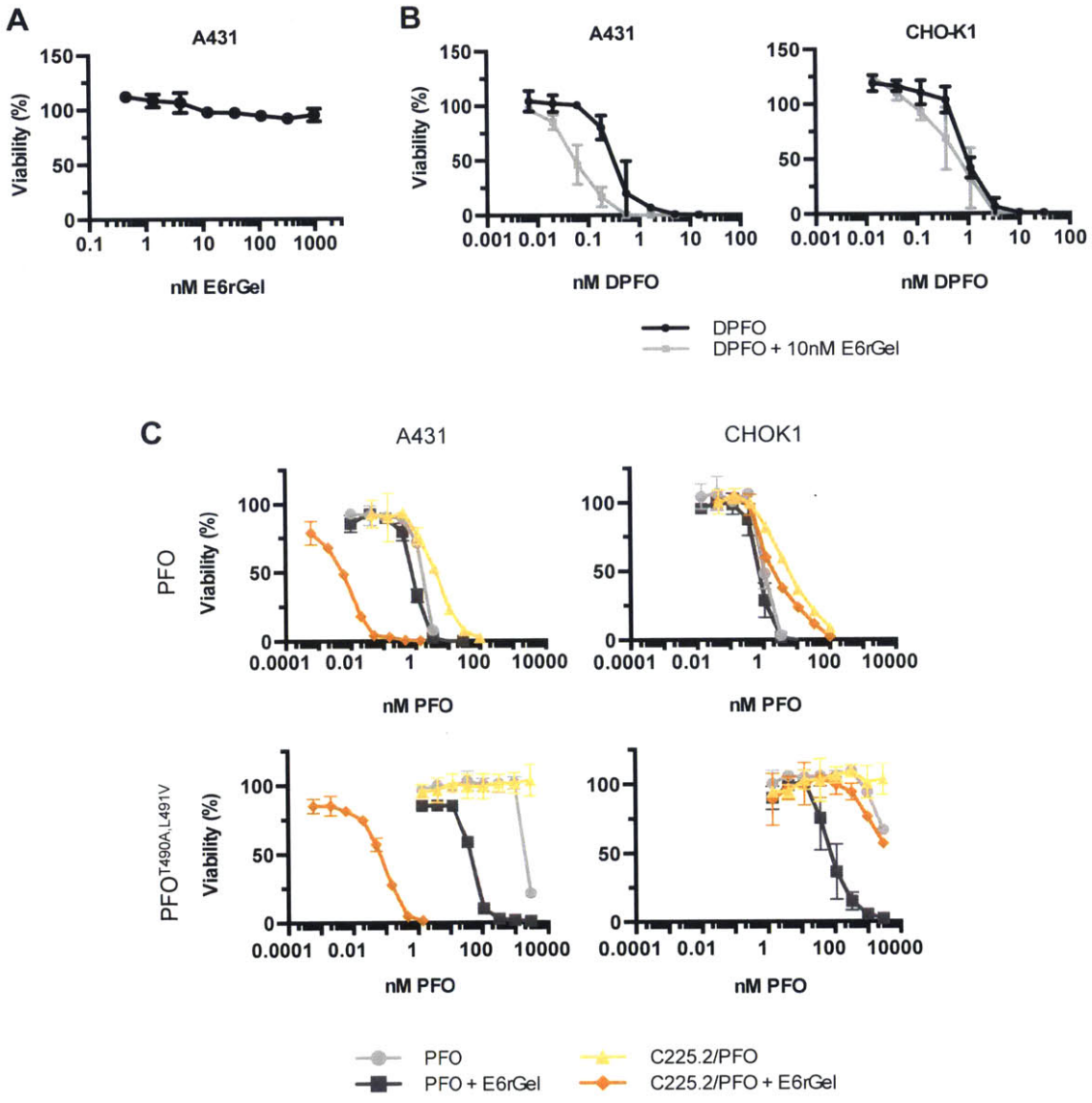

Figure 2.4. The C225.2/PFO system efficiently mediates the cytosolic delivery of targeted gelonin with low toxicity and high specificity. Viability of the indicated cell lines treated overnight at 37°C with **(a)** E6rGel alone or **(b)** in combination with DPFO. DPFO is a fusion protein consisting of the Fn3 clone D[2], which targets EGFR, and PFO[3]. Viability was measured using the WST-1 reagent and measured values were normalized to that of untreated cells. **(c)** PFO or PFO^{T490A,L491V}, in free form or in complex with C225.2, were incubated with cells at 37°C overnight in the presence or absence of 10nM E6rGel in complete media. Viability was measured using the WST-1 reagent and measured values were normalized to that of untreated cells.

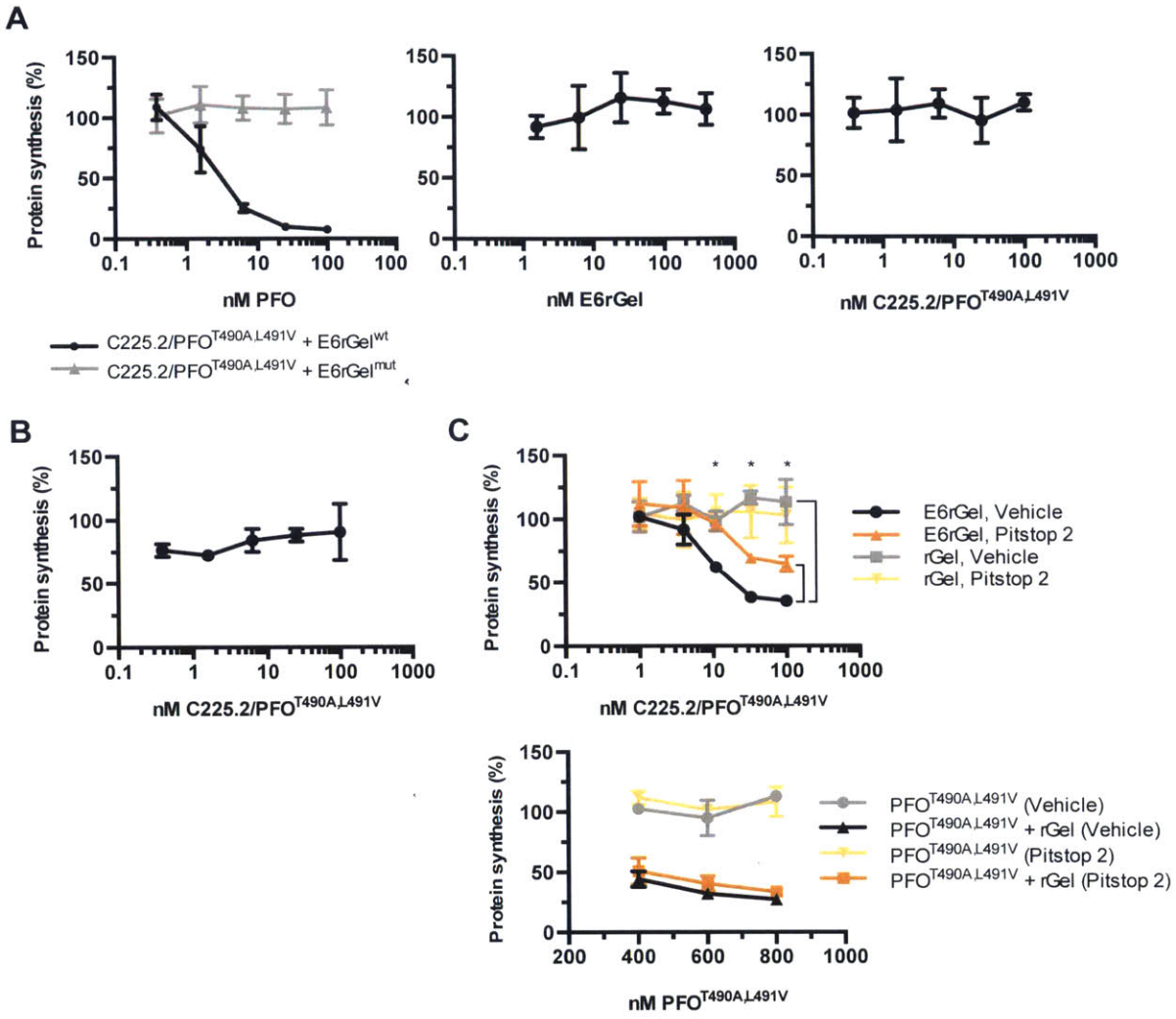

Figure 2.5. EGFR-mediated binding and internalization is critical for efficient delivery. Protein synthesis levels in all panels were measured after the indicated treatment by incubating cells with 1μCi/mL of 1-^{14}C leucine for 20 minutes, then measuring the incorporated radioactivity by solid scintillation. All measurements were normalized to that of untreated cells. **(a) Left:** C225.2/PFO^{T490A,L491V} complexes were incubated with A431 cells for 2 hours at 37°C, in combination with 10nM E6rGel (E6rGel^{wt}) or an inactive mutant (E6rGel^{mut}; contains Y74A, Y133A, E166K, R169Q). **Middle and Right:** A431 cells were treated with E6rGel or C225.2/PFO^{T490A,L491V} alone for 2 hours at 37°C. **(b)** C225.2/PFO^{T490A,L491V} and E6rGel (10nM) were incubated with A431s at 37°C for 2 hours, with C225 in ten-fold molar excess over C225.2 at all points. The concentrations denote that of PFO^{T490A,L491V} in the C225.2/PFO^{T490A,L491V} complex. **(c) Top:** A431 cells were pretreated with 2.5μM Pitstop 2 or DMSO, followed by C225.2/PFO^{T490A,L491V} in combination with targeted or untargeted gelonin. Pitstop 2 or DMSO was present throughout the incubation and radiolabeling steps. The asterisks denote $P \leq 0.05$ between E6rGel,Vehicle and E6rGel,Pitstop 2, as well as E6rGel,Vehicle and rGel,Vehicle, as analyzed by two-way ANOVA. The concentrations denote that of PFO^{T490A,L491V} in the C225.2/PFO^{T490A,L491V} complex. **Bottom:** A431 cells were treated with PFO^{T490A,L491V} alone or in combination with 100nM rGel for 45 minutes at 37°C.

Works cited

1 Gu Z, Biswas A, Zhao M, Tang Y. Tailoring nanocarriers for intracellular protein delivery. *Chem Soc Rev* 2011; **40**: 3638–3655.

2 Provoda CJ, Lee K-D. Bacterial pore-forming hemolysins and their use in the cytosolic delivery of macromolecules. *Adv Drug Deliv Rev* 2000; **41**: 209–221.

3 Gottschalk S, Tweten RK, Smith LC, Woo SL. Efficient gene delivery and expression in mammalian cells using DNA coupled with perfringolysin O. *Gene Ther* 1995; **2**: 498–503.

4 El B, Fa G, Pa F. Introduction of antisense oligonucleotides into cells by permeabilization with streptolysin O. *BioTechniques* 1993; **15**: 1016–8, 1020.

5 Brito JLR, Davies FE, Gonzalez D, Morgan GJ. Streptolysin-O reversible permeabilisation is an effective method to transfect siRNAs into myeloma cells. *J Immunol Methods* 2008; **333**: 147–155.

6 Kerr DE, Wu GY, Wu CH, Senter PD. Listeriolysin O Potentiates Immunotoxin and Bleomycin Cytotoxicity. *Bioconjug Chem* 1997; **8**: 781–784.

7 Walev I, Bhakdi SC, Hofmann F, Djonder N, Valeva A, Aktories K *et al.* Delivery of proteins into living cells by reversible membrane permeabilization with streptolysin-O. *Proc Natl Acad Sci* 2001; **98**: 3185–3190.

8 Walev I. Cell permeabilization with Streptolysin O. In: Harris JR, Graham J, Rickwood D (eds). *Cell Biology Protocols*. John Wiley & Sons, Ltd: Chichester, West Sussex, England, 2006, pp 248–249.

9 Brito JLR, Brown N, Morgan GJ. Transfection of siRNAs in Multiple Myeloma Cell Lines. In: Min W-P, Ichim T (eds). *RNA Interference*. Humana Press, 2010, pp 299–309.

10 Lee K-D, Oh Y-K, Portnoy DA, Swanson JA. Delivery of Macromolecules into Cytosol Using Liposomes Containing Hemolysin from Listeria monocytogenes. *J Biol Chem* 1996; **271**: 7249–7252.

11 Kullberg M, Mann K, Anchordoquy TJ. Targeting Her-2+ Breast Cancer Cells with Bleomycin Immunoliposomes Linked to LLO. *Mol Pharm* 2012; **9**: 2000–2008.

12 Li S-D, Huang L. Pharmacokinetics and Biodistribution of Nanoparticles. *Mol Pharm* 2008; **5**: 496–504.

13 Mandal M, Lee K-D. Listeriolysin O-liposome-mediated cytosolic delivery of macromolecule antigen in vivo: enhancement of antigen-specific cytotoxic T lymphocyte frequency, activity, and tumor protection. *Biochim Biophys Acta BBA - Biomembr* 2002; **1563**: 7–17.

14 Sun X, Provoda C, Lee K-D. Enhanced in vivo gene expression mediated by listeriolysin O incorporated anionic LPDII: Its utility in cytotoxic T lymphocyte-inducing DNA vaccine. *J Controlled Release* 2010; **148**: 219–225.

15 Pirie CM, Liu DV, Wittrup KD. Targeted Cytolysins Synergistically Potentiate Cytoplasmic Delivery of Gelonin Immunotoxin. *Mol Cancer Ther* 2013; **12**: 1774–1782.

16 Liu DV, Yang NJ, Wittrup KD. A Nonpolycationic Fully Proteinaceous Multiagent System for Potent Targeted Delivery of siRNA. *Mol Ther — Nucleic Acids* 2014; **3**: e162.

17 Hotze EM, Tweten RK. Membrane assembly of the cholesterol-dependent cytolysin pore complex. *Biochim Biophys Acta BBA - Biomembr* 2012; **1818**: 1028–1038.

18 Maynard JA, Maassen CBM, Leppla SH, Brasky K, Patterson JL, Iverson BL *et al.* Protection against anthrax toxin by recombinant antibody fragments correlates with antigen affinity. *Nat Biotechnol* 2002; **20**: 597–601.

19 Orth P, Xiao L, Hernandez LD, Reichert P, Sheth PR, Beaumont M *et al.* Mechanism of Action and Epitopes of Clostridium difficile Toxin B-neutralizing Antibody Bezlotoxumab Revealed by X-ray Crystallography. *J Biol Chem* 2014; **289**: 18008–18021.

20 Hackel BJ, Kapila A, Dane Wittrup K. Picomolar Affinity Fibronectin Domains Engineered Utilizing Loop Length Diversity, Recursive Mutagenesis, and Loop Shuffling. *J Mol Biol* 2008; **381**: 1238–1252.

21 Bloom L, Calabro V. FN3: a new protein scaffold reaches the clinic. *Drug Discov Today* 2009; **14**: 949–955.

22 Shepard LA, Heuck AP, Hamman BD, Rossjohn J, Parker MW, Ryan KR *et al.* Identification of a Membrane-Spanning Domain of the Thiol-Activated Pore-Forming Toxin Clostridium perfringens Perfringolysin O: An α-Helical to β-Sheet Transition Identified by Fluorescence Spectroscopy. *Biochemistry (Mosc)* 1998; **37**: 14563–14574.

23 Farrand AJ, LaChapelle S, Hotze EM, Johnson AE, Tweten RK. Only two amino acids are essential for cytolytic toxin recognition of cholesterol at the membrane surface. *Proc Natl Acad Sci* 2010; **107**: 4341–4346.

24 Ramachandran R, Heuck AP, Tweten RK, Johnson AE. Structural insights into the membrane-anchoring mechanism of a cholesterol-dependent cytolysin. *Nat Struct Mol Biol* 2002; **9**: 823–827.

25 Hotze EM, Heuck AP, Czajkowsky DM, Shao Z, Johnson AE, Tweten RK. Monomer-Monomer Interactions Drive the Prepore to Pore Conversion of a β-Barrel-forming Cholesterol-dependent Cytolysin. *J Biol Chem* 2002; **277**: 11597–11605.

26 Wiley HS. Trafficking of the ErbB receptors and its influence on signaling. *Exp Cell Res* 2003; **284**: 78–88.

27 Goldstein NI, Prewett M, Zuklys K, Rockwell P, Mendelsohn J. Biological efficacy of a chimeric antibody to the epidermal growth factor receptor in a human tumor xenograft model. *Clin Cancer Res* 1995; **1**: 1311–1318.

28 Pirie CM, Hackel BJ, Rosenblum MG, Wittrup KD. Convergent Potency of Internalized Gelonin Immunotoxins across Varied Cell Lines, Antigens, and Targeting Moieties. *J Biol Chem* 2011; **286**: 4165–4172.

29 Provoda CJ, Stier EM, Lee K-D. Tumor Cell Killing Enabled by Listeriolysin O-liposome-mediated Delivery of the Protein Toxin Gelonin. *J Biol Chem* 2003; **278**: 35102–35108.

30 Selbo PK, Weyergang A, Høgset A, Norum O-J, Berstad MB, Vikdal M *et al.* Photochemical internalization provides time- and space-controlled endolysosomal escape of therapeutic molecules. *J Controlled Release* 2010; **148**: 2–12.

31 Hackel BJ, Neil JR, White FM, Wittrup KD. Epidermal growth factor receptor downregulation by small heterodimeric binding proteins. *Protein Eng Des Sel* 2012; **25**: 47–57.

32 de Virgilio M, Lombardi A, Caliandro R, Fabbrini MS. Ribosome-Inactivating Proteins: From Plant Defense to Tumor Attack. *Toxins* 2010; **2**: 2699–2737.

33 Nato F, Reich K, Lhopital S, Rouyre S, Geoffroy C, Mazie JC *et al.* Production and characterization of neutralizing and nonneutralizing monoclonal antibodies against listeriolysin O. *Infect Immun* 1991; **59**: 4641–4646.

34 Schlesinger BC, Cheng L. Characterization of a novel monoclonal antibody against human perforin using transfected cell lines. *Immunology* 1994; **81**: 291–295.

35 Sawada-Hirai R, Jiang I, Wang F, Sun SM, Nedellec R, Ruther P *et al.* Human anti-anthrax protective antigen neutralizing monoclonal antibodies derived from donors vaccinated with anthrax vaccine adsorbed. *J Immune Based Ther Vaccines* 2004; **2**: 5.

36 Law RHP, Lukoyanova N, Voskoboinik I, Caradoc-Davies TT, Baran K, Dunstone MA *et al.* The structural basis for membrane binding and pore formation by lymphocyte perforin. *Nature* 2010; **468**: 447–451.

37 Spangler JB, Manzari MT, Rosalia EK, Chen TF, Wittrup KD. Triepitopic Antibody Fusions Inhibit Cetuximab-Resistant BRAF and KRAS Mutant Tumors via EGFR Signal Repression. *J Mol Biol* 2012; **422**: 532–544.

38 Schuck P. Size-Distribution Analysis of Macromolecules by Sedimentation Velocity Ultracentrifugation and Lamm Equation Modeling. *Biophys J* 2000; **78**: 1606–1619.

39 Chen TF, de Picciotto S, Hackel BJ, Wittrup KD. Engineering Fibronectin-Based Binding Proteins by Yeast Surface Display. In: *Methods in Enzymology*. Elsevier, 2013, pp 303–326.

40 Ackerman M, Levary D, Tobon G, Hackel B, Orcutt KD, Wittrup KD. Highly avid magnetic bead capture: An efficient selection method for de novo protein engineering utilizing yeast surface display. *Biotechnol Prog* 2009; **25**: 774–783.

Chapter 3. Enhanced siRNA Delivery using High-Affinity dsRNA-Binding Proteins

Introduction

Most siRNA delivery systems are internalized into cells via endocytosis, often via a targeting moiety that binds to specific cell surface receptors for receptor-mediated uptake[1]. Thus, it is expected that the siRNA must first escape the endosome to reach the RNAi machinery in the cytoplasm. Although the exact mechanisms of this process are not fully known for most delivery systems, it is understood to be an inefficient step even for some of the most clinically advanced delivery vehicles[2,3]. Thus, large gains in silencing efficacy are expected to be made by improving the efficiency of endosomal escape.

However, at a given escape efficiency, additional factors may also impact the potency of silencing. In cases where a targeting moiety triggers receptor-mediated endocytosis, such factors can include the expression level of the receptor[4], its rate of internalization and recycling[5], and its internalization route and trafficking pathways. In cases where the siRNA is complexed non-covalently to a delivery vehicle, such factors can include the stability of the complex in the extracellular space, or its rate or timing of disassembly in the intracellular space[6]. Examples of systems that utilize such non-covalent complexation strategies include non-specific assemblies of siRNA with positively charged peptides[7], proteins[8], or ionizable lipid-like materials[9], or specific assemblies with dsRNA-binding proteins[10,11].

Although many proposed delivery systems rely on non-covalent binding to siRNA, systematic studies have been lacking of how the strength of that interaction can affect delivery. Partly, this absence is due to binding affinity not being appreciated as an impactful variable, and partly due to the difficulties of independently modulating it without affecting others (such as the escape efficiency). Indeed, in the examples mentioned above, a single molecule may function both as the carrier and putative releaser, such as with positively charged proteins and peptides; or the carrier and releaser may be packaged into the same vehicle that undergoes global disassembly, such as with certain nanoparticulate formulations; or the agent mediating endosomal release may be unobvious or unknown in the first place, complicating efforts to investigate one variable at a time.

The question of how tightly siRNA should be bound to its delivery vehicle, intuitively, seems to have a simple answer. If the association is too weak, siRNA will dissociate prematurely from its vehicle and suffer from inefficient internalization or prompt degradation in the extracellular space. If the association is too strong, siRNA will not be released from its vehicle for loading onto RISC (assuming

that binding to the vehicle prevents this process). Thus, it is expected that an affinity optimum exists between these two extremes, which maximizes intracellular uptake, protection from degradation and RISC loading. However, the quantitative range of this affinity optimum and how it may depend on other parameters governing the system is not obvious.

Previously, we have reported a multi-agent siRNA delivery system[12] involving a targeted double-stranded RNA binding domain (dsRBD) to complex and deliver siRNA into cells, and an *in trans* targeted pore-forming protein Perfringolysin O (PFO) for endosomal release. The unique modularity of this system, where the siRNA binding moiety is physically separate from the endosomal release moiety, combined with established directed evolution techniques that experimental tuning of affinity, makes it well suited for investigating the affinity dependence of silencing.

Here, we report the affinity maturation of the dsRNA binding protein p19 expressed by the Carnation Italian Ringspot Virus (CIRV)[13]. (For background and rationale, see "P19 as a siRNA Carrier.") Using directed evolution and yeast surface display techniques, we obtained three mutants that demonstrated a 10-fold, 70-fold and 760-fold increase in affinity compared to the wild-type protein. The tightest binding mutant had a K_D of approximately 5pM, the highest affinity reported to date against siRNA for a protein. The affinity-matured p19 mutants were then developed into siRNA carriers targeting the epidermal growth factor receptor (EGFR). Combined with an endosomal release strategy based on a neutralized-PFO system described in Chapter 2[14], we observed that tighter binding consistently correlated with more efficient silencing. With the tightest binding mutant, we achieved 50% silencing of a GFP reporter with pM concentrations of siRNA, rivaling the *in vitro* potency of lipid-based delivery systems. Although we were unable to determine the optimum affinity experimentally, our results suggest that it may lie below 5pM, an unexpectedly low value. The increase in silencing potency was partially due to increased uptake. However, we also observed that the tighter-binding mutant enabled stronger silencing even under experimental conditions where similar numbers of siRNAs were taken up into cells by the high- and low-affinity clones. This observation suggested that providing prolonged protection of siRNA throughout the endosomal pathway may be a strategy for further improving the efficiency of delivery, even when the endosomal escape efficiency is fixed.

Results

Engineering and characterization of affinity-matured CIRV p19 mutants. To develop CIRV p19 into a siRNA carrier, we first mutated its solvent-exposed cysteines to non-reactive residues. Wild-type p19 contains three free cysteines, two out of which are exposed to solvent (C133, C159) and one is embedded

within the core of the protein (C106) without forming any polar contacts with other residues. The reactive cysteines on the surface caused multimers of various sizes to form (data not shown). Introducing the C133S and C159A substitutions[15] effectively eliminated crosslinking and yielded a monomeric peak when analyzed by size-exclusion chromatography (SEC). The clone $p19^{C133S,C159A}$ is herein referred to as "p19."

p19 displayed well on the surface of yeast, either by itself or as a C-terminal fusion to human Fc (IgG1) linked by a $(G_4S)_5$ linker. There were no significant differences in display levels or binding between the two formats. We decided to proceed with the latter configuration in anticipation of potentially fusing p19 to antibodies for targeting. A hFc-p19 library was created by random mutagenesis using error-prone PCR with a low or high error rate, and transformed into yeast to yield libraries with $1x10^7$ or $2x10^7$ different clones, respectively. The two libraries were combined and subjected to six rounds of FACS, where three different siRNA sequences were used for sequential selections to maintain sequence-independent binding. Two out of the three siRNAs contained 2'OMe modifications scattered between different positions. We performed kinetic selections at 37°C in PBSA containing 55% mouse serum to mimic *in vivo* conditions. Libraries were induced at 37°C and clones were selected based on high levels of display in addition to strong binding, to isolate high affinity clones that are also stable.

Sequence analysis of the enriched library revealed strong convergence to a single clone, $p19^{G16R,D47N}$ (19 out of the 20 clones analyzed). The remaining clone outside of this family contained the mutations N15K and I123V. Interestingly, N15 and G16 were positioned in close proximity to the siRNA backbone, suggesting that the positively charged side chains of Lys and Arg may form electrostatic interactions with negatively charged phosphates (**Figure 3.1A**). D47N was positioned in an unstructured loop that was not resolved in the crystal structure and likely uninvolved in binding. However, this substitution also introduced a N-glycosylation site that could potentially improve the solubility or stability of the protein. I123V was positioned at the dimerization interface. Eight different clones of p19 containing different combinations of the aforementioned mutations were expressed solubly. The D47N mutation was found to affect neither soluble expression levels nor binding affinities, and I123V had a destabilizing effect (data not shown). Thus, these mutations were not pursued further.

The three mutants selected for further analysis contained the substitutions N15K and G16R, singly or both (**Figure 3.1D**). All three clones expressed well with comparable yields to p19. The A_{260}/A_{280} ratios of the clones following his-tag chromatography were between 0.8 and 1.3, indicating that likely, contaminating nucleic acids were bound non-specifically. Anion exchange chromatography (AEX) reduced the A_{260}/A_{280} ratios down to between 0.59 and 0.64, effectively stripping away fugitive nucleic acids. All p19 clones eluted as monomeric peaks without evidence for larger aggregates immediately following purification (**Figure 3.1B**). However, after a single freeze-thaw cycle, we did observe a right-

shifted peak for the $p19^{N15K,G16R}$ mutant, indicating lesser stability. In contrast, p19, $p19^{N15K}$ and $p19^{G16R}$ remained monomeric following freeze-thaw (**Figure 3.1B**) and also after one month of storage at 4°C (data not shown).

The binding kinetics of the p19 clones were analyzed using BioLayer Interferometry (BLI), where strepdavidin-coated tips were loaded with biotinylated siRNA. The siRNA used for this analysis contained scattered 2'OMe modifications, and the conjugated biotin was separated from the 3' end of the sense strand by a $(PEG)_6$ linker. The K_D of p19 was measured to be 3.8 nM, higher than the initial report (170 pM measured by gel-shift assays[13]). This discrepancy may be due to the different assay format or the 2'OMe modifications present in our siRNA. The mutants displayed substantially improved affinity compared to p19, with $p19^{N15K,G16R}$ displaying the lowest K_D as expected (**Figure 3.1C**). However, it must be noted that with $p19^{G16R}$ and especially $p19^{N15K,G16R}$, mass-transport limitations were observed which could not be resolved by either lowering the loading concentration of siRNA or increasing the shake speed (to minimize protein depletion near the tip). As the affinity of these clones are likely reaching the detection limit of BLI, their K_Ds remain to be measured with higher accuracy using other methods. Solution-based techniques such as KinExA may be more appropriate.

Development and characterization of p19-based targeted siRNA carriers. In anticipation of using the EGFR-targeted, neutralized PFO system[14] for endosomal escape, we created p19 constructs targeted to the same receptor using two different EGFR binders (**Figure 3.2A**). The first binder was engineered on the fibronectin (Fn3) scaffold, termed "E6" herein (originally E6.2.6; reported K_D is 0.26 nM at pH 7.4[16]), and the second binder was engineered on a modified sso7d scaffold (originally E18.6; reported K_D is 73 nM at pH 7.4[17]), termed "E18" herein. Both binders were previously shown to be non-competitive with C225[16,17] and thus were not expected to compete with C225.2/PFO. Fusing the EGFR binders to the C terminus allowed slightly better silencing compared to the N-terminal fusions (data not shown), and thus all further analyses were performed with the C-terminal fusions only. All EGFR binders were separated from p19 by a flexible $(G_4S)_3$ linker.

The p19-E6 constructs demonstrated significantly lower yields compared to both untargeted p19s and the p19-E18 constructs. The p19-E18 constructs were expressed at comparable yields to the untargeted p19 clones, which may reflect the higher starting stability of the hyperthermophilic sso7d scaffold[18] compared to the Fn3 scaffold. All constructs were stripped of fugitive nucleic acids and were confirmed to elute as monomeric peaks from SEC (data not shown).

Next, the affinities of p19-E6 and p19-E18 against EGFR were analyzed by BLI (**Figure 3.2B**). We performed the analysis at pH 7.4, mimicking extracellular pH, and pH 5.5, mimicking endsomal pH. We also compared the affinities of the targeted constructs when they were complexed with siRNA or not

to determine whether the presence of siRNA affected receptor binding. The collected data were fitted to a 1:1 binding model to obtain apparent affinities. We observed no significant differences in binding to EGFR at the two different pHs, consistent with the absence of histidines in the paratopes of both E6 and E18. We also did not observe any statistically significant differences in binding to EGFR depending on the presence of siRNA, consistent with the modular assembly of these targeted constructs (**Figure 3.2A**).

Finally, we analyzed the size distribution of the targeted p19 constructs by Dynamic Light Scattering (DLS). Measurements were performed in the presence or absence of siRNA to discern whether larger molecular-weight aggregates formed when the constructs were mixed with siRNA. The measured diameters fell between 6.7nm and 8.8nm, roughly the length of 21 base pair siRNA, regardless of whether siRNA was present (**Figure 3.2C**). This result was consistent with the "caliper-like" mode of binding observed in the crystal structure of a p19/siRNA complex (**Figure 3.1A**). The degree of polydispersity varied between constructs with no particular pattern. Overall, a high polydispersity was expected as the flexible linker connecting p19 and the EGFR binders can adopt multiple conformations.

Although DLS does not have the resolution to resolve monomeric p19/siRNA complexes from potential oligomers, there were no evidence to support the formation of larger aggregates in the presence of siRNA. Indeed, for most samples, greater than 90% of the mass was measured to fall within the aforementioned range of diameters (**Figure 3.2C**). In theory, the p19/siRNA complexes are expected to be monomeric, as the p19 homodimer is capable of binding to only one molecule of siRNA at a time. It should be noted that, as with the untargeted p19 clones, we did observe higher A_{260}/A_{280} ratios for these constructs immediately following his-tag chromatography. This observation suggested that the constructs were capable of binding non-specifically to nucleic acids in the bacterial cytoplasm (likely DNA or RNA, as dsRNA is unlikely to be present). It was thus plausible to speculate that a lengthy piece of nucleic acid may bind multiple copies of p19 non-specifically to form a larger aggregate. However, this is unlikely to happen with siRNA, as there are no additional patches of positive charge on the protein that can potentially interact with another siRNA molecule, once the positively-charged interaction surface is shielded by the bound siRNA[13].

Efficacy of silencing using targeted p19-based siRNA carriers and neutralized PFO. Next, the intracellular delivery system based on neutralized PFO[14] was combined with the targeted p19-based siRNA carriers to enable silencing. C225.2/PFO^{T490A,L491V} was expressed, purified and prepared as previously described[14]. To load siRNA onto the p19-based carriers, both were incubated at a 1:1 molar ratio (p19 dimer : siRNA) at μM concentrations for 30 minutes at 4°C. The siRNA used for silencing experiments did not contain any chemical modifications. Silencing was measured in A431 cells stably transfected with destabilized EGFP that has a 2-hour half-life (A431-d2EGFP cells[12]). Two different

assay formats were tested, where either the siRNA concentration was fixed and PFO concentration varied, or vice versa. The constructs were diluted in complete media containing 10% FBS and incubated with cells. After 6 hours, media containing siRNA and protein were replaced with fresh media, and GFP expression was analyzed after 24 hours.

For final analysis, GFP expression was normalized to that measured from cells which received the single agent only at the fixed concentration. For example, in an experiment where the concentration of C225.2/PFO^{T490A,L491V} was fixed at 5nM and the concentration of p19-E6,E18/siRNA was varied, GFP expression was normalized to that of cells treated with 5nM C225.2/PFO^{T490A,L491V} only. This method of normalization was used to correct for the non-siRNA mediated depression of GFP caused by C225.2 (**Figure 3.3A**). While p19-E6,E18/siRNA alone did not affect GFP expression (**Figure 3.3B**), C225.2/PFO^{T490A,L491V} alone caused a dose-dependent reduction in GFP expression. C225.2 alone (without PFO^{T490A,L491V}) recapitulated this phenomena, suggesting that Cetuximab-mediated effects were responsible for the observed depression rather than effects related to pore formation. We speculate that C225.2-mediated blockage of EGF growth signaling is affecting the expression of GFP from the CMV promoter, which has been reported to be activated by the MEKK1-JNK pathway[19] downstream of EGF[20].

Both p19-E6 and p19-E18 clones demonstrated dose-dependent silencing of GFP (**Figures 3.3C** and **3.3D**). We observed that among the mutants tested, tighter binding consistently lead to greater silencing. Overall, silencing potencies were nearly identical between the p19-E6 and p19-E18 clones, which were expected given that the EGFR binders were functionally equivalent with similar affinities. Reducing the fixed concentration of C225.2/PFO^{T490A,L491V} from 5 nM to 0.5 nM affected both the EC_{50} of silencing and the maximum degree of silencing achievable (the plateau observed at high siRNA concentrations), consistent with a reduced efficiency of escape. The affinity-dependent increase in silencing was observed also when the assay orientation was reversed to fix the concentration of p19-E6/siRNA and vary the concentration of C225.2/PFO^{T490A,L491V} (**Figure 3.3E**). Differences in potencies between mutants were more pronounced at lower siRNA concentrations where their affinities start to diverge. Regardless of the concentration of siRNA used, C225.2/PFO^{T490A,L491V} demonstrated an EC_{50} of silencing in the pM range. We did observe minor discrepancies in the exact degrees of silencing depending on the orientation of the assay, although overall trends were consistent.

Removing the targeting moiety from the p19 mutants significantly reduced silencing (**Figure 3.3F**). This result was expected, as we have previously demonstrated that C225.2/PFO^{T490A,L491V} predominantly permeablizes endosomal membranes following receptor-mediated internalization[14]. Untargeted p19 clones are likely to be internalized less efficiently through non-specific pinocytic uptake, compared to the targeted p19 clones that are internalized through EGFR-mediated endocytosis. Furthermore, the p19 clones targeted to EGFR, the same receptor as C225.2/PFO^{T490A,L491V}, are more

likely to co-localize into the same endosomes as the pore-forming protein responsible for enabling release. Interestingly, the silencing potencies of the untargeted p19 mutants observed at high concentrations of siRNA were independent of their affinity. This is likely because at siRNA concentrations significantly higher than their K_Ds, all p19 clones are expected to be fully associated with siRNA.

Improved efficacy is due to increased uptake and likely prolonged protection. We hypothesized that the p19 mutants with tighter affinity were enabling greater silencing because they could internalize siRNA more efficiency, especially at low concentrations. Thus, we measured the number of siRNA molecules taken up into A431-d2EGFP cells by each p19-E18 clone over a 6 hour period. The p19-E18 constructs were complexed with siRNA labeled with Alexa Fluor 647, and incubated with cells for different periods of time in complete media. Background-subtracted fluorescence was converted to number of fluorophores (which theoretically equals the number of siRNAs) through a standard curve generated with AF647 calibration beads. As expected, the tighter-binding p19 mutants generally demonstrated faster uptake (**Figure 3.4A**), which correlated with greater silencing. However, the rate and degree of uptake mediated by $p19^{G16R}$-E18 and $p19^{N15K,G16R}$-E18 were nearly identical, whereas $p19^{N15K,G16R}$-E18 was consistently better at silencing (**Figure 3.3D**). This result suggested that the stronger affinity of $p19^{N15K,G16R}$ was affecting a step in the delivery process downstream of internalization.

To further probe this observation, we titrated down the number of siRNAs internalized into cells by fixing the p19-E18/siRNA complex at a high, saturating concentration (for binding to both siRNA and EGFR) while gradually increasing the concentration of a competitor for receptor binding. E18 (not fused to p19) with the sumo tag was used for this purpose. We deemed it unnecessary to remove the sumo tag from E18 as it was unlikely to affect binding to EGFR. With this setup, both p19-E18 and $p19^{N15K,G16R}$-E18 internalized decreasing numbers of siRNA with increasing concentrations of sumo-E18 (**Figure 3.4B**). First, this result confirmed that siRNA was being internalized specifically via EGFR for both p19 clones, as uptake could be competed off by E18. In addition, we also observed differing patterns of silencing between the two clones. Whereas p19-E18 displayed a gradual decrease in silencing with decreased uptake, $p19^{N15K,G16R}$-E18 maintained close to maximum levels of silencing even when the number of siRNAs internalized was decreased by more than 10-fold. Indeed, $p19^{N15K,G16R}$-E18 demonstrated better silencing compared to p19-E18 even when the number of internalized siRNAs were equal. This observation suggested that tighter binding to siRNA may improve silencing not only by increasing the net uptake of siRNA, but also by better maintaining association with siRNA inside the cell. We hypothesize that p19 binding to siRNA protects the siRNA from nucleases in the intracellular space, as further discussed below.

Discussion

In this study, we have extended the neutralized PFO-based delivery system to applications in siRNA delivery. Specifically, the endosomal release functionality of C225.2/PFO^{T490A,L491V} was combined with a targeted siRNA carrier based on the dsRNA-binding protein p19. Affinity-matured mutants of p19 were isolated where Lys or Arg residues were substituted into positions that allowed their positively charged side chain to interact with the negatively charged siRNA backbone. Combining these two mutations further increased the affinity to a K_D of approximately 5pM, the tightest against siRNA reported to date for a protein.

The mutants were well expressed as fusions to Fn3- or sso7d-based binders against EGFR. The binding affinity of the p19 clones generally correlated with the rate of siRNA uptake and silencing potency. This trend was not obvious to predict, as it was expected that too tight of an affinity would prevent siRNA from being released from the carrier and hinder loading onto RISC. (It is interesting to note that this is in fact the natural function of p19 expressed by viruses.) Thus, theoretically, the optimal K_D for maximizing delivery is likely below 5pM—an unexpectedly low value—for systems targeting a rapidly internalizing receptor such as EGFR. This K_D optimum may depend on the internalization rate of the target receptor, potentially even lower for slowly internalizing receptors.

Interestingly, we observed that increased siRNA uptake could not completely explain why the tighter binding p19 mutants enabled greater silencing. Under experimental conditions where similar numbers of siRNA were internalized by p19-E18 or p19^{N15K,G16R}-E18, the latter still demonstrated substantially higher potency. The most obvious difference between these two clones is their siRNA release kinetics. Indeed, the off-rates of p19 and p19^{N15K,G16R} were measured to be 8.6×10^{-4} s^{-1} and 3.8×10^{-5} s^{-1}, respectively, which correspond to dissociation half-times of 13 minutes and 5 hours. Given the rapid internalization rate of EGFR (half-time of approximately 25 minutes[21]), it is expected that much of the siRNA bound to p19^{N15K,G16R}-E18 (but not p19-E18) will remain associated to its carrier during its residence inside the cell.

Such a prolonged association could potentially improve silencing by better protecting the siRNA from nuclease-mediated degradation in endosomal or lysosomal compartments. Indeed, the degradation rate of siRNA in the endosome has been estimated to be 1.4×10^{-4} s^{-1} (half-time of 1.4 hours)[22]. Then, it is plausible for a siRNA binder that can protect its cargo for multiple hours to improve siRNA persistence in endosomes. Subsequently, maintaining a higher concentration of intact siRNAs for a longer period of time in endosomal compartments could increase the probability of successful escape. Furthermore, the siRNA may not need to be released from p19 in order to escape to the cytoplasm, as the size of the p19/siRNA complex is theoretically small enough to pass through pores formed by PFO. If so, the pool of

endosomal siRNA available for release would be even bigger, including both that are bound or unbound to p19.

Alternatively, $p19^{N15K,G16R}$ may also protect siRNA from nucleases in the cytoplasm. However, it has been suggested that siRNA has a relatively longer persistence in the cytoplasm with a degradation rate of 8.1×10^{-6} s^{-1} (half-time of 24 hours)[22]. Indeed, in rapidly dividing cells, it has been proposed that the dilution of siRNA via cell division is the limiting factor for gene silencing rather than siRNA degradation[23]. Accordingly, we have measured the doubling time of A431-d2EGFP cells to be 20.4 hours (data not shown). With cell division and intracellular degradation occurring on such slower timescales, prolonging the association between siRNA and its carrier from minutes to a couple of hours may not significantly impact siRNA persistence in the cytoplasm.

It is interesting to note that we have used siRNA without chemical modifications in our silencing assays, which is expected to degrade more rapidly than those with modifications that impart stability against nucleases, such as 2'-F or 2'-OMe. If $p19^{N15K,G16R}$ is indeed providing better protection from intracellular nucleases compared to p19, the relative differences in their silencing potencies may decrease when nuclease-stabilized siRNAs are used. Indeed, the relative timescales of degradation (by nucleases) and dissociation (from p19) may determine whether a significant improvement in siRNA persistence can be achieved in each intracellular compartment by tuning affinity.

The observations made in this study nevertheless suggest that increasing the affinity between siRNA and its carrier may be an opportunity to further improve the potencies of delivery vehicles that rely on non-covalent siRNA complexation. However, depending on the system, increasing affinity without sacrificing other key parameters such as escape efficiency may be challenging, as discussed in the introduction. From a practical standpoint, it may be possible to incorporate $p19^{N15K,G16R}$ into other delivery systems as a modular and additive unit, as p19 interacts with one surface of the siRNA only (as opposed to wrapping around the entire molecule) and may still allow charge-based interactions with other material.

Finally, ongoing and future work for this study includes mathematical modeling of the delivery system to determine whether indeed the hypothesized optimum affinity exists for maximizing delivery, and if so what K_D range it is in and how it may be affected by other parameters governing the system.

Materials and Methods

Cell lines. A431 cells (ATCC) and A431 cells stably transfected with destabilized EGFP (A431-d2EGFP) (Liu et al. 2014) were cultured in DMEM (ATCC) supplemented with 10% heat-inactivated FBS (Life

Technologies). The A431-d2EGFP cells were additionally supplemented with 0.1mg/mL G418 (Corning). All cell lines were maintained at 37°C and 5% CO_2 in a humidified incubator.

Affinity maturation of p19. Affinity maturation of p19 was performed using standard yeast surface display techniques as previously described[24] with select modifications noted below. For library construction, p19 (containing the C133S and C159A substitutions) was amplified by error-prone PCR as described[25] using either 2μM or 4μM nucleotide analogues. The 5' end of the genes contained a 39 base pair overlap with the 3' end of human Fc, followed by a $(G_4S)_5$ linker. hFc (wild-type IgG1) was amplified using Q5 hot start high-fidelity polymerase (NEB) following manufacturer's protocol. The hFc-$(G_4S)_5$-p19 gene fragments were assembled into the vector pCTCON2 by homologous recombination in yeast. The resulting libraries were screened by FACS using kinetic sorting methods described in Boder et al. Three siRNA sequences were used for selection: AllStars Negative Control siRNA labeled with Cy5, which did not have any chemical modifications (Qiagen); Factor VII siRNA labeled with Alexa Fluor 647, containing 2'OMe modifications (provided by Alnylam Pharmaceutics); and luciferase siRNA labeled with Cy5.5, containing 2'OMe modifications (provided by Alnylam Pharmaceutics). Dissociation was performed in PBSA containing 55% mouse serum (EMD Millipore) at 37°C. Unmodified and unlabeled luciferase siRNA was added at a 100-fold molar excess over the estimated concentration of labeled siRNA (final concentration was 1.7-2.5μM). A set of sequential selections using the three different siRNAs was performed twice. A dissociation time of 15 minutes was used in the first cycle, and 60 minutes in the second.

Protein expression and purification. C225.2 and $PFO^{T490A,L491V}$ were expressed, purified and complexed as previously described (Yang et al. 2015). p19, p19-E6, p19-E18 clones and E18 were expressed from the pE-SUMO vector (LifeSensors) in Rosetta 2 (DE3) E. coli (Novagen) and purified by Talon metal affinity chromatography (Clontech) as previously described (Yang et al. 2015). The sumo tag from E18 was left uncleaved, as it was expected to improve solubility without affecting binding to EGFR. All p19 constructs were purified by anion exchange chromatography (AEX) using a HiTrap Q HP anion exchange column (GE Healthcare) with an increasing salt gradient (10mM to 500mM NaCl) in 20mM bis-tris, pH 6.5. Size-exclusion chromatography (SEC) was performed using a Superdex 75 10/300 GL column (GE Healthcare) in PBS. All protein were flash frozen and stored at -80°C.

Dynamic Light Scattering. Targeted p19 constructs were analyzed at 5μM (dimer concentration; 0.31mg/mL) in PBS either alone or complexed with luciferase siRNA at a molar ratio of 1:1 (p19 dimer : siRNA) for 30 minutes at 4°C. 50μL of each sample was equilibrated to 25°C and analyzed with the

DynaPro NanoStar Light Scatterer (Wyatt Technology, Santa Barbara, CA) using the Dynamics software (Wyatt Technology, Santa Barbara, CA). Each run consisted of 20 acquisitions (10 seconds per acquisition), and two runs were performed per sample.

Biolayer Interferometry. All measurements were performed in citrate-phosphate buffer containing 100mM NaCl, 0.1% BSA and 0.002% tween-20 (at pH 7.4 or 5.5) at 37°C using an Octet RED96 instrument (Pall ForteBio LLC). Biotinylated hFc-EGFR (Traxylmayr et al) or biotinylated siRNA (provided by Alnylam Pharmaceutics) was captured on streptavidin-coated BLI tips (Pall ForteBio). The siRNA contained scattered 2'OMe modifications and biotin was conjugated to the 3' end of the sense strand, separated by a hexaethyleneglycolphosphate linker. Binding to EGFR was measured for both empty p19-E6,E18 constructs and p19-E6,E18/siRNA complexes. The complexes were prepared by incubating p19-E6,E18 and siRNA at a 1:1 molar ratio (p19 dimer : siRNA) for 30 minutes at 4°C. The siRNA used for complexation was against luciferase and did not contain any chemical modifications. Association to EGFR was analyzed at various concentrations of targeted p19 constructs (2-fold dilutions from 10nM to 0.16nM for p19-E6,E18 and p19-E6,E18/siRNA binding to EGFR; 2-fold dilutions from 25nM to 0.78nM for untargeted p19 binding to siRNA; 2-fold dilutions from 10nM to 0.31nM for untargeted p19 mutants binding to siRNA), followed by dissociation in buffer. The buffer baseline from loaded tips was subtracted from the data, which were then globally fitted to a 1:1 binding model to obtain apparent affinities.

Silencing assays. A431 or A431-d2EGFP cells were seeded at a density of 15,000 cells/well in 96 well plates 16-20 hours prior to the experiment, in media containing 0.1mg/mL G418. p19 constructs were mixed with either Negative Control AllStars siRNA (Qiagen) or GFP Duplex I siRNA (Dharmacon) at a 1:1 molar ratio (p19 dimer : siRNA) for 30 minutes at 4°C. The p19/siRNA complexes were then serially diluted in DMEM, 10% FBS containing either 5nM C225.2/10nM $PFO^{T490A,L491V}$ or 0.5nM C225.2/1nM $PFO^{T490A,L491V}$, and added to cells. In the alternative assay orientation, C225.2/ $PFO^{T490A,L491V}$ was serially diluted in DMEM, 10% FBS containing 50 nM, 5 nM or 0.5 nM of p19/siRNA. Cells were transfected for 6 hours, followed by incubation in fresh, complete media for an additional 18 hours. Cells were then trypsinized, neutralized by PBSA + 2% FBS, and analyzed on the BD LSR II HTS cytometer (BD Biosciences). Background from A431 cells (no EGFP) was subtracted from all measurements. The background-subtracted measurements were then normalized to that of untreated cells (when p19/siRNA or C225.2/$PFO^{T490A,L491V}$ was used alone) or of cells treated only with the single agent whose concentration was fixed (when both p19/siRNA and C225.2/$PFO^{T490A,L491V}$ were used in combination).

Viability assays. Cell viability was measured using the WST-1 reagent (Roche) with a 40 minute incubation at 37°C, following previously described methods (Liu et al. MTNA 2014). Background-subtracted measurements were normalized following the scheme described in *Silencing assays*.

Uptake assays. A431-d2EGFP cells were seeded at a density of 15,000 cells/well in 96 well plates 16-20 hours prior to the experiment, in media containing 0.1mg/mL G418. Targeted p19 constructs were mixed with Factor VII siRNA labeled with AF647 (provided by Alnylam Pharmaceutics) for 30 minutes at 4°C. The p19/siRNA complexes were then diluted in DMEM, 10% FBS and incubated with cells for varying periods of time up to 6 hours. Cells were washed twice with PBS, trypsinized, washed twice with cold PBSA + 2% FBS and analyzed on an iQue Screener (IntelliCyt). All liquid handling was performed using an EL406 plate washer (BioTek) and a Freedom EVO 150 liquid handling system (Tecan) to minimize variability during processing. Background from untreated cells were subtracted from all measurements, which were then converted to number of fluorophores using Quantum Alexa Fluor 647 MESF beads following manufacturer's protocol (Bangs Laboratories).

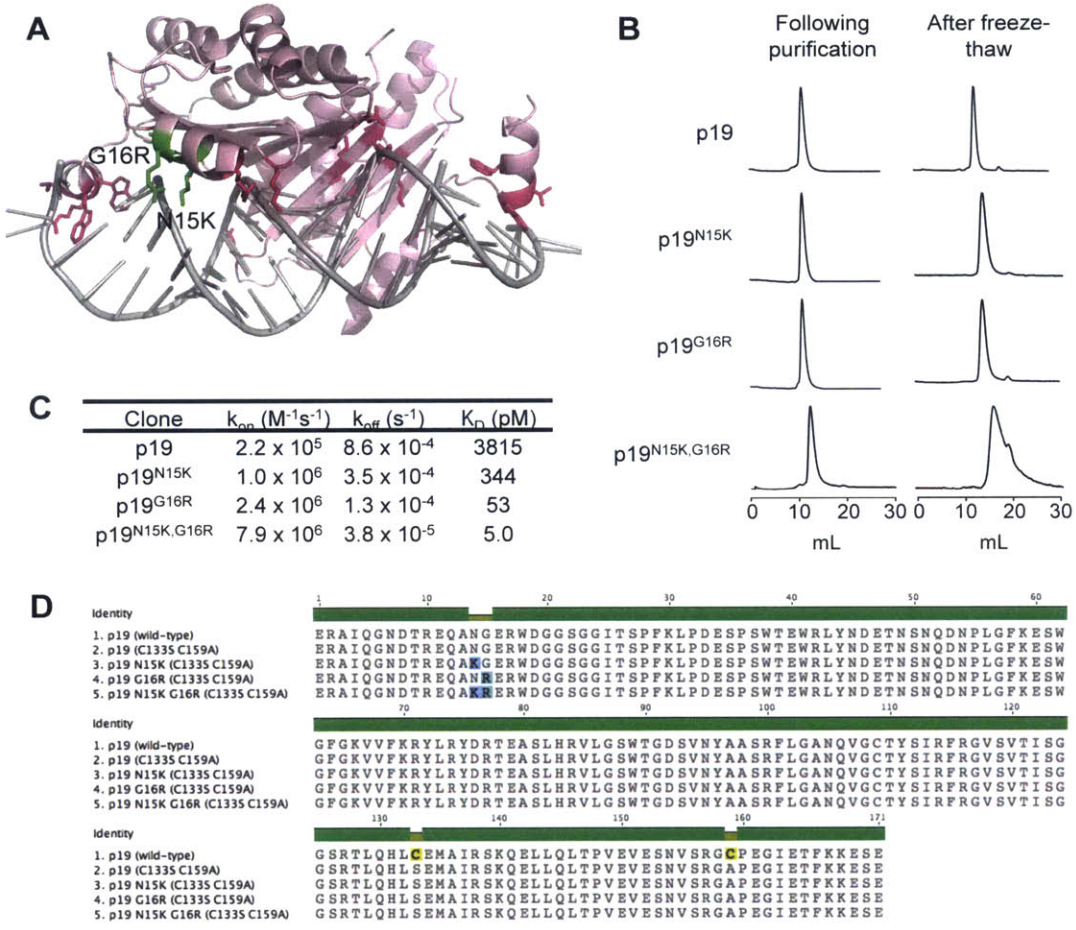

Clone	k_{on} ($M^{-1}s^{-1}$)	k_{off} (s^{-1})	K_D (pM)
p19	2.2×10^5	8.6×10^{-4}	3815
$p19^{N15K}$	1.0×10^6	3.5×10^{-4}	344
$p19^{G16R}$	2.4×10^6	1.3×10^{-4}	53
$p19^{N15K,G16R}$	7.9×10^6	3.8×10^{-5}	5.0

Figure 3.1. Characterization of affinity-matured p19 clones. (a) Crystal structure of CIRV p19 (PDB 1RPU). Native residues involved in electrostatic or stacking interactions with the dsRNA are highlighted in pink. The N15K and G16R substitutions identified from directed evolution screens are highlighted in green. **(b)** Sequences of the p19 clones used in this study. All clones used for functional analysis contained the C133S and C159A substitutions to prevent crosslinking. **(c)** SEC analysis of the p19 clones. 30µg of protein at 1.0 mg/mL was analyzed on a Superdex 75 column. **Left:** Analysis of proteins immediately following purification. **Right:** Analysis after a single freeze-thaw cycle. **(e)** Binding kinetics of the p19 clones (containing the C133S, C159A substitutions) analyzed by Biolayer Interferometry (BLI). Shown are the averages of two measurements.

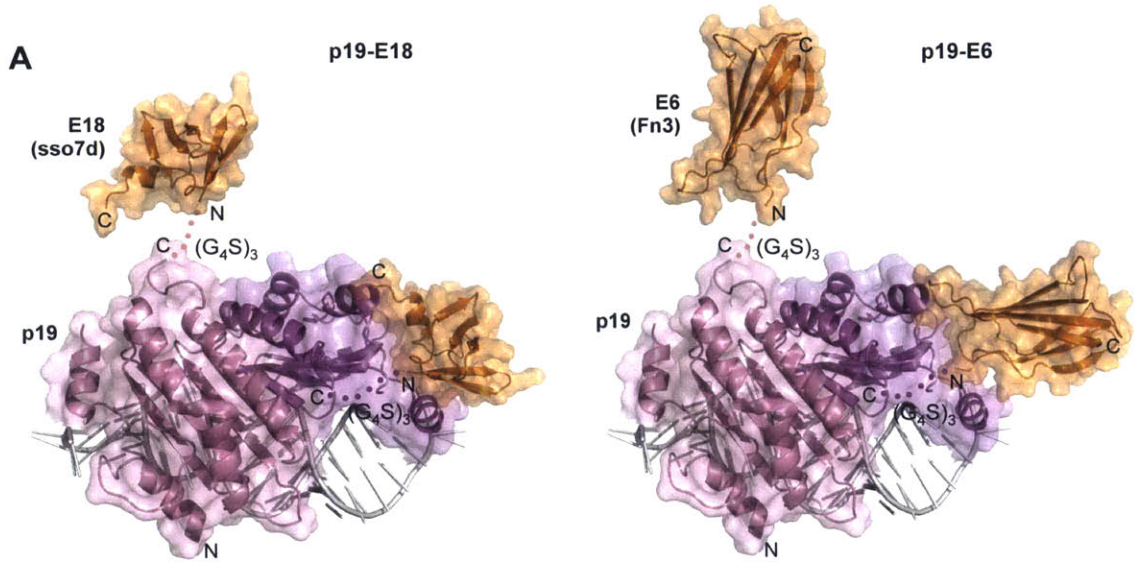

B

	pH 7.4			pH 5.5		
Clone	k_{on} ($M^{-1}s^{-1}$)	k_{off} (s^{-1})	K_D (nM)	k_{on} ($M^{-1}s^{-1}$)	k_{off} (s^{-1})	K_D (nM)
p19-E6	1.4×10^5	1.6×10^{-4}	1.2	1.5×10^5	1.6×10^{-4}	1.1
p19-E6/siRNA	1.6×10^5	1.0×10^{-4}	0.6	2.9×10^5	1.3×10^{-4}	0.4
p19-E18	1.8×10^5	4.0×10^{-4}	2.2	2.0×10^5	4.0×10^{-4}	2.8
p19-E18/siRNA	1.6×10^5	1.5×10^{-4}	0.9	4.1×10^5	2.4×10^{-4}	0.6

C

	w/o siRNA			w/siRNA		
Clone	Diameter (nm)	% Polydispersity	% Mass	Diameter (nm)	% Polydispersity	% Mass
p19-E6	7.1	13	98	7.9	20	97
$p19^{N15K}$-E6	7.5	10	90	7.3	12	82
$p19^{G16R}$-E6	8.1	10	95	8.3	22	99
$p19^{N15K,G16R}$-E6	7.6	8	92	8.3	11	99
p19-E18	6.7	13	97	6.8	23	100
$p19^{N15K}$-E18	8.2	15	100	8.2	28	100
$p19^{G16R}$-E18	7.6	37	100	8.8	35	100
$p19^{N15K,G16R}$-E18	8.2	24	100	8.7	29	100

Figure 3.2. Characterization of EGFR-targeted p19 clones. (a) Schematic of the two fusion formats used in the study (modified from PDB ID 1RPU, 1TTG and 1SSO). **Left:** E18 (orange), an EGFR binder engineered on a modified sso7d scaffold, was fused to the C terminus of p19 (each monomer in pink and purple) separated by a $(G_4S)_3$ linker. **Right:** Analogous fusion construct with E6 (orange), an EGFR binder engineered on the Fn3 scaffold. **(b)** Binding kinetics of empty or siRNA-loaded p19 constructs measured by Biolayer Interferometry (BLI). All analyses were performed in citrate-phosphate buffer at 37°C. Shown are the averages of two independent measurements. **(c)** Size distribution of empty or siRNA-loaded p19 constructs measured by Dynamic Light Scattering (DLS). All samples were analyzed at 5μM (p19 dimer concentration; 0.31mg/mL) in PBS at 25°C. Shown are the averages of two independent measurements.

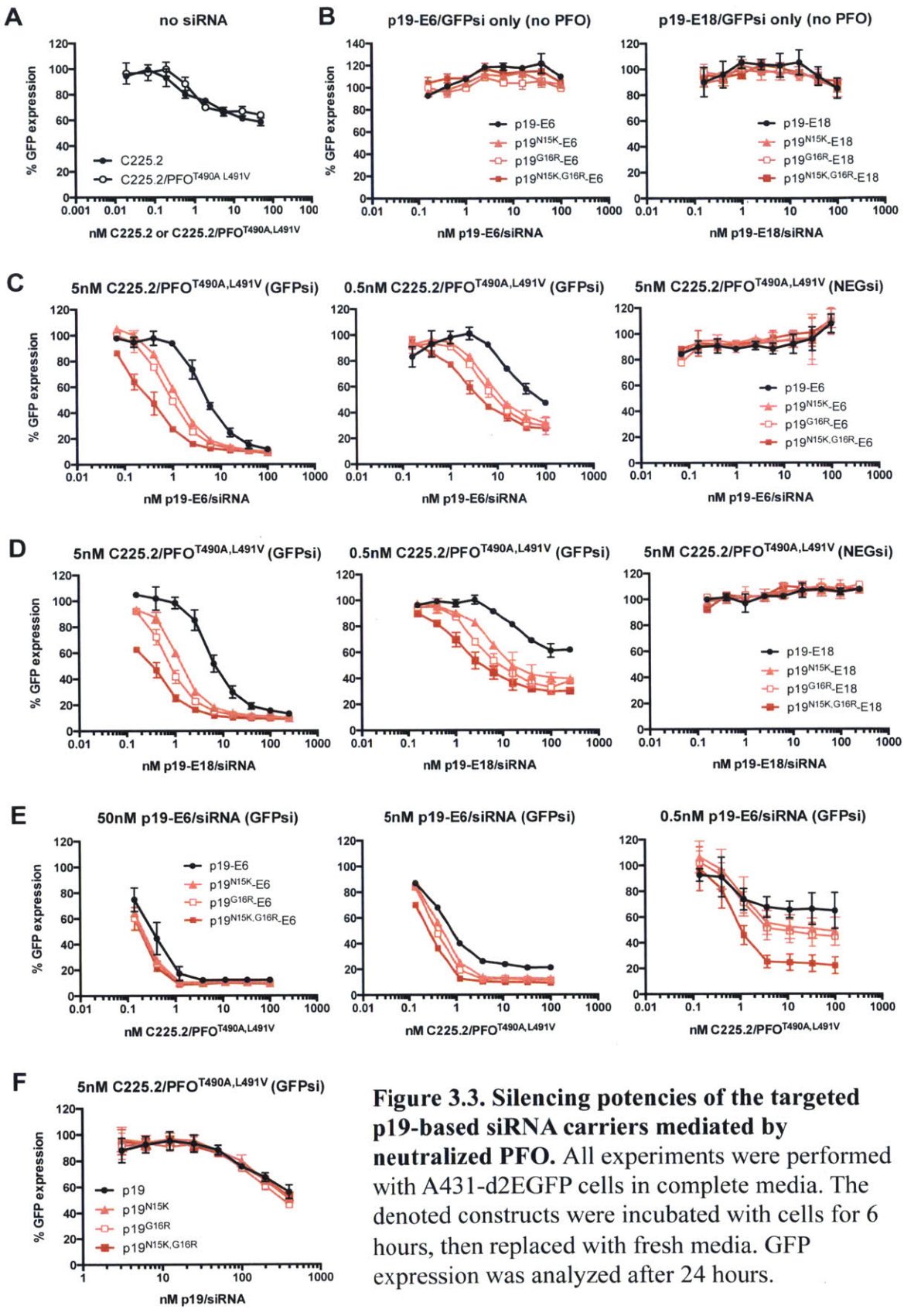

Figure 3.3. Silencing potencies of the targeted p19-based siRNA carriers mediated by neutralized PFO. All experiments were performed with A431-d2EGFP cells in complete media. The denoted constructs were incubated with cells for 6 hours, then replaced with fresh media. GFP expression was analyzed after 24 hours.

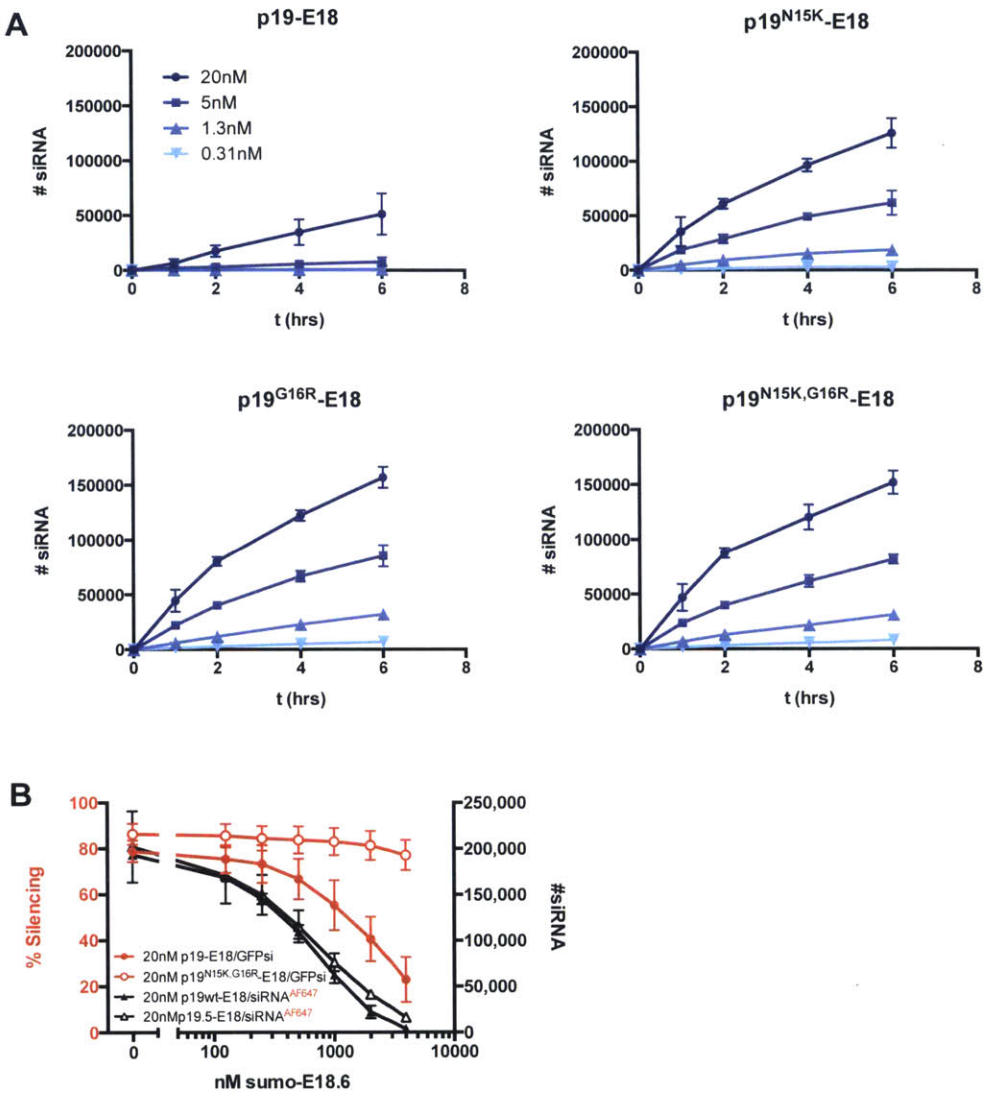

Figure 3.4. Comparing siRNA uptake and silencing between p19 mutants. (a) Time- and concentration-dependent uptake of siRNA mediated by each p19-E18 clone. p19-E18 constructs were complexed with AF647-conjugated siRNA, diluted in complete media to the indicated concentrations, and incubated with A431-d2EGFP cells for varying periods of time. **(b)** siRNA uptake and silencing in the presence of a competitor for receptor binding. The concentration of p19-E18/siRNA and $p19^{N15K,G16R}$-E18/siRNA complexes were fixed at 20nM, a saturating concentration for binding to both siRNA and EGFR. Increasing concentrations of sumo-tagged E18 (without p19) were included to titrate down the number of internalized siRNAs. Fluorescently labeled siRNA were used for quantitating uptake, and unlabeled GFP siRNA were used to measure silencing under matching conditions.

Works cited

1 Kanasty R, Dorkin JR, Vegas A, Anderson D. Delivery materials for siRNA therapeutics. *Nat Mater* 2013; **12**: 967–977.

2 Wittrup A, Ai A, Liu X, Hamar P, Trifonova R, Charisse K *et al.* Visualizing lipid-formulated siRNA release from endosomes and target gene knockdown. *Nat Biotechnol* 2015; **33**: 870–876.

3 Gilleron J, Querbes W, Zeigerer A, Borodovsky A, Marsico G, Schubert U *et al.* Image-based analysis of lipid nanoparticle-mediated siRNA delivery, intracellular trafficking and endosomal escape. *Nat Biotechnol* 2013; **31**: 638–646.

4 Cuellar TL, Barnes D, Nelson C, Tanguay J, Yu S-F, Wen X *et al.* Systematic evaluation of antibody-mediated siRNA delivery using an industrial platform of THIOMAB–siRNA conjugates. *Nucleic Acids Res* 2015; **43**: 1189–1203.

5 Sahay G, Querbes W, Alabi C, Eltoukhy A, Sarkar S, Zurenko C *et al.* Efficiency of siRNA delivery by lipid nanoparticles is limited by endocytic recycling. *Nat Biotechnol* 2013; **31**: 653–658.

6 Alabi CA, Love KT, Sahay G, Yin H, Luly KM, Langer R *et al.* Multiparametric approach for the evaluation of lipid nanoparticles for siRNA delivery. *Proc Natl Acad Sci* 2013; **110**: 12881–12886.

7 Kumar P, Ban H-S, Kim S-S, Wu H, Pearson T, Greiner DL *et al.* T Cell-Specific siRNA Delivery Suppresses HIV-1 Infection in Humanized Mice. *Cell* 2008; **134**: 577–586.

8 Song E, Zhu P, Lee S-K, Chowdhury D, Kussman S, Dykxhoorn DM *et al.* Antibody mediated in vivo delivery of small interfering RNAs via cell-surface receptors. *Nat Biotechnol* 2005; **23**: 709–717.

9 Love KT, Mahon KP, Levins CG, Whitehead KA, Querbes W, Dorkin JR *et al.* Lipid-like materials for low-dose, in vivo gene silencing. *Proc Natl Acad Sci* 2010; **107**: 1864–1869.

10 Eguchi A, Meade BR, Chang Y-C, Fredrickson CT, Willert K, Puri N *et al.* Efficient siRNA delivery into primary cells by a peptide transduction domain–dsRNA binding domain fusion protein. *Nat Biotechnol* 2009; **27**: 567–571.

11 Choi K, Park GL, Hwang KY, Lee J-W, Ahn HJ. Efficient siRNA Delivery into Tumor Cells by p19-YSA Fusion Protein. *Mol Pharm* 2013; **10**: 763–773.

12 Liu DV, Yang NJ, Wittrup KD. A Nonpolycationic Fully Proteinaceous Multiagent System for Potent Targeted Delivery of siRNA. *Mol Ther — Nucleic Acids* 2014; **3**: e162.

13 Vargason JM, Szittya G, Burgyán J, Hall TMT. Size Selective Recognition of siRNA by an RNA Silencing Suppressor. *Cell* 2003; **115**: 799–811.

14 Yang NJ, Liu DV, Sklaviadis D, Gui DY, Vander Heiden MG, Wittrup KD. Antibody-Mediated Neutralization of Perfringolysin O for Intracellular Protein Delivery. *Mol Pharm* 2015; **12**: 1992–2000.

15 Cheng J, Koukiekolo R, Kieliszkiewicz K, Sagan SM, Pezacki JP. Cysteine residues of Carnation Italian Ringspot virus p19 suppressor of RNA silencing maintain global structural integrity and

stability for siRNA binding. *Biochim Biophys Acta BBA - Proteins Proteomics* 2009; **1794**: 1197–1203.

16 Hackel BJ, Neil JR, White FM, Wittrup KD. Epidermal growth factor receptor downregulation by small heterodimeric binding proteins. *Protein Eng Des Sel* 2012; **25**: 47–57.

17 Traxlmayr MW, Kiefer JD, Srinivas RR, Lobner E, Tisdale AW, Mehta N *et al.* Strong enrichment of aromatic residues in binders from a charge-neutralized hyperthermostable Sso7d-library. *Manuscript in preparation.*

18 Gera N, Hussain M, Wright RC, Rao BM. Highly Stable Binding Proteins Derived from the Hyperthermophilic Sso7d Scaffold. *J Mol Biol* 2011; **409**: 601–616.

19 Rodova M, Jayini R, Singasani R, Chipps E, Islam MR. CMV promoter is repressed by p53 and activated by JNK pathway. *Plasmid* 2013; **69**: 223–230.

20 Fanger GR, Johnson NL, Johnson GL. MEK kinases are regulated by EGF and selectively interact with Rac/Cdc42. *EMBO J* 1997; **16**: 4961–4972.

21 Wiley HS. Trafficking of the ErbB receptors and its influence on signaling. *Exp Cell Res* 2003; **284**: 78–88.

22 Bartlett DW, Davis ME. Insights into the kinetics of siRNA-mediated gene silencing from live-cell and live-animal bioluminescent imaging. *Nucleic Acids Res* 2006; **34**: 322–333.

23 Bartlett DW, Davis ME. Effect of siRNA nuclease stability on the in vitro and in vivo kinetics of siRNA-mediated gene silencing. *Biotechnol Bioeng* 2007; **97**: 909–921.

24 Angelini A, Chen TF, de Picciotto S, Yang NJ, Tzeng A, Santos MS *et al.* Protein Engineering and Selection Using Yeast Surface Display. *Methods Mol Biol Clifton NJ* 2015; **1319**: 3–36.

25 Chen TF, de Picciotto S, Hackel BJ, Wittrup KD. Engineering Fibronectin-Based Binding Proteins by Yeast Surface Display. In: *Methods in Enzymology*. Elsevier, 2013, pp 303–326.

Ch4. Perspectives on In Vivo Delivery using Antibody-Neutralized Perfringolysin O

Introduction

Given the widened therapeutic window of PFO achieved with the neutralizing antibody system in vitro (Chapter 2), we next sought to determine whether this improvement could be extended to an in vivo setting. Thus, we investigated whether the C225.2/PFO system was capable of delivering E6rGel intracellularly in an A431 tumor model, a setup that was analogous to our in vitro experiments. The degree of delivery was measured by the degree of synergistic cell killing occurring between C225.2/PFO and E6rGel, evidenced at a gross level by a regression in tumor growth. The toxicity of the system was measured by monitoring the body weight of treated animals.

Precedent using PFO or other cholesterol-dependent cytolysins (CDCs) as a delivery tool in vivo is limited, likely mirroring the same challenges of having a narrow therapeutic window. Despite so, three different approaches have been proposed with utilizing CDCs for in vivo delivery.

First, live, attenuated *Listeria monocytogenes* that secrete tumor-associated antigens (TAAs) has been used to deliver antigens to antigen-presenting cells (APC) as a cancer vaccine[1]. *Listeria monocytogenes* expresses the CDC Listerolysin O (LLO), which along with two phospholipases, allows the bacteria to escape from phagosomes to colonize the host cell[2]. Interestingly, the TAAs were also fused to a truncated form of LLO[3] that lacks the domain responsible for membrane binding. While this truncated LLO construct had severely reduced hemolytic function, it acted as an effective adjuvant that stimulated the secretion of proinflammatory cytokines and induced APC maturation[4]. Overall, this live bacteria-based cancer vaccine demonstrated efficacy in preclinical models[5] and is currently undergoing clinical evaluation. However, while this approach is suitable for targeting APCs such as macrophages, which actively phagocytose pathogens, it is unclear how readily malignant tissue and cell types can be targeted using this strategy. Furthermore, systemic administration of bacteria may elicit immune responses that compromise safety or preclude multiple dosing.

Second, LLO has been incorporated into liposomes, along with payloads such as protein antigens or DNA vaccines, for delivery to APCs. This system was reported to generate specific cytolytic T cell (CTL) responses to the model antigen OVA and the nucleoprotein (NP) of the lymphocytic choriomeningitis virus (LCMV), leading to protection in an OVA-expressing cancer model or against viral challenge[6–8]. However, given that LLO is an adjuvant that has been incorporated as part of a vaccine, it is difficult to differentiate its effect in mediating cytosolic delivery versus stimulating the immune

response. Alternatively, a design variation where LLO was fused to protamine for gene delivery was also proposed, with preliminary results reporting luciferase expression in the spleen and lung following intravenous admistration[9]. Further characterization of this system remains to demonstrate its efficacy.

Third, from our own group, Pirie et al. showed that an EGFR-targeted PFO construct (E6-PFO) can potentiate the cell-killing activity of a carcinoembryonic antigen (CEA)-targeted gelonin construct (C7-rGel) in vivo, using a xenograft model of a cell line that expresses both receptors[10]. The synergistic cell killings that were observed was likely due to PFO mediating the intracellular delivery of gelonin, demonstrating proof-of-concept that a payload and a membrane-permeablizing agent can be administered *in trans* to allow cytosolic delivery in vivo. However, the toxicity accompanying this combination treatment (necessitating the euthanasia of one out of the three treated mice) underscored that the central problem of having a narrow therapeutic window remained unresolved.

Thus, we investigated whether the antibody-neutralized PFO system could provide an extended therapeutic window necessary for it to be a viable therapeutic strategy. Two PFO mutants were considered for this application, both of which had shown effective delivery with low toxicity in vitro: $PFO^{T490G,L491G}$, which is strongly attenuated, and $PFO^{T490A,L491V}$, which is attenuated to a lesser degree. We found that C225.2/$PFO^{T490G,L491G}$ was well-tolerated in vivo in combination with E6rGel, but was unable to deliver the payload to a significant degree enough to affect tumor growth. C225.2/$PFO^{T490A,L491V}$ demonstrated poor biodistribution properties, accumulating mainly in the liver. The resulting hepatotoxicity, caused in combination with E6rGel, was dose limiting. Overall, the antibody-neutralized PFO system successfully improved the in vivo tolerance of PFO but will require further improvements to effectively target the tumor compartment for specific delivery. Considerations and ideas for such are discussed.

Results

C225.2 improves the in vivo tolerance of PFO. To determine whether the reduction in PFO's toxicity by C225.2 observed in vitro also extended to an in vivo setting, we performed dose-escalation studies in healthy NOD scid gamma (NSG) mice comparing the tolerance of PFO in free or C225.2-loaded form. The NSG model was chosen to isolate effects of toxicity from immunogenicity, and in anticipation of using an A431 xenograft tumor model for assessing delivery. The complexes C225.2/PFO, C225.2/$PFO^{T490A,L491V}$ and C225.2/$PFO^{T490G,L491G}$ were prepared as previously described[11]. Mice were administered with each complex at varying doses every three days, for a total of five treatments. Body weight was monitored daily and normalized to that at Day 0.

For all PFO clones, we observed an oscillating pattern where body weight decreased sharply in a dose-dependent manner immediately following administration, followed by gradual recovery over the course of days (**Figure 4.1A**). This result suggested that while C225.2-loaded PFO can possess residual toxicity at higher doses, the conflicted damage is reversible, at least within the two-week period of continual dosing. In addition, we did not observe any accumulative toxicity from repeated dosing. Generally, a dose that was well tolerated after a single administration was also well tolerated after repeated dosing. Conversely, signs of dose-limiting toxicity were evident immediately following administration for ill tolerated doses. Overall, the toxicities caused by the C225.2/PFO complexes were acute and reversible, consistent with its pore-forming mode of action.

The highest dose at which no loss in body weight was observed at the end of the two-week monitoring period was defined as the maximum tolerated dose (MTD) (**Figure 4.1B**). As expected, the attenuated mutants PFO^{T490A,L491V} and PFO^{T490G,L491G} were significantly better tolerated than wild-type PFO. Loading the PFO clones onto C225.2 consistently increased their respective MTDs, indicating that C225.2 and PFO were maintaining association *in vivo* and the neutralizing antibody C225.2 was functioning as intended.

C225.2/PFO^{T490G,L491G} demonstrates favorable targeting but weak delivery. To further confirm that C225.2 and PFO were maintaining association *in vivo*, leading to better tumor targeting properties, we first characterized the pharmacokinetics and biodistribution of PFO^{T490G,L491G} in free or C225.2-loaded form. Healthy NSG mice were used for pharmacokinetics measurements, and mice bearing subcutaneous xenografts of the A431 cell line were used for biodistribution measurements. We hypothesized that association with C225.2 would extend the circulation time of PFO^{T490G,L491G} through the long half-life of the antibody. Subsequently, the high concentration gradient maintained between the plasma compartment and the tumor, combined with active targeting of EGFR via C225.2, were expected to increase the fraction of injected PFO^{T490G,L491G} accumulating at the target tumor site.

Indeed, whereas PFO^{T490G,L491G} was rapidly cleared from plasma, as expected for a molecule its size (53kDa) without an active retention mechanism, C225.2/PFO^{T490G,L491G} displayed significantly slower clearance, with a half-time of 4 hours and 59 hours for the α- and β-phase, respectively (**Figure 4.2A**). In addition, PFO^{T490G,L491G} loaded onto C225.2, but not C225, showed significantly higher levels of accumulation in the tumor compared to free PFO^{T490G,L491G} (C225.2/PFO^{T490G,L491G} vs PFO^{T490G,L491G} $P = 0.0263$; C225.2/PFO^{T490G,L491G} vs C225/PFO^{T490G,L491G} $P = 0.0266$) (**Figure 4.2B**). Overall, these results demonstrated that C225.2 was simultaneously neutralizing PFO^{T490G,L491G} and targeting it to the tumor compartment as designed.

Next, to determine whether C225.2/PFO^{T490G,L491G} is capable of mediating intracellular delivery *in vivo*, we employed an experimental setup analogous to that used *in vitro* (Chapter 2). In short, mice bearing subcutaneous xenografts of A431 cells were treated with either C225.2/PFO^{T490G,L491G} alone, E6rGel alone, or both in combination. We reasoned that C225.2/PFO^{T490G,L491G}-mediated release of E6rGel in the tumor would enable synergistic cell killing, resulting in a retardation or regression in tumor growth at the gross level. Constructs were administered either intratumorally, bypassing transport to the tumor, or intravenously (retro-orbitally), a more physiologically relevant route. The combination treatment with both C225.2/PFO^{T490G,L491G} and E6rGel was well tolerated following intravenous administration, with no loss in body weight (**Figure 4.2D**). However, with neither routes of administration was there a significant growth delay observed in groups treated with both agents in combination, compared to those that received each agent individually (**Figure 4.2C** and **4.2D**). Although we could estimate that the amount of C225.2/PFO^{T490G,L491G} and E6rGel accumulating in the tumor was sufficient to enable release, based on biodistribution data and the *in vitro* potency curve, the lack of synergistic cell killing suggested that achieving similar potencies *in vivo* may require higher concentrations of C225.2/PFO^{T490G,L491G} or the payload due to properties unique to the tumor microenvironment.

C225.2/PFO^{T490A,L491V} is limited by potent delivery occurring off-target. As the more attenuated PFO^{T490G,L491G} clone failed to enable delivery *in vivo*, we next investigated the pharmacokinetics, biodistribution and delivery potency of the lesser attenuated PFO^{T490A,L491V} clone. In contrast to previous experiments where only the PFO^{T490G,L491G} portion of the C225.2/PFO^{T490G,L491G} complex was tracked, we labeled both C225.2 and PFO^{T490A,L491V} with separate dyes to gain a more complete understanding of their individual behaviors. The dual-labeled C225.2/PFO^{T490A,L491V} complex was prepared in an identical manner as with the unlabeled complex.

In contrast to previous observations with PFO^{T490G,L491G}, where loading onto C225.2 extended its serum persistence and tumor accumulation, PFO^{T490A,L491V} demonstrated rapid clearance and dominant liver accumulation despite being loaded onto C225.2 (**Figure 4.3A** and **4.3B**). In addition, the C225.2 portion of the complex showed extremely rapid clearance in the α-phase, followed by slower clearance in the β-phase (**Figure 4.3A**). Tumor accumulation was poor also for C225.2 (**4.3B**). The molar ratio of PFO^{T490A,L491V} to C225.2 accumulated in the tumor following intravenous (retro-orbital) administration was 0.26, indicating that most of PFO^{T490A,L491V} had dissociated from C225.2 prior to entering the tumor compartment (**Figure 4.3C**). In contrast, C225.2/PFO^{T490A,L491V} administered intratumorally had an average molar ratio of 2.9 (PFO^{T490A,L491V} : C225.2), closer to the theoretical value of 2. Overall, these results suggested that PFO^{T490A,L491V} may be causing the C225.2/PFO^{T490A,L491V} complex to have faster

plasma clearance and increased liver capture, and that $PFO^{T490A,L491V}$ is dissociating prematurely from C225.2 without benefiting from the targeting functionality of C225.2.

$PFO^{T490A,L491V}$'s premature dissociation from C225.2 was particularly puzzling in comparison with $PFO^{T490G,L491G}$'s extended association with C225.2. As both PFO clones were loaded onto C225.2 via the same PFO binder, it had been expected that their dissociation kinetics from C225.2 would also be identical. A potential explanation for this discrepancy is that $PFO^{T490G,L491G}$ also dissociates rapidly from C225.2, but at high concentrations in the plasma, is able to rebind to the bi-specific antibody. In contrast, $PFO^{T490A,L491V}$, whose affinity for membrane cholesterol is less attenuated than $PFO^{T490G,L491G}$, may be captured onto "membrane sinks" in the vicinity instead of rebinding to C225.2. This explanation was plausible given that we measured dissociation rate of (avi-tagged) PFO from C225.2 to be 9.5×10^{-5} s^{-1} (in 2mL of 50% serum at 37°C; data not shown), which translates to a half-life of 2 hours. In addition, the C225.2/$PFO^{T490A,L491V}$ complex may also suffer from non-specific binding mediated by $PFO^{T490A,L491V}$, leading to faster clearance. Although previous *in vitro* experiments demonstrated that loading $PFO^{T490A,L491V}$ onto C225.2 blocks the former protein from associating with mammalian membranes (**Figure 2.3B**), likely via steric hindrance from C225.2, we speculate that this steric hindrance may be reduced in a sheer flow environment.

To investigate whether C225.2/$PFO^{T490A,L491V}$ could mediate intracellular delivery should its transport problem is solved, we treated xenografted A431 tumors intratumorally with C225.2/$PFO^{T490A,L491V}$ alone, E6rGel alone, or both in combination. The combination treatment showed strong regression of tumor growth under conditions where the individual agents had no effect (**Figure 4.3D**). The synergistic cell killing observed only when both agents were present strongly indicated that C225.2/$PFO^{T490A,L491V}$ was enabling E6rGel to access the cytoplasm. In contrast, intravenous (retro-orbital) administration of the C225.2/$PFO^{T490A,L491V}$ and E6rGel combination caused no significant regression of tumor growth, while causing substantial weight loss even when the dose was reduced (**Figure 4.4E**). It should be noted that the dose of C225.2/$PFO^{T490A,L491V}$ and E6rGel had to be significantly reduced for the treatment to be tolerable. Despite so, a significant loss in body weight was observed, which was reversible once treatment ceased. We observed histological signs of severe hepatotoxicity in mice that received the combination treatment intravenously (in consultation with veterinary pathologist Dr. Roderick Bronson, Harvard Medical School; data not shown). In combination with earlier results which showed that the majority of injected C225.2/$PFO^{T490A,L491V}$ accumulates in the liver, the dose-limiting hepatotoxicity suggests that C225.2/$PFO^{T490A,L491V}$ is effectively mediating the delivery of E6rGel in the liver.

Discussion

In this study, we demonstrated that the C225.2-loaded $PFO^{T490G,L491G}$ and $PFO^{T490A,L491V}$ clones have differing in vivo properties. While their net tolerances were both improved by complexation onto C225.2, C225.2/$PFO^{T490G,L491G}$ preferentially accumulated in the tumor, whereas C225.2/$PFO^{T490A,L491V}$ preferentially accumulated in the liver. Despite localizing to the tumor, C225.2/$PFO^{T490G,L491G}$ failed to deliver E6rGel intracellularly to an appreciative degree to affect tumor growth. In contrast, when combined with E6rGel, C225.2/$PFO^{T490A,L491V}$ caused dose-limiting hepatotoxicity, which suggested that efficient delivery of gelonin was occurring in the liver. Reducing the dose of C225.2/$PFO^{T490A,L491V}$ to a tolerable level did not cause a significant regression in tumor growth, indicating that the delivery efficiency was sub-optimal in the tumor compartment.

Comparing the pharmacokinetics of C225.2/$PFO^{T490G,L491G}$ and C225.2/$PFO^{T490A,L491V}$ suggested that PFO may be dissociating and rebinding to C225.2 during circulation. This was certainly plausible given that the dissociation half-time of PFO from C225.2 was measured to be 2 hours. Then, following dissociation, $PFO^{T490A,L491V}$ was more likely to become captured on other cell membranes in the vicinity compared to $PFO^{T490G,L491G}$, due to its higher affinity for membrane cholesterol. The rapid clearance of C225.2 (in the C225.2/$PFO^{T490A,L491V}$ complex) in the α-phase suggested that the non-specific interaction between $PFO^{T490A,L491V}$ and cell membranes may also cause the entire C225.2/$PFO^{T490A,L491V}$ complex to become sequestered on irrelevant membranes as well.

Based on this reasoning, two potential directions may be taken to improve the tumor-targeting properties of $PFO^{T490A,L491V}$. First, to prevent $PFO^{T490A,L491V}$ from prematurely dissociating from C225.2 in the first place, the affinity of the PFO binder 1.2 may be further matured. While this approach is relatively straightforward to pursue using established directed evolution techniques, care must be given to ensure that PFO can be readily dissociated in endosomal compartments even if it is more tightly bound in the extracellular space. One way to assure prompt dissociation in endosomes is to maintain a low affinity at pH 5.5, although we have previously found the affinities at the different pHs tend to go hand-in-hand (**Figure 2.1B**). Alternatively, different stimuli-responsive elements may be incorporated to impart specificity for the endosomal environment, such as protease cleavage sites.

Second, in the event that C225.2/$PFO^{T490A,L491V}$ is still capable of associating with off-target cell membranes, an alternative binder to 1.2 that can directly interact with the membrane-binding loops of PFO may be engineered. As shown in Chapter 2, 1.2 interacts with the oligomerization interface of PFO, which is distinct and separated in distance from the membrane-binding domain of PFO (**Figure 2.1E**). Thus, 1.2 by itself is likely unable to prevent $PFO^{T490A,L491V}$ from binding to cell membranes. Having a binder that physically shields the membrane-binding loops of PFO would unequivocally prevent

C225.2/PFO^{T490A,L491V} from associating non-specifically with cell membranes. However, as before, with any binder, it must be ensured that PFO can dissociate promptly in endosomes.

If the tumor-targeting properties of C225.2/PFO^{T490A,L491V} can be improved even slightly, alternative approaches may be explored to increase the specificity of the treatment, such as using a payload with higher specificity. If the payload is capable of producing a biological response only in the tumor compartment, off-target responses (potentially causing dose-limiting toxicity) may be dramatically reduced. Indeed, the dose-limiting toxicity observed in this current study was partly a consequence of employing gelonin as the payload. While gelonin is a potent toxin that can provide a very sensitive readout for delivery, its mechanism of action cleaving ribosomal RNA and arresting translation is completely non-specific and harmful to overall health when carried out in other organs. If the payload can be chosen judiciously such that it exerts an effect only in the cytoplasm of cancerous cells, having some degree of off-target delivery in vital organs may not be as detrimental. Examples of such payloads include siRNA designed against oncogenes or genes that are synthetic-lethal with such.

Finally, although we have employed an immune-compromised mouse model for the current study to use the model cell line A431 (a human epithelial cancer cell line), it is anticipated that in a more realistic setting involving an intact immune system, the immunogenicity of PFO may be a problem. Humoral responses raised against PFO may limit efficacy by promoting clearance and preventing repeated dosing. Thus, for the reported pore-forming protein-based delivery system to be a viable therapeutic strategy in the long term, it may be necessary to substitute PFO with a pore-forming protein of human origin. Indeed, the pore-forming protein perforin secreted by CTLs has a structure very similar to that of PFO[12], indicating that its mechanism of action may also be similar. Consequently, successful design principles and strategies identified in the process of developing PFO as an intracellular system may be potentially transferable to perforin, to yield a delivery system with higher translatability.

Materials and Methods

Mice. Male NOD.Cg-*Prkdc*^{scid} *Il2rg*^{tm1Wjl}/SzJ (NSG) mice (Jackson Laboratory) were aged between 6 to 10 weeks for all studies. All animal work was conducted under the approval of the Massachusetts Institute of Technology (MIT) Division of Comparative Medicine (DCM) in accordance with federal, state, and local guidelines.

Dose escalation studies. PFO, PFO^{T490A,L491V} and PFO^{T490G,L491G}, in free or C225.2-loaded form, were administered retro-orbitally to NSG mice at the indicated doses every three days for five treatments total.

Body weight was monitored daily and normalized to the value at day 0 prior to the first injection. Mice were monitored daily for signs of morbidity, and euthanized when such were significant or when loss of body weight exceeded 15%.

Pharmacokinetic studies. C225.2, $PFO^{T490A,L491V}$ and $PFO^{T490G,L491G}$ were labeled with Alexa Fluor 488 NHS-Ester (Life Technologies), Alexa Fluor 647-NHS Ester (Life Technologies) and DyLight 800 NHS Ester (Thermo Fisher Scientific), respectively, following manufacturers' instructions, and unlabeled dye was removed using the HiPrep 26/10 Desalting column (GE Healthcare). The degree of labeling was determined by absorbance and the absence of free dye was confirmed by thin layer chromatography in 70% EtOH. C225.2/$PFO^{T490A,L491V}$ and C225.2/$PFO^{T490G,L491G}$ complexes with the labeled constructs were prepared as previously described[11]. 100μg of $PFO^{T490G,L491G}$, 159μg C225.2/100μg $PFO^{T490G,L491G}$ and 129μg C225.2/ 80 μg $PFO^{T490A,L491V}$ were administered retro-orbitally to NSG mice. Tail bleeds were performed at the indicated time intervals and collected in heparin-coated tubes (VWR). Blood samples were centrifuged at 600xg for 5 min, after which the serum was transferred to a fresh tube. All tubes were protected from light and kept at 4°C until analysis. Fluorescence was measured using the Typhoon FLA 7000 scanner (GE Healthcare) or Odyssey Infrared Imaging System (Li-Cor) and analyzed using ImageJ (NIH). Background from PBS-treated mice was subtracted from all measurements, followed by normalization to values at the first time point (30s). Data was fit to a two-phase decay ($Ae^{-\alpha t} + Be^{-\beta t}$) to obtain clearance fractions and rates.

Biodistribution studies. Labeled C225.2, $PFO^{T490A,L491V}$, $PFO^{T490G,L491G}$ and corresponding complexes were prepared as described in "Pharmacokinetic studies." A431 xenografts were established as described in "Tumor inoculation and treatment." Tumors were 10 to 20 days post-inoculation with an area between 60 and 100 mm^2. PBS, $PFO^{T490G,L491G}$ (100μg), C225.2/$PFO^{T490G,L491G}$ (159μg/100μg), C225 + $PFO^{T490G,L491G}$ (140μg + 100μg) and C225.2/$PFO^{T490A,L491V}$ (216μg/190μg) were administered retro-orbitally 24 hours prior to analysis. C225.2/$PFO^{T490A,L491V}$ (4.8μg/3μg) were administered intratumorally 2 hours prior to analysis. The indicated organs and tumors were harvested, weighed and homogenized using 1.0 mm zirconium beads in 2 mL tubes (KSE Scientific) using a Mini-Beadbeater-16 (Biospec Products) in 5 volumes of PBS. Samples were centrifuged for 20,000xg for 15 min at 4°C, and fluorescence in the supernatant was measured with an Infinite 200 Pro plate reader (Tecan). Background from PBS-treated mice was subtracted from all organ-matched measurements. A standard curve for each organ was generated by spiking in known amounts of labeled protein into organ samples collected from untreated mice and used to calculate respective concentrations.

Tumor inoculation and treatment. For induction of A431 tumors, 10^6 cells in 50μL of PBS were injected subcutaneously into the flanks of NSG mice. Intratumoral injections of PBS, C225.2/PFO^{T490G,L491G} (26μg/16μg), E6rGel (1.5μg) and C225.2/PFO^{T490G,L491G} (26μg/16μg) + E6rGel (1.5μg) were performed on days 7, 10 and 13 after tumor inoculation. Retro-orbital injections of PBS, C225.2/PFO^{T490G,L491G} (289μg/180μg), E6rGel (60μg) and C225.2/PFO^{T490G,L491G} (289μg/180μg) + E6rGel (60μg) were performed on days 6, 11, 16 and 21 after tumor inoculation. Intratumoral injections of PBS, C225.2/PFO^{T490A,L491V} (19μg/12μg), E6rGel (1.0μg) and C225.2/PFO^{T490A,L491V} (19μg/12μg) + E6rGel (1.0μg) were performed on days 5, 8 and 11 after tumor inoculation. Retro-orbital injections of PBS and C225.2/PFO^{T490A,L491V} (41μg/26μg) + E6rGel (3.4μg) were performed on days 5, 8 and 11 after tumor inoculation. Tumor area was calculated by multiplying length and width.

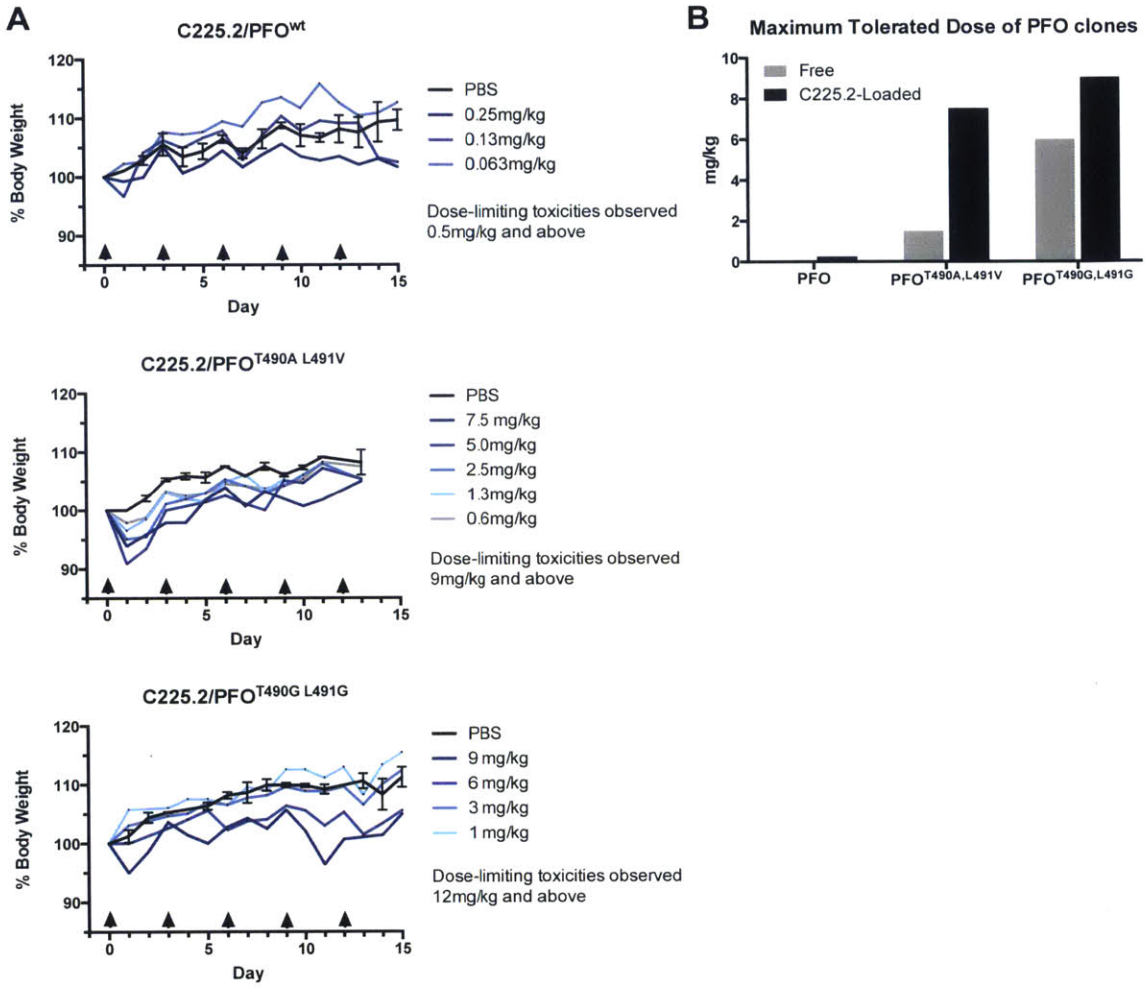

Figure 4.1. C225.2 improves the in vivo tolerance of PFO clones. (a) Changes in body weight following repeated dosing of C225.2/PFO. C225.2/PFO complexes at the indicated doses and timing were administered retro-orbitally to healthy NOD scid gamma (NSG) mice. Body weight was monitored daily and normalized to that measured at day 0 prior to the first injection. **(b)** The maximum tolerated dose (MTD) was defined as the highest dose of PFO that did not cause any loss of body weight at the end of the two-week monitoring period in (a). The indicated doses for the C225.2/PFO complexes are those of the PFO portion only.

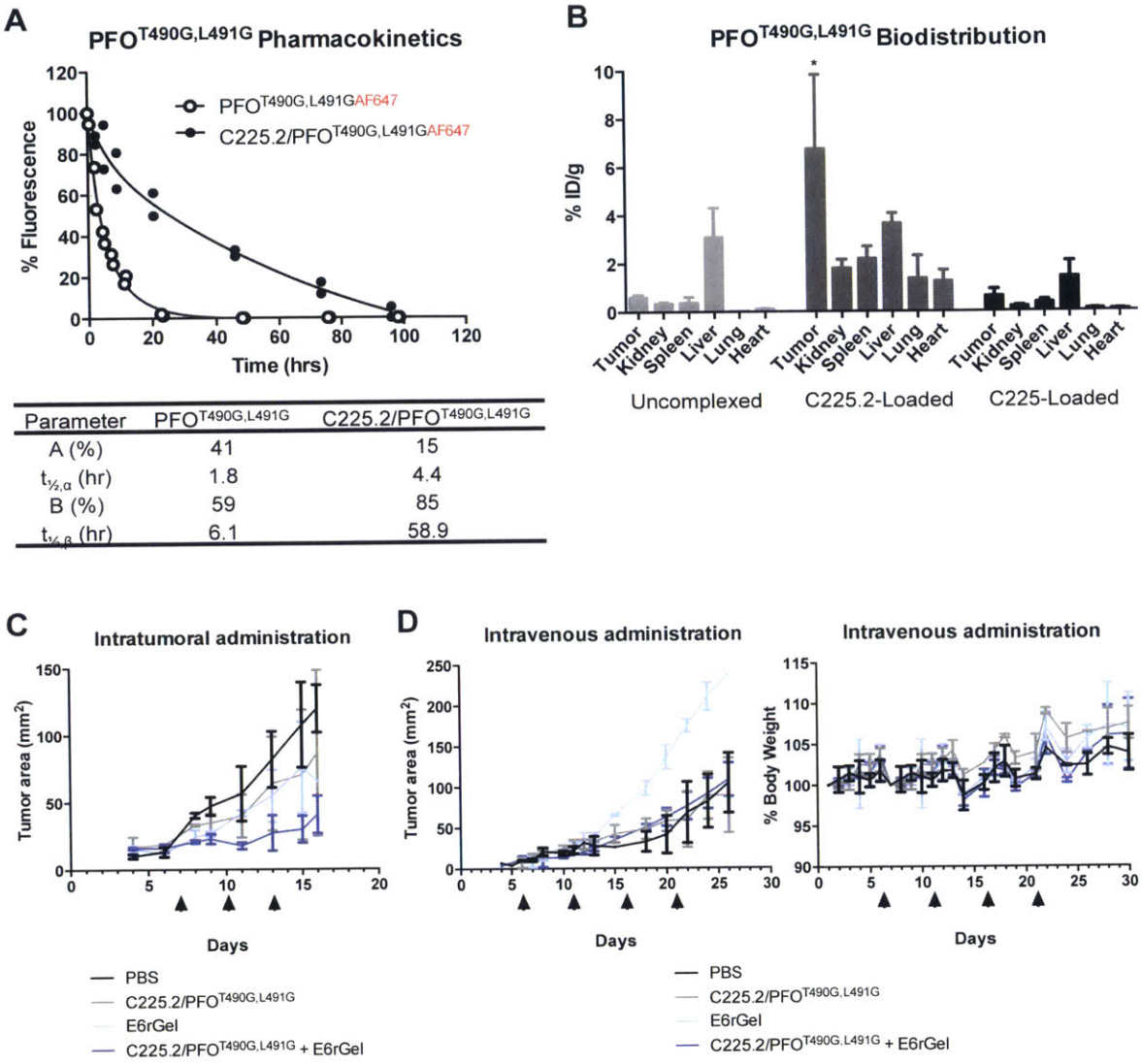

Parameter	PFO^{T490G,L491G}	C225.2/PFO^{T490G,L491G}
A (%)	41	15
$t_{½,\alpha}$ (hr)	1.8	4.4
B (%)	59	85
$t_{½,\beta}$ (hr)	6.1	58.9

Figure 4.2. Characterization of C225.2/PFO^{T490G,L491G} in vivo properties. (a) Pharmacokinetic analysis comparing free PFO^{T490G,L491G} and C225.2/PFO^{T490G,L491G}. PFO^{T490G,L491G} was labeled with Alexa Fluor 647 and loaded onto unlabeled C225.2. Tail bleeds were performed at the indicated intervals following retro-orbital administration in healthy NSG mice (n = 2). The background-subtracted fluorescence in serum was normalized to that of the first time point and fitted globally to a two-phase exponential decay ($Ae^{-\alpha t} + Be^{-\beta t}$). **(b)** Biodistribution of free PFO^{T490G,L491G}, C225.2/PFO^{T490G,L491G} and a C225 + PFO^{T490G,L491G} mixture. PFO^{T490G,L491G} was labeled with Alexa Fluor 647. Indicated constructs were administered retro-orbitally to NSG mice bearing A431 tumors (n = 3). After 24 hours, the fluorescence in each homogenized organ was quantified and converted to concentrations. **(c)** PBS, C225.2/PFO^{T490G,L491G} (26μg/16μg), E6rGel (1.5μg) or C225.2/PFO^{T490G,L491G} (26μg/16μg) + E6rGel (1.5μg) were administered intratumorally to NSG mice bearing A431 tumors (n = 3). Arrows indicate dosing. **(d)** PBS, C225.2/PFO^{T490G,L491G} (289μg/180μg), E6rGel (60μg) and C225.2/PFO^{T490G,L491G} (289μg/180μg) + E6rGel (60μg) were administered retro-orbitally to NSG mice bearing A431 tumors (n = 3). Arrows indicate dosing. **Left:** Change in tumor area. **Right:** Change in body weight of corresponding mice.

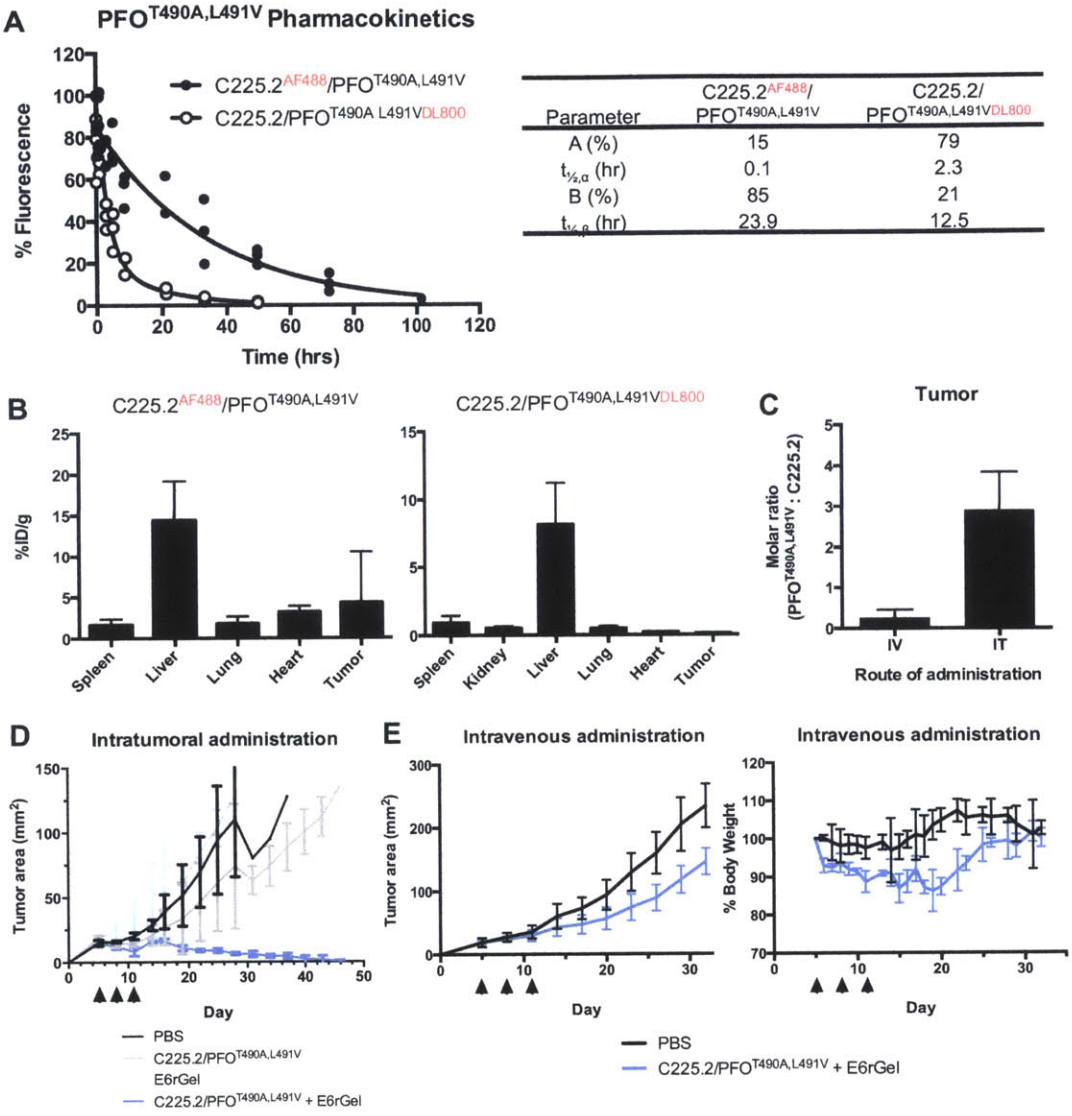

Parameter	C225.2 AF488/ PFO T490A,L491V	C225.2/ PFO T490A,L491V DL800
A (%)	15	79
$t_{½,\alpha}$ (hr)	0.1	2.3
B (%)	85	21
$t_{½,\beta}$ (hr)	23.9	12.5

Figure 4.3. Characterization of C225.2/PFO^{T490A,L491V} in vivo properties. (a) Pharmacokinetic analysis of C225.2/PFO^{T490A,L491V}. C225.2 was labeled with Alexa Fluor 488, PFO^{T490A,L491V} with DyLight 800. Tail bleeds were performed at the indicated intervals following retro-orbital administration in healthy NSG mice (n = 3). The background-subtracted fluorescence in serum was normalized to that of the first time point and fitted globally to a two-phase exponential decay ($Ae^{-\alpha t} + Be^{-\beta t}$). **(b)** Biodistribution of C225.2/PFO^{T490A,L491V} measured in NSG mice bearing A431 tumors (n = 3). C225.2 was labeled with Alexa Fluor 488, PFO^{T490A,L491V} with DyLight 800. C225.2/PFO^{T490A,L491V} was administered retro-orbitally. After 24 hours, the fluorescence in each organ was quantified and converted to concentrations. **(c)** The molar ratio of PFO^{T490A,L491V} to C225.2 in the tumor following retro-orbital (IV) or intratumoral (IT) administration (n = 3). C225.2/PFO^{T490A,L491V} was administered 24 hours (IV) or 2 hours (IT) prior to analysis. **(d)** PBS, C225.2/ PFO^{T490A,L491V} (19μg/12μg), E6rGel (1.0μg) or C225.2/PFO^{T490A,L491V} (19μg/12μg) + E6rGel (1.0μg) were administered intratumorally to NSG mice bearing A431 tumors (n = 4). Arrows indicate dosing. **(e)** PBS or C225.2/PFO^{T490A,L491V} (41μg/26μg) + E6rGel (3.4μg) were administered retro-orbitally to NSG mice bearing A431 tumors (n = 4). **Left:** Change in tumor area. **Right:** Change in body weight of corresponding mice.

Works cited

1 Rothman J, Paterson Y. Live-attenuated Listeria-based immunotherapy. *Expert Rev Vaccines* 2013; **12**: 493–504.

2 Portnoy DA, Auerbuch V, Glomski IJ. The cell biology of Listeria monocytogenes infection the intersection of bacterial pathogenesis and cell-mediated immunity. *J Cell Biol* 2002; **158**: 409–414.

3 Gunn GR, Zubair A, Peters C, Pan Z-K, Wu T-C, Paterson Y. Two Listeria monocytogenes Vaccine Vectors That Express Different Molecular Forms of Human Papilloma Virus-16 (HPV-16) E7 Induce Qualitatively Different T Cell Immunity That Correlates with Their Ability to Induce Regression of Established Tumors Immortalized by HPV-16. *J Immunol* 2001; **167**: 6471–6479.

4 Wallecha A, Wood L, Pan Z-K, Maciag PC, Shahabi V, Paterson Y. Listeria-derived Listeriolysin O has PAMP-like properties independent of its hemolytic ability. *Clin Vaccine Immunol* 2012. doi:10.1128/CVI.00488-12.

5 Sewell DA, Pan ZK, Paterson Y. Listeria-based HPV-16 E7 vaccines limit autochthonous tumor growth in a transgenic mouse model for HPV-16 transformed tumors. *Vaccine* 2008; **26**: 5315–5320.

6 Mandal M, Lee K-D. Listeriolysin O-liposome-mediated cytosolic delivery of macromolecule antigen in vivo: enhancement of antigen-specific cytotoxic T lymphocyte frequency, activity, and tumor protection. *Biochim Biophys Acta BBA - Biomembr* 2002; **1563**: 7–17.

7 Andrews CD, Huh M-S, Patton K, Higgins D, Van Nest G, Ott G *et al.* Encapsulating Immunostimulatory CpG Oligonucleotides in Listeriolysin O-Liposomes Promotes a Th1-Type Response and CTL Activity. *Mol Pharm* 2012; **9**: 1118–1125.

8 Mandal M, Kawamura KS, Wherry EJ, Ahmed R, Lee K-D. Cytosolic Delivery of Viral Nucleoprotein by Listeriolysin O-Liposome Induces Enhanced Specific Cytotoxic T Lymphocyte Response and Protective Immunity. *Mol Pharm* 2004; **1**: 2–8.

9 Kim NH, Provoda C, Lee K-D. Design and Characterization of Novel Recombinant Listeriolysin O–Protamine Fusion Proteins for Enhanced Gene Delivery. *Mol Pharm* 2015; **12**: 342–350.

10 Pirie CM, Liu DV, Wittrup KD. Targeted Cytolysins Synergistically Potentiate Cytoplasmic Delivery of Gelonin Immunotoxin. *Mol Cancer Ther* 2013; **12**: 1774–1782.

11 Yang NJ, Liu DV, Sklaviadis D, Gui DY, Vander Heiden MG, Wittrup KD. Antibody-Mediated Neutralization of Perfringolysin O for Intracellular Protein Delivery. *Mol Pharm* 2015; **12**: 1992–2000.

12 Law RHP, Lukoyanova N, Voskoboinik I, Caradoc-Davies TT, Baran K, Dunstone MA *et al.* The structural basis for membrane binding and pore formation by lymphocyte perforin. *Nature* 2010; **468**: 447–451.